REPORT DOCUMENTATION PAGE

Form Approved
OMB No. 0704-0188

Public reporting burden for this collection of information is estimated to average 1 hour per response, including the time for reviewing instructions, searching existing data sources, gathering and maintaining the data needed, and completing and reviewing the collection of information. Send comments regarding this burden estimate or any other aspect of this collection of information, including suggestions for reducing this burden, to Washington Headquarters Services, Directorate for Information Operations and Reports, 1215 Jefferson Davis Highway, Suite 1204, Arlington, VA 22202-4302, and to the Office of Management and Budget, Paperwork Reduction Project (0704-0188), Washington, DC 20503.

1. AGENCY USE ONLY *(Leave blank)*	2. REPORT DATE	3. REPORT TYPE AND DATES COVERED
	2.Jul.99	THESIS

4. TITLE AND SUBTITLE
A FOUR-YEAR SUMMER TIME MICROBURST CLIMATOLOGY AND RELATIONSHIP BETWEEN MICROBURSTS AND CLOUD-TO-GROUND LIGHTNING FLASH RATE FOR THE NASA KENNEDY SPACE CENTER,

5. FUNDING NUMBERS

6. AUTHOR(S)
1ST LT SANGER NEIL T

7. PERFORMING ORGANIZATION NAME(S) AND ADDRESS(ES)
TEXAS A&M UNIVERSITY

8. PERFORMING ORGANIZATION REPORT NUMBER

9. SPONSORING/MONITORING AGENCY NAME(S) AND ADDRESS(ES)
THE DEPARTMENT OF THE AIR FORCE
AFIT/CIA, BLDG 125
2950 P STREET
WPAFB OH 45433

10. SPONSORING/MONITORING AGENCY REPORT NUMBER

FY99-149

11. SUPPLEMENTARY NOTES

12a. DISTRIBUTION AVAILABILITY STATEMENT
Unlimited distribution
In Accordance With AFI 35-205/AFIT Sup 1

12b. DISTRIBUTION CODE

13. ABSTRACT *(Maximum 200 words)*

14. SUBJECT TERMS

15. NUMBER OF PAGES
141

16. PRICE CODE

17. SECURITY CLASSIFICATION OF REPORT	18. SECURITY CLASSIFICATION OF THIS PAGE	19. SECURITY CLASSIFICATION OF ABSTRACT	20. LIMITATION OF ABSTRACT

Standard Form 298 (Rev. 2-89) (EG)
Prescribed by ANSI Std. 239.18
Designed using Perform Pro, WHS/DIOR, Oct 94

A FOUR-YEAR SUMMERTIME MICROBURST CLIMATOLOGY AND RELATIONSHIP BETWEEN MICROBURSTS AND CLOUD-TO-GROUND LIGHTNING FLASH RATE FOR THE NASA KENNEDY SPACE CENTER, FLORIDA: 1995-1998
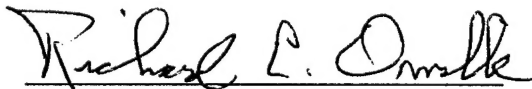
A Thesis

by

NEIL THOMAS SANGER
Captain, USAF

128 pages

MASTER OF SCIENCE

Texas A&M University

1999

Major Subject: Meteorology

A FOUR-YEAR SUMMERTIME MICROBURST CLIMATOLOGY AND

RELATIONSHIP BETWEEN MICROBURSTS AND CLOUD-TO-GROUND

LIGHTNING FLASH RATE FOR THE NASA KENNEDY SPACE CENTER,

FLORIDA: 1995-1998
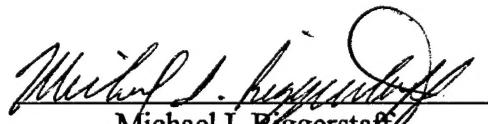
A Thesis

by

NEIL THOMAS SANGER

Submitted to the Office of Graduate Studies of
Texas A&M University
in partial fulfillment of the requirements for the degree of

MASTER OF SCIENCE

August 1999

Major Subject: Meteorology

A FOUR-YEAR SUMMERTIME MICROBURST CLIMATOLOGY AND RELATIONSHIP BETWEEN MICROBURSTS AND CLOUD-TO-GROUND LIGHTNING FLASH RATE FOR THE NASA KENNEDY SPACE CENTER, FLORIDA: 1995-1998

A Thesis

by

NEIL THOMAS SANGER

Submitted to Texas A&M University
in partial fulfillment of the requirements
for the degree of

MASTER OF SCIENCE
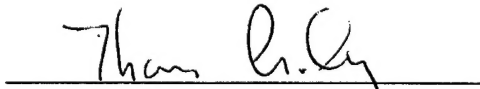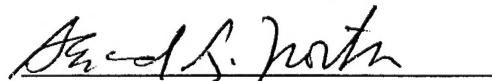
Approved as to style and content by:

_____
Richard E. Orville
(Chair of Committee)

_____
Michael I. Biggerstaff
(Member)

_____
Thomas J. Crowley
(Member)

_____
Gerald R. North
(Head of Department)

August 1999

Major Subject: Meteorology

ABSTRACT

A Four-Year Summertime Microburst Climatology and Relationship Between Microbursts and Cloud-to-Ground Lightning Flash Rate for the NASA Kennedy Space Center, Florida: 1995-1998. (August 1999)

Neil Thomas Sanger, B.S., Florida State University;

M.H.R., University of Oklahoma

Chair of Advisory Committee: Dr. Richard E. Orville

In order to ameliorate the forecasting of microbursts, the first summertime microburst climatology in the United States was produced. This climatology was based on a four year wind data base during the summer months (May – September) of 1995-1998 for 50 mesonet wind towers that encompasses the KSC. An investigation into the microburst characteristics of frequency, diurnal variation, spatial variation, speed frequency distribution, and the wind direction was accomplished. Finally, an examination into the relationship between microbursts and lightning was conducted.

A total of 282 microbursts were observed during this four-year period. There were 114 microburst days with 59 of these days having more than one microburst. The most prominent months of microbursts are June, July, and August with July being the most dominant.

Several important characteristics of wind speed and direction were found. The median wind speed was 34 knots. The majority of microburst wind speeds fell within 25 and 44 knots. As the wind increases above 43 knots, the frequency decreases exponentially, reaching virtually zero at 65 knots. The predominant wind direction of the microbursts is from southeast through the west-northwest with a maximum from the southwest.

The spatial variation of the microbursts revealed an interesting pattern. Some areas received a substantial amount of microbursts, while others received few, if any. It is

hypothesized that this difference is due to the sea breeze interacting with the abundant river breezes causing the formation of convection over the same areas on a daily basis.

The diurnal variation also uncovered a revealing pattern. The most favorable time for microbursts is between 1600 UTC (12 P.M. EDT) and 2200 UTC (6 P.M. EDT) with the peak occurring between 2000 UTC (4 P.M. EDT) and 2200 UTC (6 P.M. EDT). Directly after this peak the number of microbursts drops drastically.

The investigation into the relationship between lightning and microbursts revealed that in most cases there was an evident increase in the CG flash rate up to 25 minutes prior to the microburst. Moreover, a clear peak often occurred 5-10 minutes before the microburst. Thus, CG lightning may also improve microburst forecasting.

DEDICATION

I would like to dedicate this thesis to my beautiful fiancée Lily Landaverde, and my wonderful parents Stephen and Jeannette Sanger. Their unconditional love, support, encouragement, and patience have enabled me to make this dream a reality.

Ever since we met in February 1998, Lily has been the light in my life that has gotten me through the rigors of graduate school. She has endured my long hours spent at school and been a sounding board for my research problems. After a long day at school, her smile and encouragement would give me the strength to continue on this journey. The thing that I cherish most about Lily is that she is my best friend and companion. I am indeed a lucky man to have a woman like Lily in my life.

My parents have made me the person I am today. They have always supported me in all my endeavors. My parents sent me care packages and mail that kept my spirits up. They also talked to me every week and emboldened me to complete this important research. I am grateful to my parents because without them, none of this would have been possible.

I am also dedicating this research to the late Dr. Theodore Fujita. His extensive research into microbursts gave me the guidance I needed for my research. May he rest in peace with the Lord.

ACKNOWLEDGEMENTS

TABLE OF CONTENTS

LIST OF FIGURES

LIST OF TABLES

CHAPTER I

INTRODUCTION

During the summer, the area of maximum thunderstorm frequency in the United States is in central Florida, near the NASA Kennedy Space Center (KSC) (Boyd et al., 1993). The NASA Kennedy Space Center is located on the East Coast of central Florida at 28.61° N, 80.69°W. The persistent occurrence of sea breezes interacting with the irregular shape of the east coast, small inland bodies of water, and deep tropical moisture leads to a nearly daily occurrence of airmass thunderstorms. These storms are the primary producers of cloud-to-ground (CG) lightning and are the reason central Florida has the highest frequency of CG lightning, as shown by Orville (1991,1994). Moreover, these thunderstorms account for most of the non-tornadic severe weather events that occur at the KSC.

The most damaging of these events are downbursts. According to Fujita (1985), a downburst is a strong downdraft that causes an outburst of damaging winds on or near the surface. These destructive winds are extremely divergent. The divergence can be as large as 0.5 s^{-1}. The sizes of downbursts vary from less than one kilometer to tens of kilometers. These downbursts are subdivided into macrobursts and microbursts according to their horizontal scale of damaging winds.

Fujita (1985) defines a macroburst as a large downburst with outburst winds extending greater than 4 km (2.5 miles) in horizontal dimension. An intense macroburst can often cause widespread, tornado-like damage. The destructive winds of a macroburst can last from five to 30 minutes and can be as high as 60ms^{-1}(116 kts). Fujita (1985) defines a microburst as a small downburst with outburst winds extending only 4 km (2.5 miles) or less. Although the microburst has a small horizontal scale, an intense one can inflict damaging winds as high as 75ms^{-1} (146 kts). Kelly et al. (1985) reported wind damage and strong gusts in Florida are most prevalent during the summer. Hence, damaging

---

This thesis follows the style and format of *Journal of Climate*.

downburst winds most often occur at KSC during the summer months. The most treacherous downburst is the microburst due to its small size and short life span of less than five minutes. A microburst often eludes detection by radars and ground-based anemometers. Consequently, an aircraft at low altitude can encounter a microburst with little or no notice.

A vivid example of this was seen in three major airline accidents that were a direct result of a microburst. The first of these was the Eastern Flight 66 accident on 24 June 1975 at Kennedy airport. The second was the Pan Am Flight 759 accident on 9 July 1982 at the New Orleans airport. Finally, the Delta Flight 191 accident occurred on 2 August 1985 at the Dallas/Fort Worth airport. These three accidents caused 394 fatalities. Consequently, the study of microbursts is vital to improving aviation safety.

The perils of a microburst not only affect aviation, but also affect the daily space operations at the KSC. For instance, exposed vehicles, such as the Space Shuttle, along with other facilities and equipment, can be toppled over from an unexpected microburst. In addition, exposed workers on tall structures could be endangered. Several strong wet microbursts of up to 65 knots occurred without warning on 16 August 1994 (Wheeler, 1997). Microbursts are considered the number two weather hazard behind lightning at the KSC. The majority of the microbursts at the KSC are wet microbursts. Thus, this research will focus on the study of wet microbursts and lightning at KSC.

Eastern Florida's high frequency of thunderstorm activity produces the two most destructive weather phenomena on the plethora of daily weather sensitive ground and launch operations at KSC: lightning and microbursts. One-half of all Space Shuttle countdowns between 1981 and 1994 were scrubbed due to weather (Bauman and Businger,1996). The majority of the United State's space launches occur at the Air Force's Eastern Range (ER) and NASA's Kennedy Space Center. The ER launch complexes are located on the Cape Canaveral Air Station (CCAS), adjacent to KSC. The 45th Weather Squadron at Patrick Air Force Base, Florida provides weather support for approximately forty launches per year that include: Space Shuttle; Titan, Atlas, Athena, Pegasus, and Delta rockets; and Trident ballistic missiles (Harms et al. 1999). They issue

TABLE 1. Convective wind warning criteria for Kennedy Space Center (KSC) and Cape Canaveral Air Station (CCAS).

Area	Wind (kts)	Height (ft)	Lead-Time (min)
KSC	≥ 35	sfc – 200	30
	≥ 50	sfc – 200	60
	≥ 60	sfc – 200	60
CCAS	≥ 35	sfc – 300	30
	≥ 50	sfc – 300	60

convective wind warnings for the KSC area and CCAS (Table 1). The KSC area includes the Shuttle launch pads, areas where people are working outside, and other elevated structures. All KSC vehicles have 'exposure' wind requirements. The term exposure means the mobile service towers have been rolled back and the vehicle has lost the safeguard of the towers. These exposure wind requirements vary by vehicle and configuration. Since the mobile service towers give some protection for downwind directions, the wind limits vary in direction. The Space Shuttle launch pad limits are for a height of 60 feet AGL, and vary between 24 knots (18°-189°) to 34 knots (0°-90°). Consequently, accurate forecasts of microbursts are essential to ensure the safety of invaluable personnel and expensive Department of Defense (DoD) launch equipment.

This research will focus on analyzing a four year wind data base during the summer months (May – September) of 1995-1998 for 50 mesonet wind towers that encompasses CCAS, KSC, and remote sites surrounding CCAS and KSC. A map of Florida with the areas of interest is shown in Figure 1. This summer months time frame will be used since the majority of typical wet microbursts occur in the low shear summer regime. Microbursts will be identified and plotted using a computer algorithm written in the Interactive Data Language (IDL). An investigation into the microburst characteristics of frequency, diurnal variation, spatial variation, speed frequency distribution, and the wind direction was accomplished. Finally, an examination of the lightning characteristics using data from the National Lightning Detection Network (NLDN) will be conducted in order to find a possible link between lightning and microbursts.

Area of Study

Fig. 1. Map of Florida displaying area of study. Solid box denotes the area of study where top crosshair identifies the location of the KSC Shuttle Landing Facility (SLF) and the bottom crosshair identifies the location of the CCAS. The SLF is also the location of the KSC.

CHAPTER II

BACKGROUND

A microburst climatology for a given area has never been accomplished; however, there were a few projects in late 1970's and early to mid 1980's that analyzed microburst activity over the span of a few months. These were the Northern Illinois Meteorological Research on Downburst (NIMROD), Joint Airport Weather Studies (JAWS), and the National Science Foundation (NSF) component of the Cooperative Huntsville Meteorological Experiment (COHMEX), MIST (Microburst and Severe Thunderstorm) (Dodge et al. 1986). As a result, the purpose of this research is to develop the first short-term climatology of microbursts utilizing the state of the art mesonet of wind towers in the KSC area. The two main projects used to construct this climatology are NIMROD and JAWS.

This climatology of microbursts will give forecasters at the 45th Weather Squadron an essential tool for improving microburst forecasting. This research will help ameliorate microburst nowcasting with a more accurate lead-time of menacing microburst winds. Currently, the lead-time at KSC is 30 to 60 minutes, depending on speed threshold; however, there is a large false alarm rate of 40-60 percent. The climatology developed in this research will also be used in conjunction with lightning data from the NLDN. This data will be used to examine the temporal relationship between microbursts and cloud-to-ground (CG) lightning flash rate.

1. Description of Microbursts

a. Characteristics

All microbursts are not identical to each other. Some microbursts are accompanied by heavy rain, while others form underneath small virga. Moreover, the parent clouds which induce microbursts are not always associated with thunderstorms. Frequently, isolated rainshowers spawn relatively strong microbursts. Consequently, there are a variety of characteristics associated with microbursts.

According to Fujita (1985), no microbursts develop on or near the ground. Rather, they descend from the bases of convective clouds. The microburst that has its

characteristic winds located above anemometer heights is called a "midair microburst". A midair microburst may remain aloft until it dissipates, or it may keep descending to the surface.

After a microburst has made it to the surface it is called a "surface microburst". When a surface microburst spreads out onto a large area, the downflow continues to supply the mass until it sinks to the surface (Fujita, 1985). After this, the microburst flattens and its expansion ends.

Fujita (1985) hypothesizes there can be either stationary or traveling microbursts. If a stationary microburst spreads out inside an unperturbed environment, a perfect starburst outflow with an annular ring of high winds will be observed. In reality, the majority of microbursts are traveling microbursts. The traveling microburst and its associated motion distorts the airflow from a circular to an elliptical shape. The front-side wind increases while the backside weakens, resulting in a crescent-shaped area of high winds. A fast-moving microburst is characterized by surface winds with straight, or mostly parallel streamlines. These type of microburst winds are frequently called "straight-line winds.

These straight-line winds are associated with radial microbursts. These radial streamlines are observed if the microburst winds are irrotational. The outflow winds of microbursts are typically irrotational. This means that the streamlines of the outflow winds spread out radially without rotating around the center. However, when a microburst descends inside a strong mesocyclone, its airflow at the surface is characterized by cyclonically curved or twisting streamlines. This type of microburst is often labeled a twisting microburst and has been confirmed during aerial surveys of tornadoes spawned by supercell thunderstorms (Fujita, 1985).

According to Fujita (1985), a microburst associated with a strong downflow and outflow is called an "outflow microburst". The outflow microburst is the most prevalent type of microburst. Observational evidence has discovered that a slow-moving outflow microburst is often encircled by a vortex ring.

The ring vortex keeps stretching until it reaches a limit. Once this limit is reached, the vortex is sliced into several pieces of horizontal roll vortices. Some of these vortices speed

away from their source region, inducing bands of high winds that last two to three minutes. According to Fujita (1985), this horizontal vortex roll is called a "rotor microburst". A rotor microburst leaves a band of wind damage in its wake. This type of microburst acts like a steamroller, or a tornado with a horizontal vortex axis, damaging structures and uprooting trees inside a narrow area. Due to the fact a rotor microburst has a roaring sound and a narrow damage path, it has been erroneously identified as a tornado.

As mentioned earlier, there can be both wet and dry microbursts; however, certain regions usually experience the predominance of one or the other. In dry areas such as Denver, raindrops in microbursts often completely evaporate prior to reaching the ground. This evaporation can cause a sufficient amount of downward momentum for a microburst to reach the ground without any rain. Moreover, the high cloud base in the dry region provides the descending raindrops ample time to evaporate before reaching the ground. Furthermore, the low relative humidity below the cloud base serves to accelerate the evaporation process. In stark contrast, wet areas, such as the Kennedy Space Center in Florida, are the typical breeding ground for wet microbursts.

b. Wet Microburst Mechanics

The primary source for the production of wet microbursts during the summer in the KSC area is typical air mass thunderstorms. The wet microburst has four mechanisms: 1) evaporative cooling, 2) precipitation loading, 3) melting of ice particles, and 4) downward advection of momentum. Moreover, the wet microburst is not in hydrostatic balance. Since the upper-level winds are usually quite weak in the summer regime of Florida, downward advection of momentum is assumed to play a small role in the development of wet microbursts. However, during the El-Niño year of 1997, the upper-level winds associated with the sub-tropical jet may have been strong enough to make downward advection of momentum a significant factor in wet microburst formation. Evaporative cooling takes place when relatively dry air is entrained into the storm center. The dry and moist air mixture leads to evaporation and hence cooling. This cooler air is more dense and sinks in the form of a convective outflow. Precipitation loading occurs when the weight of the hydrometeors leads to an outflow of sinking air. When the updraft of a

storm collapses, the weight of the precipitation becomes an unbalanced force that leads to the convective microburst. The melting of graupel and hail also cause low-level cooling that leads to the development of a convective outflow.

2. Summer Weather Regime

a. Thunderstorm Activity

During the summer months, there is a nearly daily occurrence of thunderstorms in Florida; however, there is usually no synoptic forcing during this time of year and the upper air pattern is weak. The daily heating and cooling of the landmass is the main reason for convective development in east-central Florida. The heating of the landmass creates a sea breeze that is the main focus for thunderstorm development. Many studies (e.g., Byers and Rodebush 1948; Gentry and Moore 1954; Frank et al. 1967; Nicholls et al. 1991; Lyons et al. 1992) have shown that thunderstorms often develop near and ahead of sea breeze fronts.

Laird et al. (1995) found that the variations in the direction of the sea breeze in the vicinity of irregular coastlines, such as Cape Canaveral, can lead to persistent zones of convergence within the sea breeze air. Moreover, several numerical studies (e.g., McPherson, 1970; Abbs 1983; Arritt 1989; Cautenet and Rosset 1989) have revealed that convergence patterns associated with the sea breeze are altered along asymmetrical coastlines. In a modeling effort associated with the Kennedy Space Center Atmospheric Boundary Layer Experiment (KABLE), Zhong et al. (1991) discovered that the presence of the Indian River, Banana River, and the Mosquito Lagoon resulted in a convergence pattern that did not resemble a simple sea breeze circulation. Due to the surface heat flux differential between the rivers and adjacent land areas, weak subsidence developed over the rivers and lagoon, and areas of convergence evolved adjacent to bodies of water. Consequently, the normal convergence pattern associated with a simple sea breeze front was disrupted.

These atypical zones of convergence can locally increase the depth of the sea breeze air and create circulations at the top of the sea breeze that can support the development of convection. Moreover, small inland water bodies, such as the Indian River, can have a

strong influence on location of thunderstorm development as the sea breeze moves inland. Divergence over the small, relatively cooler Indian River during daytime was shown to be enough to maintain a quasi-stationary convergence zone which, when approached and disrupted by the sea breeze front, initiated thunderstorm development.

Laird et al. (1995) noted the development of a trailing convergence line behind the sea breeze front. They showed that the trailing convergence line deepened the sea breeze in a local area and played a key role in the development of a thunderstorm behind the sea breeze front. The trailing convergence line is typically perpendicular to the north-south oriented sea breeze.

Pielke (1974); Atchison and Taylor (1992); Zhong and Takle (1993) found that the anomalous convergence pattern found at the KSC was quite sensitive to the direction and speed of synoptic-scale winds for a given region. Watson et al. (1987) found that low-level offshore flow would develop vigorous convection inland that would move eastward across KSC. Conversely, low-level onshore flow would tend to generate less intense convection. The southwesterly flow regime is moist, unstable, and offshore. Hence, it is the most favorable environment for deep convection and subsequent microburst activity. This flow regime increases the eastward propagation of the West Coast sea breeze from the Gulf of Mexico. The thunderstorms associated with the West Coast sea breeze move eastward across the Florida peninsula throughout the day and can reach the KSC area in the late afternoon or early evening. In general, a northeasterly flow regime is the most stable and driest of all regimes. Thus, it is the least favorable for deep convection and microburst activity.

b. Diurnal Cycle

Neumann (1971) observed that during the summer (May through September) almost all thunderstorm activity occurred from 1400 UTC (10 A.M. EDT) to 0200 UTC (10 P.M. EDT). The diurnal cycle of CG flashes can reveal the most frequent time of thunderstorm activity for a given area. Studies show that the maximum lightning activity at KSC occurs between May and September especially in July and August. Hinson (1997) found that the three most active CG activity months of June, July, and August account for 73% of all CG

flashes for the entire year. He also discovered that the diurnal maximum occurs between 1700 UTC (12 P.M. EDT) and 0000 UTC (8 P.M. EDT).

Maier et al. (1984) analyzed the diurnal variability of lightning during the summers of 1976-78 and 1980. They observed a peak in lightning occurred at KSC and CCAS between 2000 UTC (4 P.M. EDT) and 2100 UTC (5 P.M. EDT). Hinson (1997) noted a rapid increase in lightning activity beginning at 1600 UTC (12 P.M. EDT) with a lucid diurnal maximum at 2000 UTC (4 P.M. EDT) and a precipitous decline from 2100 UTC (5 P.M. EDT) until 0300 UTC (11 P.M. EDT). This coincides well with Neumann (1968) who studied 13 years of thunder data (1951-52, 1955-67) at Cape Canaveral. He determined it was likely to have at least one thunderstorm in progress peaking between 2000 UTC (4 P.M. EDT) and 2200 UTC (6 P.M. EDT) for the months of June through August. All of these studies point to lightning as a strong indication of how much convection is occurring at a given time over the KSC region. Thus, it can be inferred that these peak times of convective activity will be the most probable times for microburst activity.

3. Microburst Studies

a. NIMROD and JAWS

The first field program that investigated microbursts was NIMROD (Northern Illinois Meteorological Research on Downburst). The Eastern 66 accident at JFK airport on 24 June 1975 initiated this experiment. In order to distinguish relatively small downbursts from their larger counterparts, the downburst was sub-classified into macroburst and microburst according to the horizontal extent of the damaging winds. A macroburst contains outburst winds that extend in excess of 4 km (2.5 miles) in horizontal dimension. A microburst has outburst winds that extend only 4 km (2.5 miles) or less in the horizontal dimension.

The program was conducted in 1978 by the University of Chicago, with principal investigators Ted Fujita and Ramesh Srivastava. The project network, located in the western suburbs of Chicago, Illinois, was designed to depict the structure of downbursts by using three Doppler radars and 27 PAM (Portable Automated Mesonet) stations. The

PAM stations were placed inside a triangular grid with dimensions 56x57x60 km.

During the first quarter of the experiment, it was discovered that not all microbursts were associated with severe thunderstorms. In fact, some microbursts were observed to occur in relatively weak echoes without thunder. The role of evaporational cooling aloft associated with elevated convection may have been responsible for producing these irregular microbursts. Moreover, these microbursts were probably dry microbursts, which are not the focus of this research. The duration of the NIMROD project lasted from 19 May to 1 July 1978 (42 days).

The second microburst field project in 1982, called JAWS (Joint Airport Weather Studies) was conducted jointly by the University of Chicago and the National Center for Atmospheric Research (NCAR), with principal investigators Ted Fujita of the University of Chicago, John McCarthy, and Jim Wilson of NCAR. It was hypothesized that a deep sub-cloud layer of dry adiabatic lapse rate over the high plains would produce a new type microburst quite different from those found in the NIMROD experiment. The JAWS network, located in the northern suburbs of Denver, Colorado, was designed to find microbursts, rather than macrobursts. As a result, the PAM stations were spread out over a much smaller area than in the NIMROD case. The PAM stations were located inside a triangular grid with dimensions 15x18x28 km.

This second experiment was conducted since a number of microburst–related accidents kept occurring in various parts of the world. The PAN American 759 accident at New Orleans on 9 July 1982 occurred during the JAWS project. It was later determined that a microburst on the eastern side of the airport was a strong factor in the crash. Thus, the JAWS researchers felt that the workings of the microburst needed to be understood as soon as possible in order to ameliorate aviation safety. The length of the JAWS project was from 15 May to 9 August 1982 (86 days).

b. *Identification of Microbursts by Computer*

Each PAM station in the NIMROD and JAWS networks continuously gathered wind speeds once every minute. These speeds included the one-minute mean wind and the one-minute maximum wind. The maximum wind speeds were used in identifying the

microbursts that affected the PAM stations. The PAM stations in the NIMROD and JAWS networks collected a large amount of maximum wind data during operations: 61,766 from NIMROD and 123,956 from JAWS (Fujita, 1985). The gross number of winds collected from both NIMROD and JAWS was 5,014,494.

The only way to efficaciously identify the microburst winds from these data was to single out all possible wind characteristics utilizing a microburst identification algorithm. The algorithm detected a first-guess microburst if it was characterized by a mound-shaped wind profile with a peak center wind. In order to determine the magnitude of the rise and fall of the winds in the mound, the pre-peak mean speed (2-7 minutes before) and post peak mean speed (2-7 minutes after) were computed. Since the mound-shaped wind in a microburst lasts two to five minutes, using the winds one minute before and after the peak center wind could result in an unusual increase in the mean speeds. The first-guess algorithm consisted of six conditions that had to be met simultaneously (Table 2). The center wind in Table 2 refers to the peak wind associated with the microburst. Condition 1 specifies that the peak wind must be greater than or equal to 20 knots for it to be labeled a microburst. Conditions 2 and 3 require that the mound-shaped profile must be elevated at least 10 knots above the level of the pre and post-peak mean wind speeds. Conditions 4 and 5 reject a small mound superimposed upon sustained high winds. Condition 6 will eliminate the gust front that is characterized by an exponential decay of the gusty winds behind a front.

This first-guess algorithm was applied to the 5 million winds and obtained 143 first-guess microbursts in NIMROD and 436 first-guess microbursts in JAWS. However, a detailed look into the PAM data and the known cases of microbursts revealed that the number of first guess microbursts was excessive. In order to overcome this difficulty, the variation of winds in every first guess microburst was plotted on a misoanalysis (4-40 km) wind chart. The final decision of whether a first guess microburst was real or not was subjectively made by meteorologists. In the end, there were 50 microbursts in NIMROD and 186 microbursts in JAWS.

TABLE 2. First guess algorithm conditions to identify microbursts from (Fujita, 1985).

Condition 1	Center wind (peak wind) greater than or equal to 20 kts
Condition 2	Center wind (peak wind) at least 10 kts faster than pre-peak mean speed
Condition 3	Center wind (peak wind) at least 10 kts faster than post-peak mean speed
Condition 4	Center wind (peak wind) is $1.25 \times$ (pre-peak mean speed) or faster
Condition 5	Center wind (peak wind) is $1.25 \times$ (post-peak mean speed) or faster
Condition 6	Pre-peak mean speed does not exceed $1.5 \times$ (post-peak mean speed)

c. Meteorological Parameters of Microbursts

There are a myriad of meteorological parameters that accompany microbursts. According to Fujita (1985), most macrobursts are followed by a high pressure dome induced by rain-cooled air. A pressure jump takes place along the leading edge of the macroburst followed by gusty winds and sharp temperature drop. In contrast, microbursts have a strong downflow that descends all the way to the surface before spreading. The downflow air warms up dry-adiabatically unless embedded raindrops evaporate quick enough to maintain a moist adiabatic descent; however, this is extremely rare in a strong microburst. The air temperature in microbursts can be warmer or colder than their environment. Moreover, the surface pressure in a microburst can be higher or lower than the ambient pressure due to the fact that microburst winds lose their pressure head while being accelerated outward from the center. Fujita (1985) observed that the pressure does not always increase during high winds. On average, the surface pressure only increases several tenths of a millibar; however, individual cases could experience an increase or decrease of 2 to 3 mb.

The main reason for the abnormal pressure change is the conversion of total pressure into velocity pressure. The total pressure is sum of the static pressure and the velocity pressure or dynamic pressure. At the dead center of a microburst the air is calm and the surface pressure is high. The high pressure at the center of the microburst accelerates the air outward. The atmospheric pressure decreases as the outflow speed increases and reaches a minimum at the location of the peak wind. If a frictionless outflow is assumed, Bernoulli's Theorem can be applied for computing the pressure change as a function of wind speed.

The dew-point temperature in microbursts can be higher or lower than their environment. A higher dew-point temperature is expected in a precipitation-cooled microburst. The unexpected lower dew-point temperature is likely attributed to dry air entrainment into the microburst during its fast descent to the ground. Subsequently, the changes in meteorological conditions associated with microbursts are quite complicated.

Several important meteorological parameters pertaining to microbursts were analyzed

from NIMROD and JAWS. These were direction of peak winds, peak wind speed of microbursts, duration of half-speed winds, diurnal variations of microbursts, and spatial variations of microbursts. According to Fujita (1985), the peak winds microbursts generate can come from any direction; however, peak winds from the easterly direction are seldom. The direction of peak winds in the NIMROD network was mainly from 135° (southeast) through 360° (north). The peak winds in the JAWS network exhibited a sinusoidal distribution with a maximum frequency at 290° (west-northwest).

Since microbursts typically descend from a traveling parent cloud, the direction of peak winds should follow the direction of the parent cloud. For example, if a parent cloud is traveling from west to east, the microburst will induce a peak microburst wind from the west. When a microburst center passes to the south of a wind sensor it will measure a wind from the south. Thus, the direction of the starburst winds differs markedly depending on the relative location of the microburst center and wind sensor. Moreover, the pressure field of an earlier microburst affects the pattern of the outburst winds on or near the surface.

The frequencies of microburst winds from both NIMROD and JAWS reveal that the probability of experiencing a certain wind speed reaches a peak within a range of 12 to 14 ms^{-1} (23 to 27 kts). As wind speed increases, the frequency decreases exponentially, reaching practically zero at 33 ms^{-1} (64 kts). The maximum wind speed measured in NIMROD and JAWS was 31.3 ms^{-1} (61 kts) and 32.6 ms^{-1} (63 kts), respectively. Fujita (1985) observed that the exponential decrease is nearly the same in both NIMROD and JAWS as well as in dry and wet microbursts.

Fujita (1985) defines the average duration of microburst winds as the period of one-half of the peak wind speed (half-speed period). He found that it varied between one and eight minutes for both NIMROD and JAWS. Since the parent clouds of microbursts are convective clouds, their diurnal and spatial variations are closely related to the time and frequency of convective activity in specific areas.

The frequency of wet microbursts in NIMROD increased progressively from 0800 UTC (3 A.M CDT). to 0500 UTC (12 A.M. CDT), reaching a peak between 2200 UTC (5

P.M. CDT) and 0500 UTC (12 A.M. CDT). For the JAWS network, wet microbursts occurred with a distinct peak between 2000 UTC (2 P.M. MDT) and 2100 UTC (3 P.M. MDT) and a secondary peak between 0100 (7 P.M. MDT) and 0200 UTC (8 P.M. MDT). The earlier peak jives with the time of small convective clouds, while the later peak coincides with the time of large thunderstorms in the late afternoon and early evening. Atkins and Wakimoto (1991) reported that MIST had somewhat similar findings to NIMROD and JAWS with a diurnal peak of microbursts at 2000 UTC (3 P.M. CDT) and a secondary peak at 1700 UTC (12 P.M. CDT).

Both the NIMROD and JAWS revealed some areas prone to experiencing microbursts with some areas receiving few, if any, microbursts. The complex interaction of the sea breeze, inland river breezes, and irregular shape of the coastline will make some areas more likely to experience convection and microbursts at KSC.

4. Lightning and Microburst Relationship

a. Cloud Physics

The relationship between lightning and microbursts can be understood better if one knows the role of cloud physics in convection. The primary initiation mechanisms for the microburst have been attributed to the low-level cooling that results from the melting of graupel and hail and to the evaporation of precipitation (Goodman et al. 1988b; Srivastava (1985, 1987). The temporal evolution of lightning activity associated with wet microbursts shows many of the same characteristics as the growth and decay life-cycle of the typical air-mass thunderstorm.

Workman and Reynolds (1949) and Dye et al. (1986) revealed clouds that contain ice-phase precipitation and intense vertical growth produced the most lightning. Laboratory studies by Jayaratne et al. (1983) revealed that ice-ice interactions in an area of supercooled water leads to a large amount of charge exchange between particles. The prototype electrostatic structures believed to be key players in producing the two most dominant lightning types, intracloud (IC) and cloud-to-ground (CG), are shown in Figure 2. Wilson (1916) and Simpson and Scrase (1937) originally advocated this figure. The main negative charge region is seen in both the dipole and tripole structures in Figure 2. It
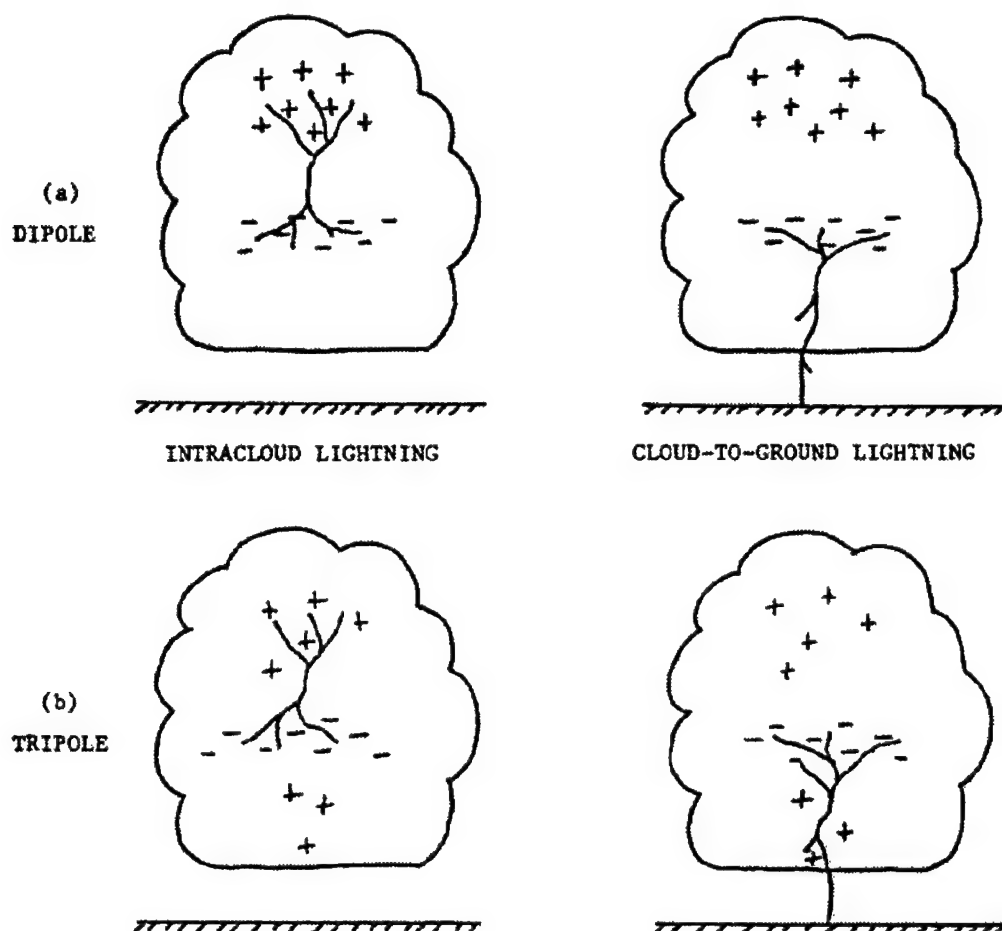
Fig. 2. Depiction of in-cloud (IC) and cloud-to-ground (CG) lightning in prototype electrostatic structures. (a) dipole and (b) tripole (From Williams et al. 1989).

has been shown that this main negative charge region is correlated with a temperature of around $-12°$ C. Balloon soundings indicate that the largest vertical fields in thunderclouds are in the upper and lower boundary of this thin (≤ 1000 m) region. Krehbiel (1981) and Taylor (1983) have shown from VHF radiation studies that IC and CG lightning are initiated at the upper and lower boundary of the main negative charge layer, respectively.

The lightning produced in these convective clouds exhibits a sound correlation with microbursts observed at the surface. During the MIST experiment in Huntsville, Alabama, the peak lightning rate preceded the maximum outflow velocity for all but one of the 33 microbursts. Moreover, the peak electrical activity is well correlated with the vertical development of clouds. The consistent temporal relationship between the electrical phenomena (lightning) and the dynamical phenomena (microburst) hints that the lightning and microburst have a common cause.

There has been a plethora of evidence proving that collisions between graupel and ice crystals are responsible for the separation of charge that accounts for the main positive dipole. According to Lhermitte and Williams (1985), the IC lightning tends to be most active in the presence of a well-developed updraft with ice crystals, supercooled droplets, and graupel all moving upward relative to the ground. A particle 'balance level' manifests itself at about 6-7 km. When the balance level disappears, and the ice particles begin to descend, the IC lightning rate and total lightning rate decrease. At this time, millions of kilograms of ice are free to fall and melt, thereby absorbing the latent heat of fusion.

Williams et al. (1989) believe the induced negative buoyancy may be the predominant drive for the formation of microbursts. Moreover, they hypothesize that the role of melting usually gets less attention than evaporation due to the large difference in latent heats of vaporization and melting; however, the rate of cooling for both of these processes is inversely proportional to the respective latent heats. As a result, the rate of cooling due to melting exceeds that due to evaporation even at small relative humidity of 40%. This result can be found in the numerical calculations of Srivastava (1987).

Williams et al. (1988) showed that intracloud lightning activity of microburst producing storms is a precursor to the maximum wind speed at the surface. The time of

peak flash rate leads precedes the maximum wind speed by five to ten minutes. They hypothesized that the consistent temporal relationship between the electrical phenomena (lightning flash rate) and the dynamical phenomena (microburst) is attributed to ice particles aloft.

b. Recent Observations

The relationship between lightning and microbursts has been the focus of several recent studies. Goodman et al. (1988b) found that total flash rates in convective storms tend to increase/decrease in-phase with the evolution of the updraft/downdraft. Hence, an abrupt decline in total flash rates was associated with storm collapse and served as a signal to the arrival of maximum microburst outflows at the surface. An examination of lightning detection and ranging (LDAR) data from Lhermitte and Krehbiel (1979) revealed that as many as 15 IC flashes precede the first CG flash in the initial stage of a Florida storm. In the second and more vigorous stage of storm development, LDAR radiation sources associated with IC lightning rise in concert with the vertical development. About three minutes later, the onset of CG lightning is well correlated with the initial descent of the 55-Dbz reflectivity core beneath the level of main negative charge.

Williams et al. (1989) found that IC lightning is most prevalent in the early stages of a thunderstorm and is well correlated with the vertical development of the cloud, the growth of ice particles, and radar reflectivity above the main negative charge region. They also found that CG lightning activity lags the initial IC lightning peak by 5-10 minutes; however, this is less systematic than IC behavior. Moreover, they observed that strong microburst outflows at the surface trail the peak lightning rate, which is dominated by IC lightning, by 5-10 minutes.

Buechler et al. (1988) observed that the flash rates of CG lightning in long-lived, microburst-producing storms increases until about 3-5 minutes prior to the microburst event. Goodman et al. (1988a) looked at the total flash rate and found similar results in a wet microburst-producing storm in the southeastern United States. They observed an apogee in the total flash rates of air-mass thunderstorms 6 minutes before the peak microburst outflow. Williams et al. (1989) studied the total flash rate of air-mass

thunderstorms that produced wet microbursts and found that microbursts lagged the peak total lightning rate by 5-10 minutes.

Biedinger and Stern (1989) studied the relationship of CG strikes with radar reflectivity and echo tops in Florida. They discovered that the peak CG lightning rate was strongly correlated with the time and location of severe weather. Maier and Krider (1982) compared CG lightning characteristics of severe storms in northern Texas and Oklahoma with normal air-mass thunderstorms in Florida. They showed that the air-mass thunderstorms produced CG mean rates of about 1 per minute, whereas severe storm rates were as high as 2 to 6 per minute. Moreover, peak rates in severe storms approached 20 per minute. The air-mass storms only had peak rates on the order of 12 per minute.

c. Discussion

Williams et al. (1989), Buechler et al.(1989), Goodman et al. (1988b), and others suggest that there is a vital microphysical nexus between ice particles and charge separation in the production of storm electrification and microbursts in air-mass thunderstorms. The presence of large amounts of supercooled water, ice crystals, and graupel inside a vigorous updraft accelerates the electrification of a convective cloud. As a result, the apex in IC lightning activity coincides with the peak updraft strength. When the updraft is no longer able to support the mass of precipitation, the core descends toward the surface. At this point, cooling from latent heat of melting supplemented by evaporative cooling drives the formation of a microburst.

Kane (1991) hypothesizes that the descending mass of ice generates a positive charge at lower levels beneath the main negative charge and produces an environment conducive for CG lightning. This is the reason for the temporal differences between the peak IC lightning, peak CG lightning, and the microburst winds at the surface. Williams et al. (1989) believe that the diminishment of IC lightning and predominance of CG lightning seen in their case studies is due to the depleted ice content in the central dipole region and the descent of large numbers of graupel particles beneath the main negative charge region. The observed 5-10 minute interval from peak IC lightning to microburst at the surface is the same time required for ice particles to travel the distance between the main negative

charge region and the surface. Based upon the results from the observations in the previous section, Williams et al. (1989) speculate that IC instead of CG lightning activity is a superior precursor of microburst activity.

A well-defined peak in activity is more difficult to detect in the comparatively infrequent CG lightning component. Goodman et al. (1988b) thinks the decreasing total flash rate may serve as an important sign of imminent microbursts since it reflects the presence of ice particles and the collapse of the storm in a favorable environment for the production of damaging microbursts. Hence, the investigation of lightning activity in deep thunderstorms in weakly sheared environments, such as the KSC area, may provide a simple short-term warning of perilous microburst hazards at low levels.

CHAPTER III
DATA AND METHODS OF ANALYSIS

The 45th Weather Squadron at Patrick Air Force Base, Florida, provided the wind tower data for this study. The Kennedy Space Center (KTTS) official surface observations that were used for verifying the presence or absence of convection in this study were obtained from the Air Force Combat Climatology Center (AFCCC) in Asheville, North Carolina. GeoMet Data Services, Inc., which operates the National Lightning Detection Network (NLDN), collected the lightning data for this research.

1. Wind Tower Data

The Weather Information Network Display System (WINDS) collects, processes, archives and disseminates data from an array of 50 instrumented meteorological towers at Cape Canaveral Air Station (CCAS) and the NASA Kennedy Space Center (KSC) and remote sites surrounding CCAS and KSC. This system began operating in 1994; however, the network consisted of only 27 wind towers. These towers make independent measurements each minute; however, the data interval for each tower used in this study is 5 minutes. Thus, a tower will provide the highest wind measured during the previous 5-minute period. The tower observations are in compliance with international meteorological observation practices.

The network covers approximately 1200 km^2 with an average station density of one tower every 27 km^2 (Figure 3). The inland bodies of water surrounding the KSC are depicted in Figure 4. This is one of the most densely instrumented mesonetworks in continuous operation in the United States. The wind towers are organized into three different groups based on their primary operational application. These three different categories are launch critical towers, safety critical towers, and forecast critical towers.

The launch critical towers are located at the launch complexes, Shuttle Landing Facility (SLF), or taller towers that provide safety information to the safety assessment program. These wind towers are equipped with the R.M. Young Model 05305-18 Wind Monitor AQ sensor and have the highest reliability and accuracy since they are used in direct evaluation
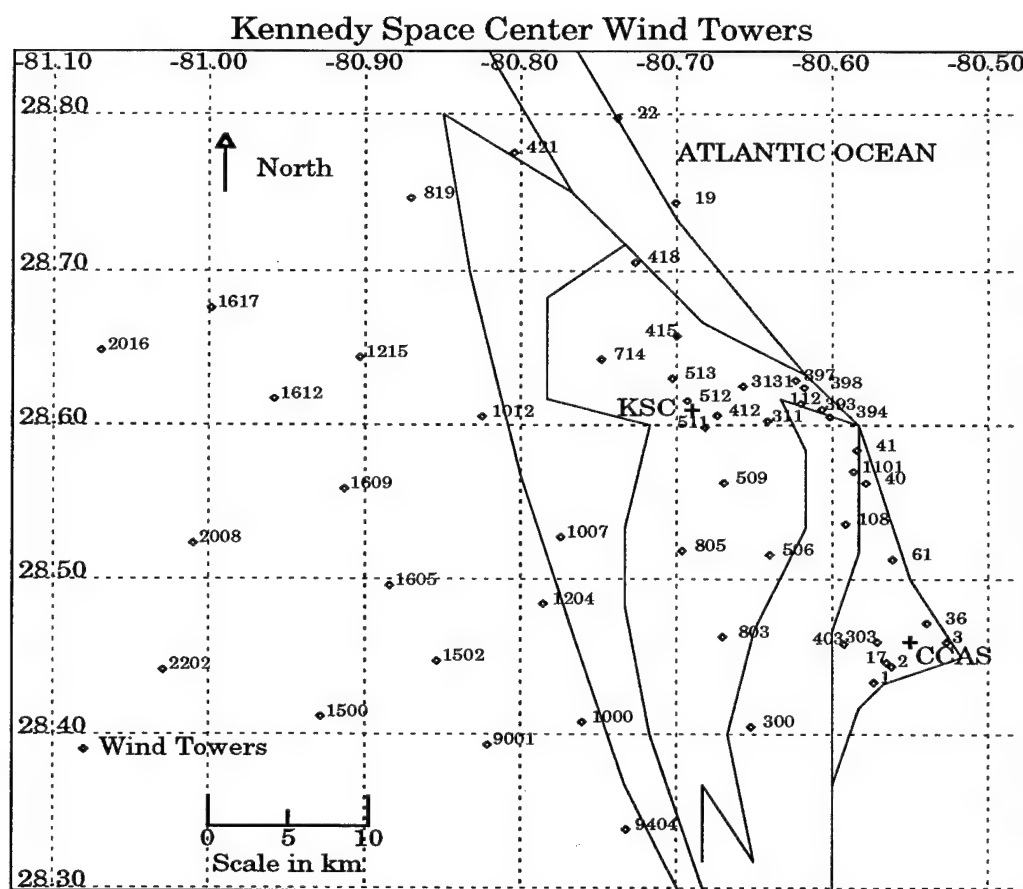
Fig. 3. Location of Kennedy Space Center wind towers. The wind tower positions are shown with a diamond. The KSC and CCAS are depicted with crosshairs.
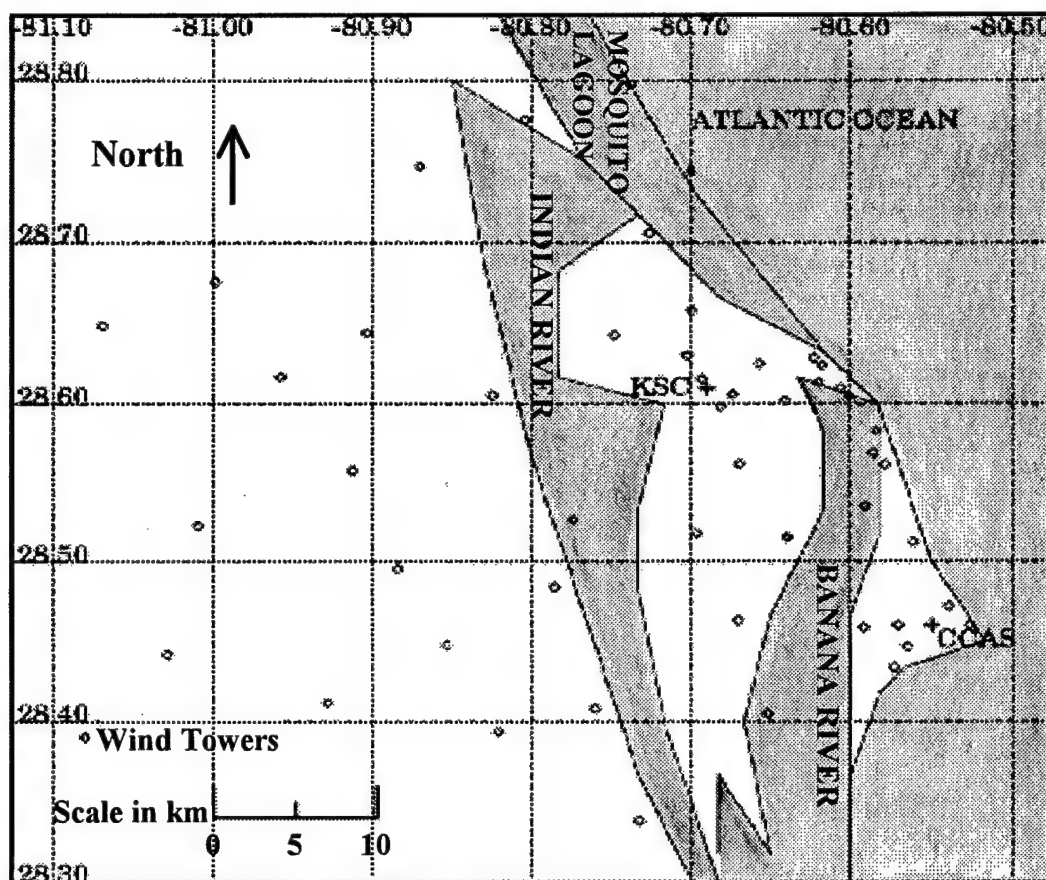
Fig. 4. Depiction of bodies of water around KSC. The bodies of water are indicated by the gray shading. The Banana River and Indian River both run parallel to each other and split the KSC to the right and left, respectively. The Mosquito Lagoon is just to the north of tower 397 and continues up the Atlantic coast.

of launch constraints.

The safety critical towers are located near the launch complexes and SLF where propellants and other potentially toxic chemicals are stored or handled. These towers are also equipped with the R.M. Young Model 05305 18 Wind Monitor AQ sensor since they support emergency response activities.

The forecast critical towers generally surround the launch and safety critical towers. These towers use the R.M. Young Model 05103 Wind Monitor sensor. This is a Commercial Off The Shelf (COTS) sensor that is widely used for standard meteorological measurements that do not require high fidelity response characteristics such as those required for air quality measurements.

The launch and safety critical towers have an operating wind speed range of 0.33-54 ms^{-1} (0.6-105 kts) and a survival range of 60 ms^{-1} (116 kts). The wind speed sensor is a 20 cm diameter 4-blade helicoid carbon fiber propeller that has a precision of $\pm$ 0.3ms^{-1} (0.58 kts). The wind direction sensor is a 38 cm turning radius balanced vane that has an accuracy of $\pm$ 3°. The forecast critical towers have a wind speed operating range of 0.9-60ms^{-1} (1.74-116 kts) and a survival range of 80ms^{-1} (155 kts). The wind speed sensor is an 18 cm diameter 4-blade helicoid polypropylene propeller that has an accuracy of $\pm$ 0.3ms^{-1} (0.58 kts). The wind direction sensor is also a 38 cm turning radius balanced vane that has a precision of $\pm$ 3°.

Although the wind towers are extremely accurate, they have several limitations that will affect this research. A key limitation is the placement of the wind towers themselves. Several towers have poor meteorological exposures and often report spurious data. In other areas, the tower spacing is too sparse, particularly south and southwest of CCAS (refer to Figure 2). This sparse spacing may inhibit the detection of a microburst if it falls between two widely spaced towers. Another limitation is the archiving process of the real-time data. Some files were corrupted with spurious wind readings of 100 knots or more on convective-free days during 1994 and 1996. Moreover, the wind towers have a varying number of sensors at different elevations. For example, tower 512 has two sensors at 6 and 30 feet, while tower 3131 has 8 sensors at 6,12,54,162,204,295,394, and

492 feet. Fortunately, most of the towers have at least one height in common; however, a few towers do not. Finally, the data interval of 5 minutes is too long for working with a short-lived phenomena such as a microburst.

The wind tower data from the mesonetwork was analyzed using Interactive Data Language (IDL) programs. Due to the serious data archiving problem in 1994, the data from 1994 was not used. Tower 2 was not used in this study since it was added in 1996 and no microbursts were reported at that tower. Moreover, tower 2 is located in an area that has good tower coverage.

There are three towers that have two wind sensors facing different directions that report as separate towers; however they are at the same location. As a result, the three pairs of towers numbered 3131 and 3132, 1101 and 1102, and 61 and 62 are actually three towers. Thus, these towers were consolidated into the three towers numbered 3131, 1101,and 61. Subsequently, if tower 3131 and 3132 both reported a microburst at the same time, the highest speed of the two was taken and labeled as tower 3131. This prevented the possibility of recording the same microburst twice. Since the KSC and CCAS wind warnings are for elevations less than or equal to 300 feet, wind data above 300 feet was not used. Wind gusts of 20 knots or greater were isolated and interrogated in order to decide if they met the microburst criteria in Fujita (1985) (refer to Table 2). Only the maximum gust at each tower was used in order to ensure multiple microbursts were not simultaneously obtained from the same tower.

Since the data interval for the towers is 5 minutes, the pre-peak and post-peak wind used was the peak wind 5 minutes before and 5 minutes after each possible microburst, respectively. In order to find divergent flow and obtain further evidence of a true microburst, wind vectors of all towers were simultaneously plotted on a map at the time of a microburst (Appendix B). Due to the wide spacing of towers, divergent flow was not always identified. The MIST project in 1986 did not utilize the subjective method of using a wind vectors map to discard microbursts. Moreover, the IDL computer program used to draw the vector interpolated between data points and smoothed out the vectors. As a result, a first-guess microburst was not removed from the data set that did not have the

classic divergent flow pattern of a microburst. In order to plot the vectors for towers that had unique sensor heights to most other towers , the vectors were plotted using a uniform height of surrounding towers. This eliminated the actual tower with the microburst; however, the low-level flow around the tower was manifested. Each microburst event was written to a file with the date, time, tower number, sensor height, direction, speed, gust, latitude, and longitude.

Upon viewing the microburst file, there were some spurious-looking cases of high winds with large gust spreads noticed. For instance, a tower had a report of sustained winds of 3 knots with a gust to 116 knots. Some cases were not this easy to identify. Therefore, in order to distinguish good data from corrupted data, all microburst observations were compared to the KSC official surface observations (KTTS), lightning data from NLDN and nearby towers. If a questionable case did not have convection reported in the KTTS observation or lightning recorded by the NLDN, and nearby towers did not have similar wind speeds, it was discarded and not used in the final dataset. It was determined that these instances of corrupted data were due to the archiving limitation mentioned earlier.

In addition to these factitious cases of microbursts, 18 microbursts associated with Hurricane Erin on 1-2 August 1995 were eliminated from the data set (Appendix A). These microbursts were eliminated due to the fact they were not produced in the typical summer low-shear regime air-mass thunderstorm. Moreover, the wind speeds would tend to be inflated as a result of the pre-existing pressure gradient winds associated with the hurricane.

A statistical summary was performed on all of the microbursts and a table was created that itemized all microburst events according to the year, day, time, tower, height, direction, speed, gust, latitude, and longitude. Another table was developed that compared the length, area, number of wind towers, and total number of microbursts divulged in NIMROD, JAWS, MIST, and this study. Two histograms were constructed for the inter-annual comparison of the total number of microbursts and microburst days. The four-year average number of microbursts per microburst day was ascertained. A

histogram was produced in order to manifest the inter-annual comparison of multiple microburst days. In order to find the most prominent month of microbursts, two histograms were formed exhibiting the total monthly distribution of microbursts and microburst days. The number of microbursts not associated with CG lightning was determined and contrasted to the number of microbursts associated with CG lightning on a histogram.

In order to investigate whether the 1997 El-Niño event produced stronger than normal microburst wind speeds, the mean and median wind speed was calculated for each year and displayed on a histogram. Moreover, to find out if the 1997 El-Niño event contributed to a decrease in the number of microbursts, the thunderstorm days were tabulated for each year.

The diurnal distribution of all microbursts was stratified into two-hour intervals beginning at 0000 UTC and shown on a histogram plot. This diurnal distribution was then compared to previous lightning activity and microburst studies. A histogram of the frequency of microburst wind speeds was done and compared to the NIMROD, JAWS, and MIST results. Another histogram was developed that revealed the frequency distribution of microburst wind speeds for 5-knot intervals. A spatial variation of microburst events was contoured on a map using an interval of 5 microbursts. A histogram of the microburst wind speed direction was constructed and compared to the previous discoveries in NIMROD, JAWS, and MIST.

2. Lightning Data

The NLDN was originally composed of three distinct networks. The Eastern United States was covered by the State University of New York at Albany (SUNYA). In 1989, the three networks were combined into a single network that monitored the entire contiguous United States. The NASA Kennedy Space Center has had continuous, network coverage since 1986. The NLDN has been in operation throughout the entire United States since 1989. The NLDN consists of 105 sensors that locate CG flashes and measure the multiplicity, polarity, and peak currents in these flashes. A mixture of magnetic direction finders (DFs) and time-of-arrival (TOA) sensors measure these

quantities (Cummins et al. 1995). The DFs detection efficiency in the United States has been estimated to be approximately 85 percent (Cummins et al., 1998; Idone et al., 1998) and have a nominal range of 600 km. The location errors are typically less than 500 meters (Cummins et al., 1998). The lightning data recorded by each instrument is transmitted to the Network Control Center in Tucson, Arizona, where it is processed to record time, location, polarity, peak current, and multiplicity of every CG lightning flash it detects. This data is encoded into binary form and disseminated to NLDN users.

The CG lightning flashes that were analyzed in this research were located within the boxed region from 28.30° N to 28.84° N and 81.10° W to 80.50° W. This region contains KSC, CCAS, and all surrounding wind sensors in the mesonet (refer to Figure 2). All CG lightning flashes detected by the NLDN, within the grid box defined above for the period of May through September of 1995 to 1998, was analyzed with the EXTHUN and IDL computer programs. The EXTHUN program was used to verify the presence of convection during questionable microburst events. It was also used to find clear cases of amplified lightning activity associated with significant microbursts greater than 34 knots. Moreover, EXTHUN ensured that the proper grid box was used for the lightning flash rate analysis of each microburst performed in the IDL computer program.

The IDL program was used to analyze the CG lightning flash rate before, during, and after all microburst events. The microburst and flash rate temporal relationship was analyzed for significant microburst cases with winds greater than 34 knots. This threshold was used since it is meets the wind warning criteria for KSC. A 20x20 km grid box centered on the appropriate wind tower was used for the CG flash rate analysis. It was assumed that all of the storms producing microbursts moved slow enough to stay within the grid box during the time of analysis. The microburst and flash rate temporal relationship for each case was plotted on a histogram using 5-minute intervals beginning 30 minutes prior to the onset of microburst winds and ending 30 minutes after the onset of microburst winds. The total number of flashes per 5-minute interval prior to and after all microbursts greater than 34 knots using the 20x20 km grid box was displayed on a histogram. In addition, the mean and median 5-minute flash rate prior to and after

microbursts greater than 34 knots was manifested on a histogram. In order to examine the utility of using flash rate to forecast the onslaught of damaging microburst winds, a grid box containing the entire area of study (refer to Figure 2) was used to examine the microburst and flash rate temporal relationship for microbursts with winds greater than 34 knots. The microburst and flash rate temporal relationship for each case was plotted on a histogram using 5-minute intervals beginning 30 minutes prior to the onset of microburst winds and ending 30 minutes after the onset of microburst winds. A histogram was made revealing the total number of flashes per 5-minute interval prior to and after all microbursts greater than 34 knots using the area of study grid box. In addition, the mean and median 5-minute flash rate prior to and after microbursts greater than 34 knots was shown on a histogram.

The temporal relationship between microbursts and flash rate was analyzed for all microburst cases found in this study utilizing both the 20x20 km grid box and area of study grid box. The total number of flashes per 5-minute interval 30 minutes before and after all microbursts was manifested on a histogram for both grid box cases. The mean and median 5-minute flash rate was computed and exhibited on a histogram plot. Finally, individual cases were subjectively identified that exhibited a rapid rise of CG flash rate before microbursts.

CHAPTER IV
RESULTS AND DISCUSSION

1. Characteristics of Microbursts

a. Frequency

The total number of microbursts found during the five summer months of 1995 through 1998 was 282. All of these microburst events are documented in Appendix C with the year, day, time, tower, height, direction, speed, and gust of each microburst. A comparison of this study to the NIMROD, JAWS, and MIST studies is displayed in Table 3. It is obvious that this study was far more comprehensive spanning a total of 612 days.

Figure 5 displays the number of microbursts that occurred during the 5-month summer period for each of the four years. There was a maximum of 76 microbursts in 1997 with a minimum of 61 in 1998. The four-year average of microbursts was 70.5. Thus, the number of microbursts found in 1998 seems to be below average.

The inter-annual comparison of thunderstorm days displayed in Figure 6 does not reveal a significant decrease in the amount of thunderstorms during the summer of 1998; however, a further look into the number of thunderstorm days during May and June of each year in Figure 7 reveals a visible decrease in thunderstorm days during May and June of 1998. Figure 8 displays the number of thunderstorm days during the remaining summer months of July, August, and September for each year. This reveals a rather high amount of thunderstorm days in 1998. This explains the reason for no apparent decrease in the amount of thunderstorm days in 1998. This decrease in thunderstorm days during the first two months of May and June of 1998 was the reason for the decreased amount of microbursts. This decrease in thunderstorm activity may have been the result of El-Niño, which caused severe drought conditions and a plethora of forest fires in Florida during May and June of 1998. Subsequently, the decrease in the number of microbursts in 1998 can be linked to El- Niño.

In addition to analyzing the total number of microbursts, the total number of microburst days was analyzed. There were a total of 114 microburst days during the time of this study. Figure 9 compares the number of microburst days recorded for each year.

TABLE 3. Comparison of the four microburst studies.

Project	NIMROD	JAWS	MIST	KSC
Length of Study	42 days	86 days	61 days	612 days
Area Covered	56x57x60 km	15x18x28 km	15x16x24 km	52x52 km
Number of towers	27	27	41	50
Total Microbursts	50	186	33	282
Dry Microbursts	18	155	0	0
Wet Microbursts	32	31	33	282
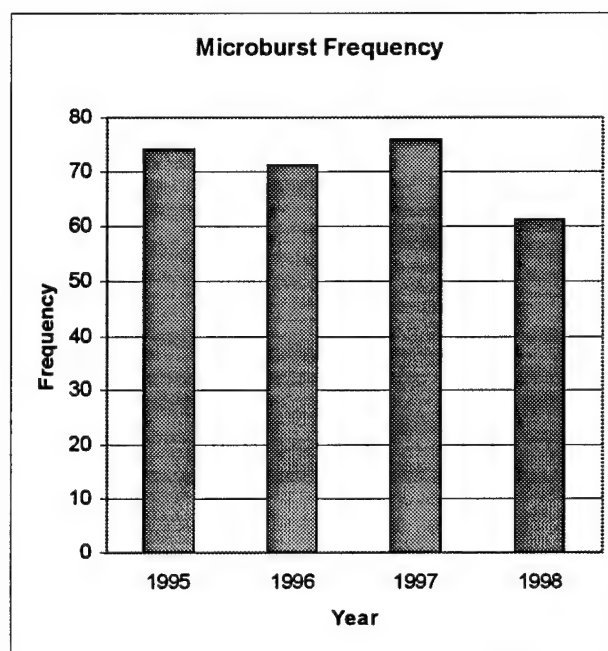
Fig. 5. Inter-annual comparison of
microbursts for the summer months of 1995 to
1998.
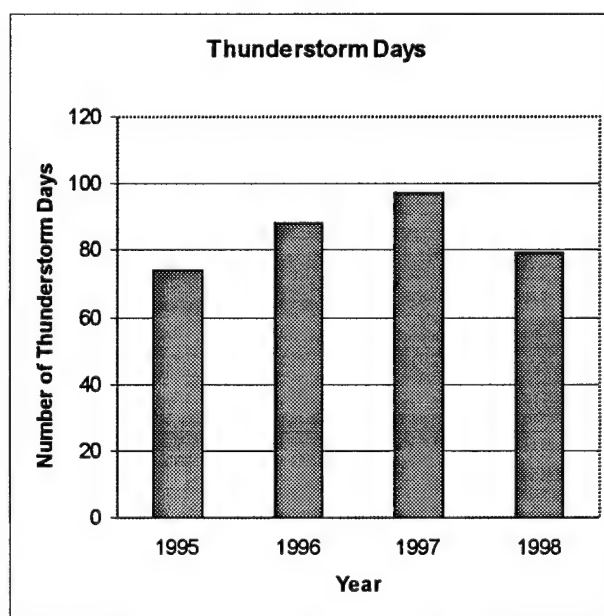
Fig. 6. Inter-annual comparison of
thunderstorm days for the summer months of
1995 to 1998.
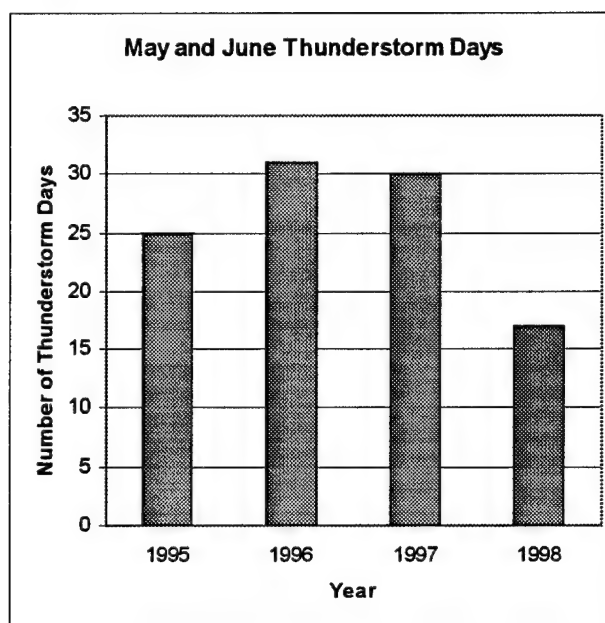
Fig. 7. Inter-annual comparison of May and June thunderstorm days.
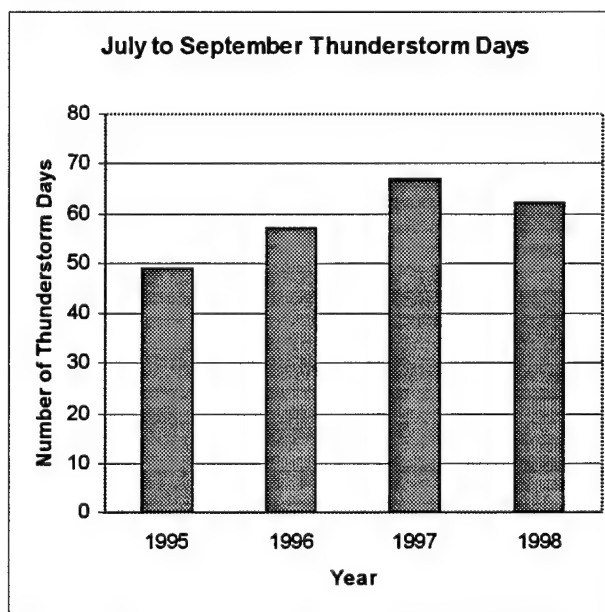
Fig. 8. Inter-annual comparison of thunderstorm days for the months of July through September.
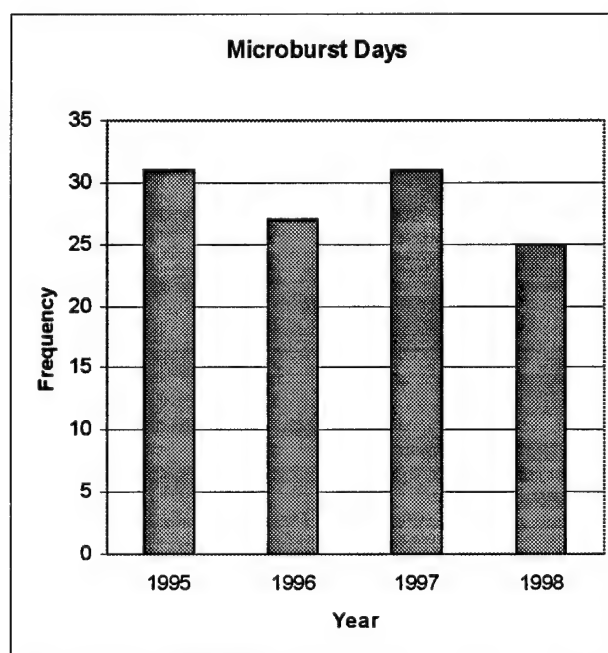
Fig. 9. Inter-annual comparison of microburst days for the summer months of 1995 to 1998.

The number of microburst days was 25 for 1998. The four-year average number of microburst days was 28.5. The minimum of 25 microburst days is congruent with the decline of microbursts noted in 1998.

The inter-annual comparison of multiple microburst days is exhibited in Figure 10. It was discovered that 59 of the 114 microburst days had multiple microbursts. The four-year average number of multiple microburst days is 14.75. There was an apogee of 18 multiple microburst days noted in 1996 and a minimum of 11 observed in 1998. Again, this minimum corresponds well to the minimum amount of microbursts observed in 1998. The mean number of microbursts per microburst day was 2.17.

The total number of microbursts was stratified into a monthly distribution of microbursts (Figure 11). There is a significant increase in the number of microbursts from a minimum of 36 in May, to 53 in June, to a peak of 86 in July. Moreover, there is a significant decrease in the number of microbursts from the peak of 86 in July, to 64 in August, and 43 in September. Thus, the prime months for microbursts are June, July, and August with a distinct peak in July. This peak of microburst activity in July occurs in conjunction with the peak in CG lightning at the KSC.

A similar trend is found in Figure 12 for the number of microburst days per month from May to July; however, there is not a substantial decrease in the amount of microburst days after July. The number of microburst days rises rapidly from a minimum of 10 in May to a peak of 31 in July. The number of microburst days dips slightly from the peak of 31 in July, to 29 in August, and then to 21 in September.

All of these previously mentioned figures show that the three months of June, July, and August are the most prominent months of microburst activity. The peak month of microburst activity is July. In contrast, May and September are the least probable months for microburst activity. The lowest month of microburst activity is May.

b. *Wind Speed and Direction*

Several important characteristics of wind speed and direction associated with the 282 microbursts were investigated. One of these characteristics was the mean and median microburst wind speed. The mean and median microburst wind speed was 34.6 and 34
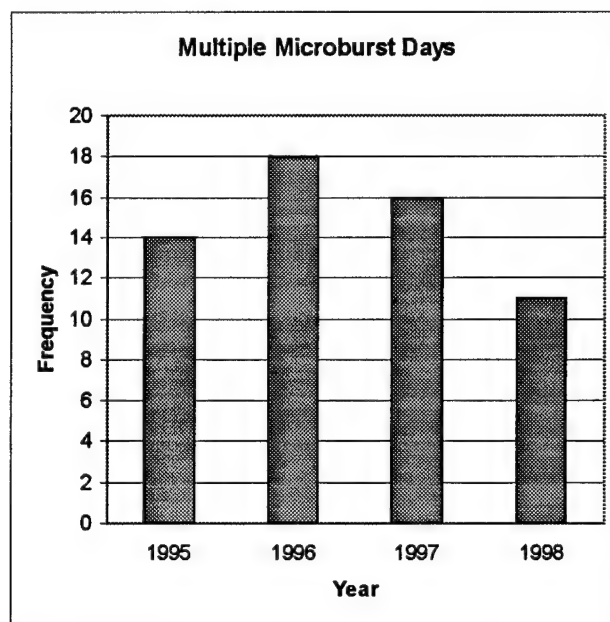
Fig. 10. Inter-annual comparison of multiple microburst days for the summer months of 1995 to 1998.
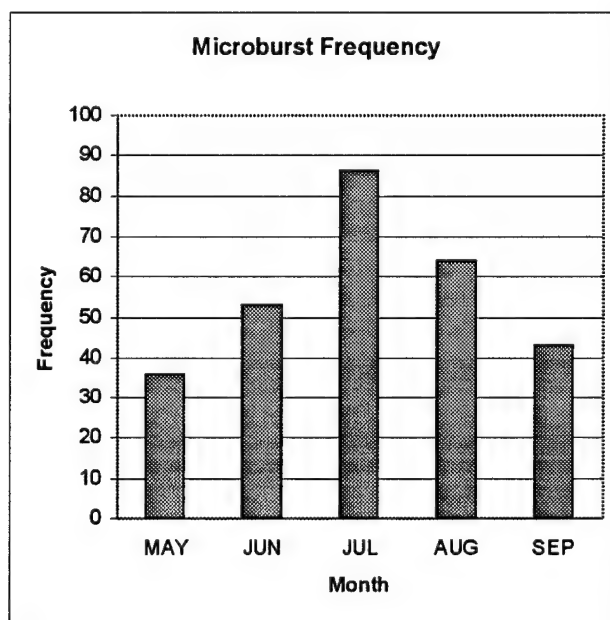
Fig. 11. Number of microbursts for each of the five summer months from 1995 to 1998.
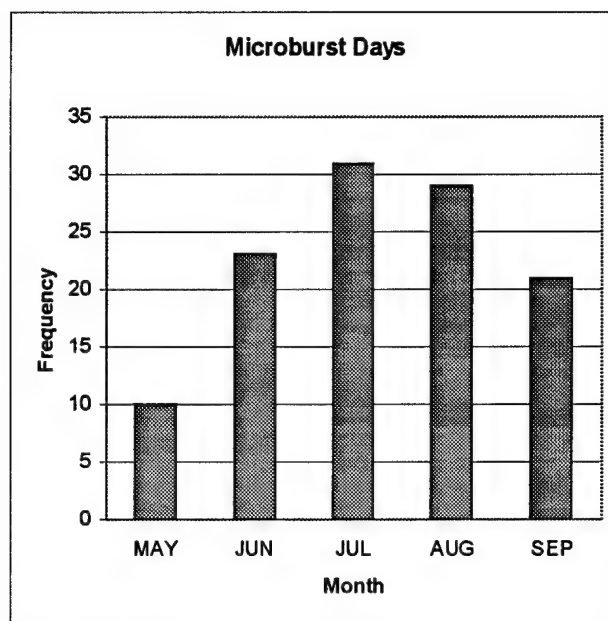
Fig. 12. Number of microburst days for each
of the five summer months from 1995 to 1998

knots, respectively. The median microburst wind speed is shown for each year in Figure 13. In 1995 and 1996, the median speed was 32 knots. The median speed for 1997 and 1998 was 34 and 36 knots, respectively. In Figure 14, the mean microburst wind speed for 1995 and 1996 was 33.1 and 34.6 knots, respectively. The mean speed for 1997 and 1998 was 34.2 and 37.1 knots, respectively. Both of these figures show a distinct increase in the microburst wind speeds during 1998. Ironically, this peak in mean and median wind speed occurred during the year with the least amount of microbursts.

In addition to the mean and median microburst wind speeds, an investigation into the frequency of microburst wind speeds was conducted. The frequency of microburst wind speeds is shown in Figure 15. Out of the 282 microbursts observed in this four-year period, only 14 were greater than or equal to 50 knots; however, there were 117 cases of microburst winds between 35 and 49 knots. Thus, 131 of the 282 cases of microburst cases met or exceeded the warning criteria for KSC operations. Most of the wind speeds were observed between 25 and 43 knots. There were two peaks of 24 found within this range of speeds for 29 and 36 knots.

The speed frequency distribution was smoothed out into 5 knot intervals and shown in Figure 16. There was a dramatic increase in frequency from the first interval of 20-24 knots and the second interval of 25-29 knots. The first interval contained 26 microbursts, while the second interval had a remarkable number of 72 microbursts. The third interval of 30-34 knot wind speeds decreased markedly to 53 microbursts; however, there was a secondary peak of 58 microbursts in the fourth interval of 35-39 knot winds. After this secondary peak, there was another substantial drop in the amount of microbursts to 44 for the fifth interval of 40-44 knots winds. After this, there was a steep drop in microburst frequency to 15 for the sixth interval of 45-49 knots. The next three intervals of 50-54 knots, 55-59 knots, and 60-64 knots contained a mere 6, 4, and 2 microbursts, respectively.

The peak wind speed for the 4 years of study was 90 knots, which occurred twice. The two graphs of the speed frequency distribution show that the most common wind speed for microbursts fall in the range of 25 and 44 knots with two distinct peaks at 29
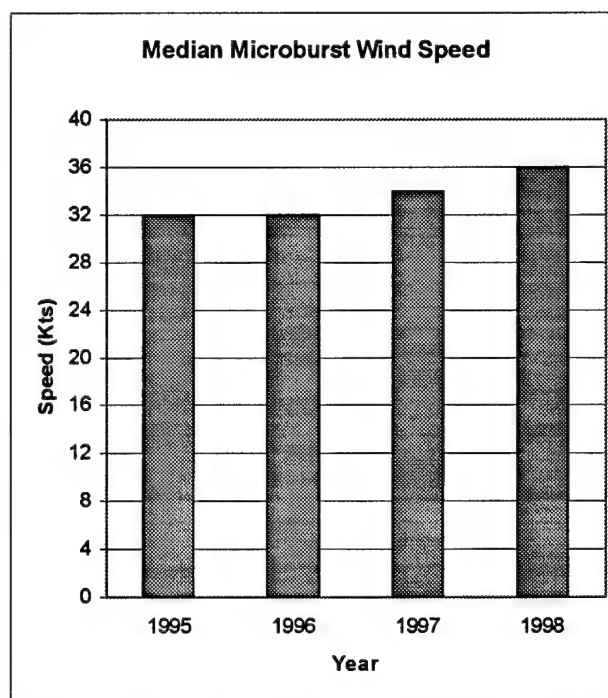
Fig. 13. Inter-annual comparison of the median microburst wind speed for the summer months of 1995-1998.
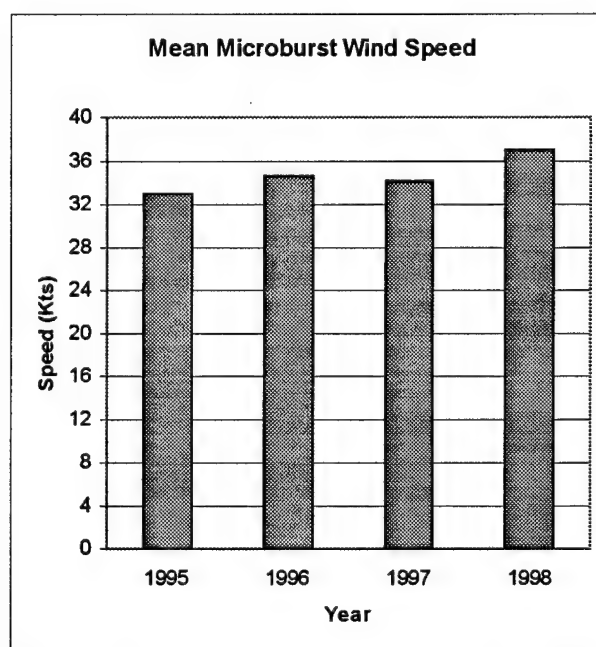
Fig. 14. Inter-annual comparison of the mean microburst wind speed for the summer months of 1995 to 1998.
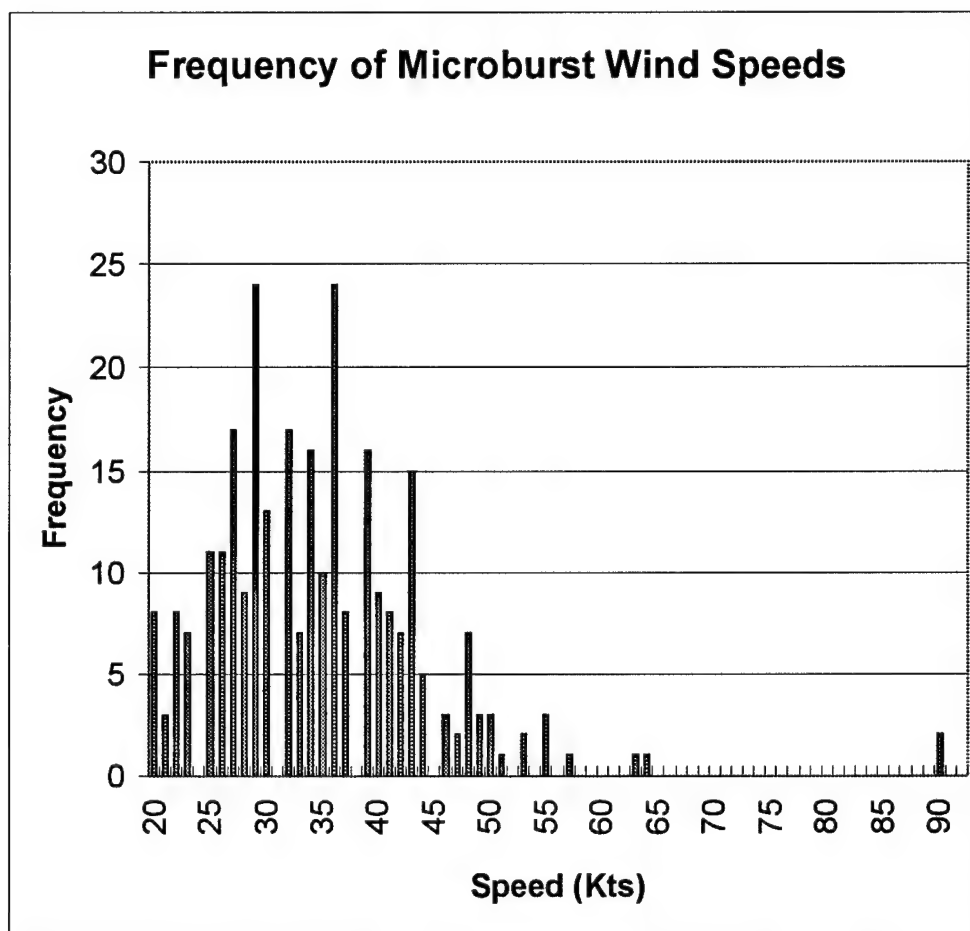
Fig. 15. Speed frequency distribution of microburst wind speeds in knots for all microbursts during the summer months of 1995 to 1998.
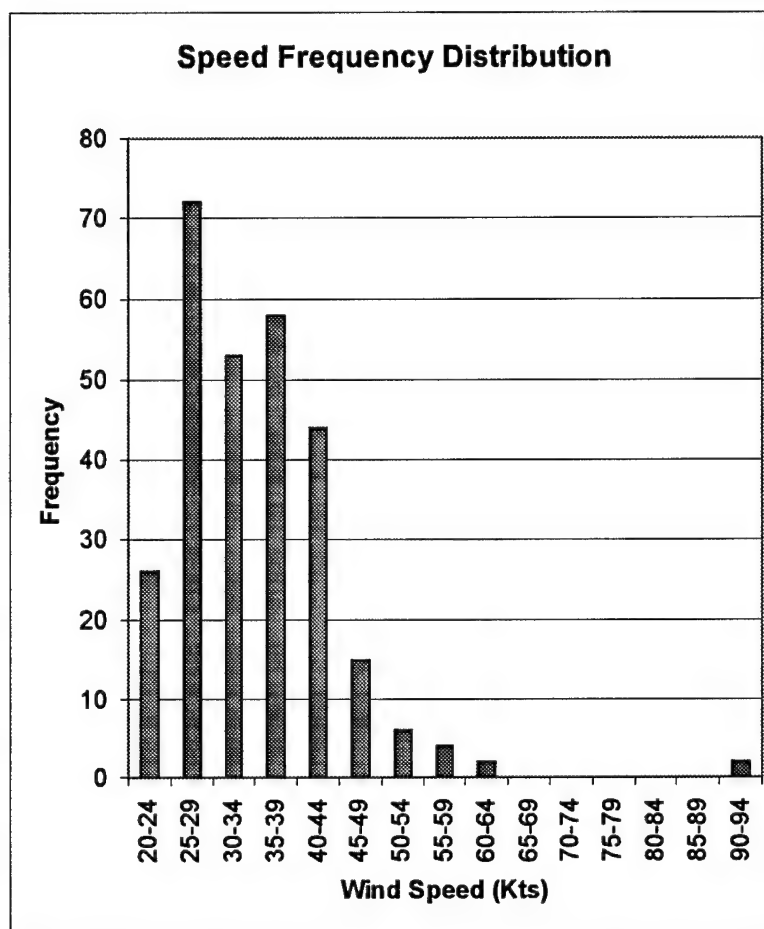
Fig.16. Speed frequency distribution in 5 knot intervals
for all microbursts recorded during the five summer months
of 1995 to 1998.

and 36 knots. Moreover, as the wind speed increases over 43 knots, the frequency decreases exponentially, reaching virtually zero at 65 knots. The peak speed interval of 25-29 knots coincides well with the peak of 23-27 knots found in the NIMROD and JAWS studies. The secondary peak of 35-39 knots was also found in NIMROD and JAWS. The sharp increase between the first and second intervals was also seen in NIMROD and JAWS; however, the exponential decrease occurred just after the first peak for the interval of 23-27 knots.

These different results can probably be attributed to the fact that this study consisted of a much larger and consistent data set of wet microbursts compared to a smaller data set of both wet and dry microbursts in NIMROD and JAWS. Moreover, there were twice as many wind towers used over a larger area for this study compared to the NIMROD and JAWS studies.

In addition to investigating the wind speed characteristics, the wind direction of each microburst was plotted using 20° intervals (Figure 17). The microburst winds can come from any direction; however, it is less likely to experience microburst winds between 80° and 100° (east). There is a gradual increase in the frequency of microbursts beginning between 120° and 139°(southeast) from 13 cases to a peak of 33 between 220° and 239° (southwest). After the peak from the southwest direction, the frequency gradually decreases at about the same rate as it increased to a frequency of 8 for the wind direction interval between 340° and 359°(north). The predominant wind direction of microbursts is from the southeast through the west-northwest with a maximum occurring from the southwest. There were only a small number of microbursts with wind directions from northerly and easterly directions.

In NIMROD and JAWS, the maximum wind direction frequency was from the west-northwest. This difference may be due to the fact that the NIMROD and JAWS studies were done in Chicago and Denver, respectively. The weather regime in Denver and Chicago is quite different from tropical Florida. The majority of mid-level steering winds in NIMROD and JAWS may have been from the west-northwest associated with synoptic disturbances. In contrast, the bulk of mid-level steering winds are light and variable in
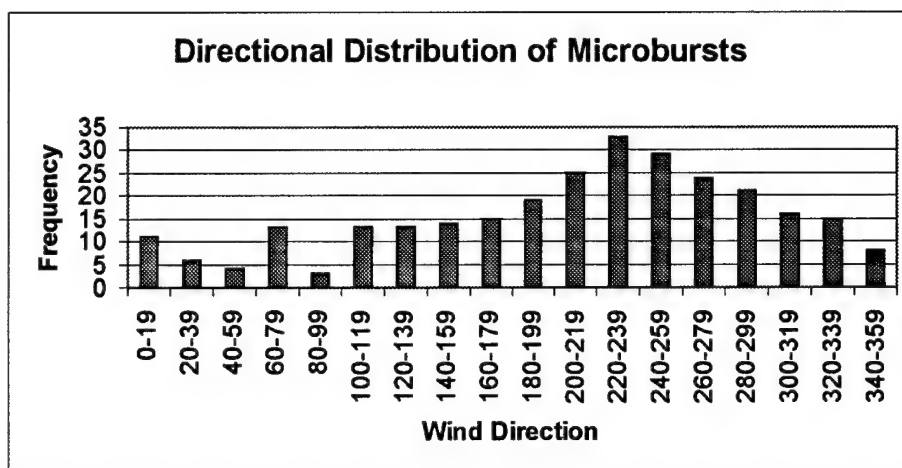
Fig. 17. Directional distribution of microburst winds for the summer months of 1995 to 1998 in 20° intervals.

Florida and are usually not associated with synoptic disturbances. This information on the preferred direction of microburst winds will enable the KSC to know which direction to expect the majority of damaging microburst winds will come from during the summer microburst season. As a result, the KSC will be better prepared for destructive microburst winds.

c. Diurnal and Spatial Variation

Two additional forecast tools that will ameliorate weather support to the KSC are the diurnal and spatial variation of microbursts. Both of these vital forecast tools were analyzed in this research. The spatial variation of the 282 microbursts was contoured on a map of the KSC mesonet using an interval of five microbursts (Figure 18). A complete listing of all the towers, along with the total number of microbursts are listed in Appendix D.

The mean and median frequency of microbursts for an individual tower is 5.6 and 6, respectively. There are two sharp peaks of microburst frequency at towers 61 and 3131 of 18 and 17, respectively. There are less distinct peaks of microburst activity at towers 513, 311, 397, and 1101 of 12, 11, 10, and 10, respectively. Some towers received few, if any, microbursts during the four-year period. Most of these towers were located in the western, northern, and southern extremes of the mesonet where the tower density is much less than near the KSC and CCAS; however some towers that are located in a dense part of the mesonet received only one to three microbursts. Interestingly, tower 61, which had the highest number of microbursts is not located in a dense part of the mesonet. Moreover, the location of the majority of microbursts seem to be located in areas of complicated land-water interactions. This land-water interaction provides an apt zone of enhanced convergence for the development of thunderstorms. Hence, the reason for the large disparity in the number of microbursts among towers is more than likely due to the location of each tower in relation to a favorable or unfavorable zone of convergence.

The two maximum at tower 61 and 3131 are both located in favorable areas of convergence where the sea breeze and river breeze often interact and produce thunderstorms on a more frequent basis. All of the other less distinct maximum at towers
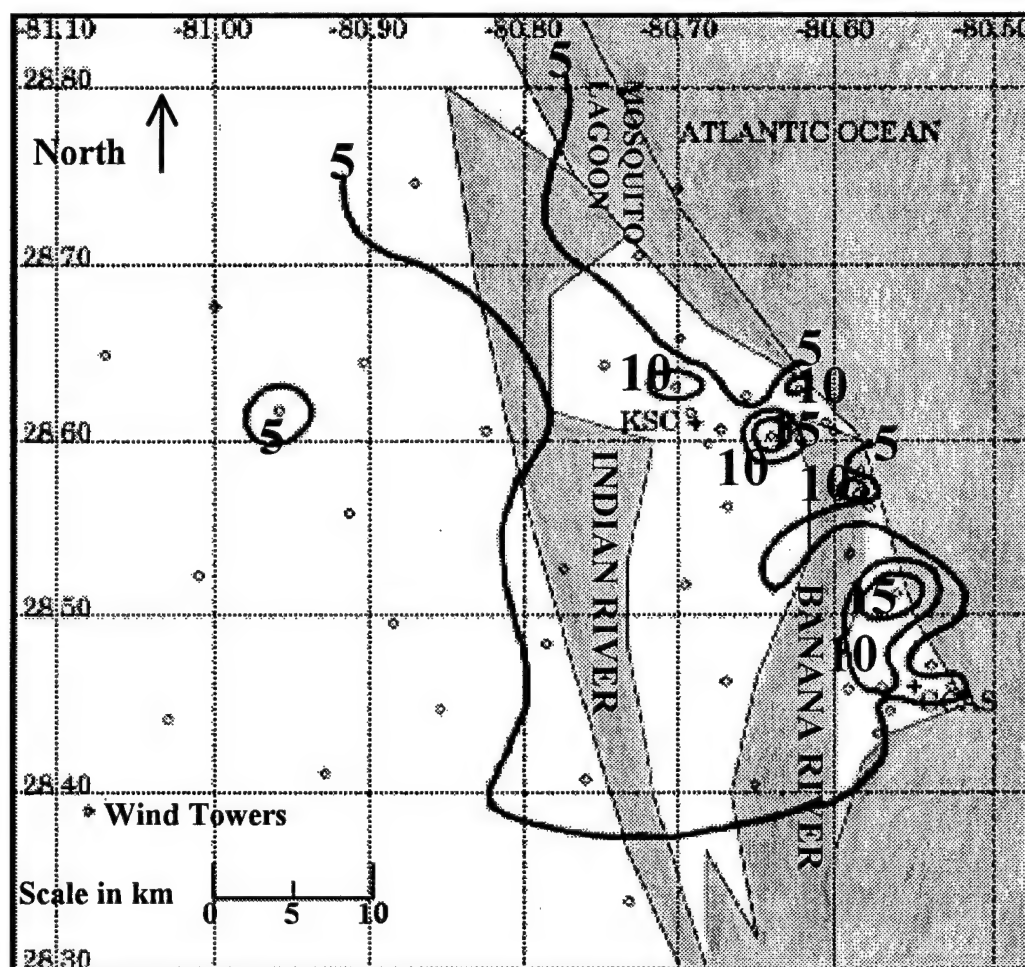
Fig. 18. Spatial variation contour plot of microburst frequency for the summer months of 1995 to 1998. The contour interval is 5 microbursts.

311, 397, 513, and 1101 are also located in favorable regions of river and sea-breeze interaction. Hence, it appears that the spatial variation pattern observed in Figure 18 is a result of certain towers residing in a favorable zone of convergence associated with the complex coastline, river breezes, and sea-breezes.

The diurnal variation of the 282 microbursts was plotted on a histogram in Figure 19. It is clear that the most favorable time for microbursts to occur is after 1600 UTC (12 P.M. EDT) until 2200 UTC (6 P.M. EDT). There is quite a substantial rise from a total of 7 microbursts occurring between 1400 and 1600 UTC, to 33 from 1600 (12 P.M. EDT) and 1800 (2 P.M. EDT), and to a peak of 99 microbursts occurring between 2000 UTC (4 P.M. EDT) and 2200 UTC (4 P.M.). The peak within this two-hour period was 56 and occurred between 2000 and 2100 UTC. After the sharp peak between 2000 UTC (4 P.M. EDT) and 2200 UTC (6 P.M. EDT), there is a steep drop in the number of microbursts from 99 to 17.

All of these diurnal variations correspond well with previous research on the diurnal cycle of lightning discussed in Chapter 2. For instance, Hinson (1997) noted a rapid increase in lightning activity beginning at 1600 UTC (12 P.M. EDT) with a distinct diurnal maximum at 2000 UTC (4 P.M. EDT) and a steep decline after 2100 UTC (5 P.M. EDT). Subsequently, it can be deduced that lightning and microbursts are highly related to each other.

2. Microburst and Flash Rate Relationship

In order to gain further evidence of the integral temporal relationship between microbursts and cloud-to-ground (CG) lightning flash rate and investigate whether the CG flash rate can be used to forecast the onslaught of damaging microburst winds, all 282 microburst cases and the associated CG flash rate were analyzed. It was found that out of the 282 microburst cases, 213 were associated with CG lightning (Figure 20). Thus, there were 213 cases of microburst and CG flash rate analysis done for this research. These 213 cases were analyzed together and separately for cases with microburst winds greater than the convective wind warning criteria of 34 knots using the area of study grid box and the 10x10 km grid box. The individual cases of the microburst and flash rate temporal
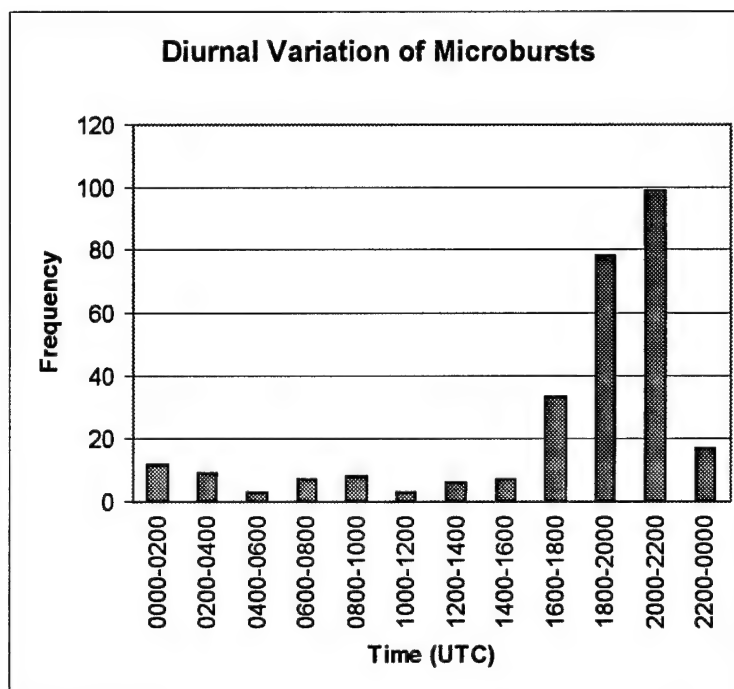
Fig. 19. Diurnal variation of microbursts for each
2-hour interval beginning at 0000 UTC (8 P.M. EDT).
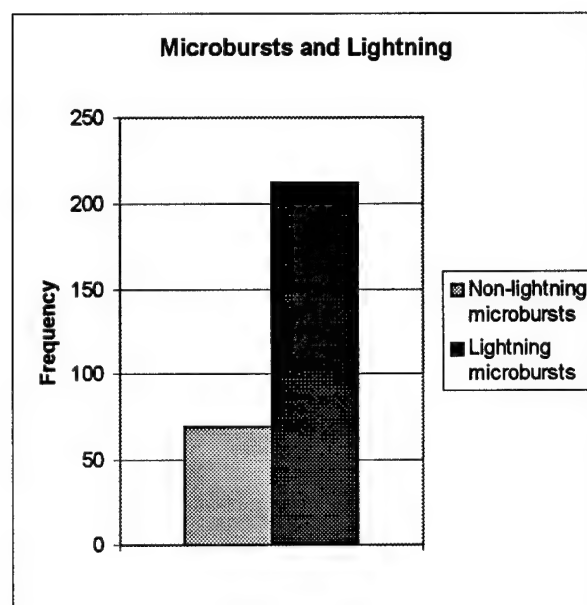
Fig. 20. Comparison between the number of microbursts associated with cloud-to-ground (CG) lightning and the number of microbursts not associated with CG lightning.

relationship for microbursts greater than 34 knots, using the 20x20km grid box, can be found in Appendix E. Out of these 104 cases, 81, or 77.8% exhibited a distinct increase in the CG lightning 5-minute flash rate at least 5-10 minutes before the microburst winds reached the wind tower. There were 25 cases of a distinct rise in the 5-minute flash rate 20-25minutes before the microburst, 18 cases 15-20 minutes prior to the microburst, 23 cases 10-15 minutes before the microburst, and 15 cases 5-10 minutes before the microburst.

The total number of flashes that occurred within each 5-minute interval before and after microbursts greater than 34 knots, using the 20x20 km grid box, is plotted in Figure 21. There is a steep rise in the number of flashes beginning 20-25 minutes before the microburst and ending with a peak of 2263 flashes 5-10 minutes before the microburst. The flash rate is about the same 0-5 minutes before the microburst and then drops off rapidly to a minimum of 473 flashes 25-30 minutes after the microburst.

The mean and median 5-minute flash rate are plotted in Figure 22 and Figure 23, respectively. Both the mean and the median resemble Figure 21 with a steep ascent starting 20-25 minutes prior to the microburst and ending with a peak 5-10 minutes before the microburst. They also exhibit the same quick decline in flash rate.

This analysis reveals that in most cases, the CG flash rate begins a rapid climb beginning 15-25 minutes before the microburst reaching a peak flash rate 5-10 minutes before the microburst event. Thus, the first increase of the flash rate may be a vital signal that can be utilized to forecast dangerous microburst events at KSC with more accuracy and lead-time.

Unfortunately, the forecasters at the 45th Weather Squadron are not able to zoom in on a 20x20 km grid box and observe the flash rate. As a result, an area of study grid box containing the entire KSC area was used to evaluate the utility of the CG flash rate as a forecast tool for microbursts. The individual cases of the microburst and flash rate temporal relationship for microbursts greater than 34 knots, using the area of study grid box, can be found in Appendix F. Out of these 104 cases, 86, or 82.6%, exhibited a distinct increase in the CG lightning 5-minute flash rate at least 5-10 minutes before the
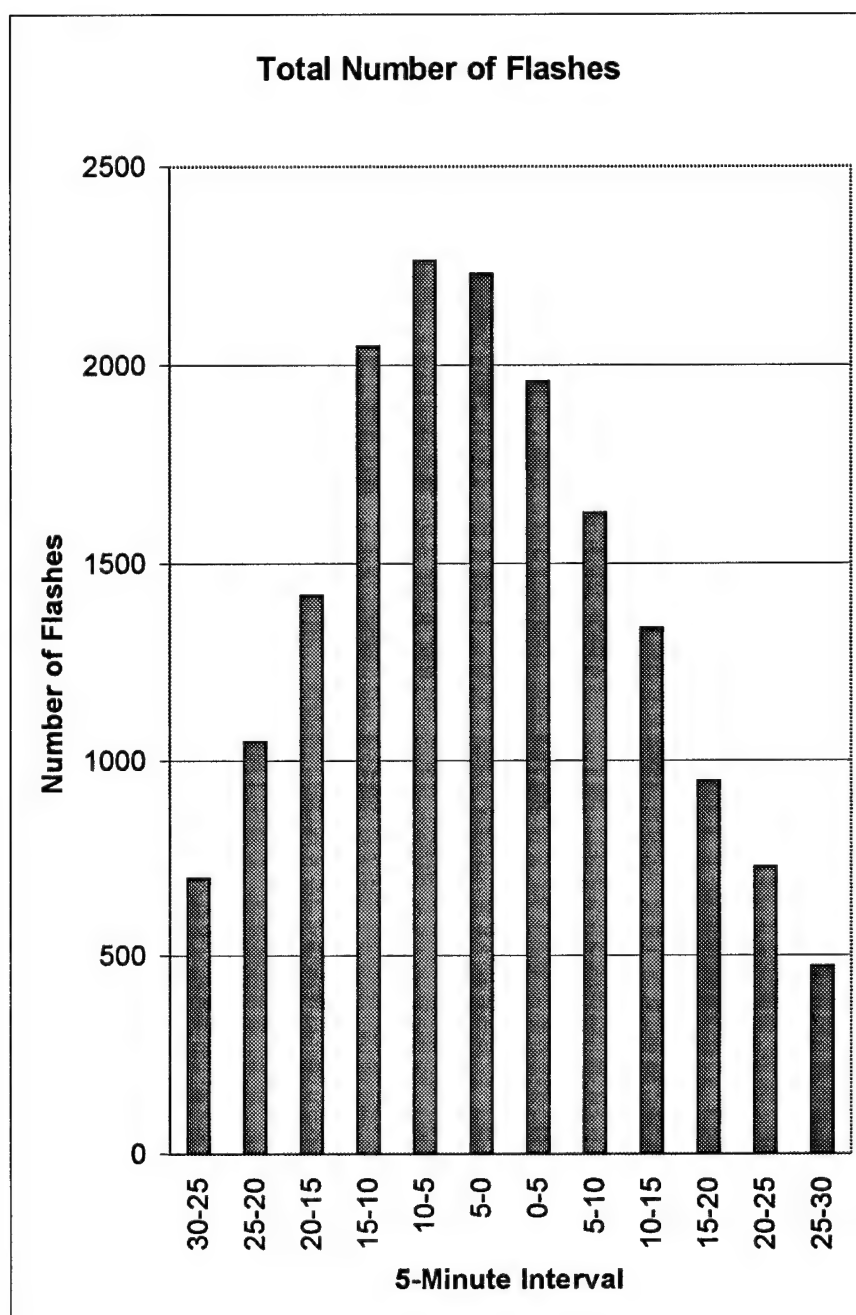
Fig. 21. Total number of cloud-to-ground (CG) flashes for each 5-minute interval 30 minutes before and after microbursts with wind speeds greater than 34 knots using the 20x20 km grid box.
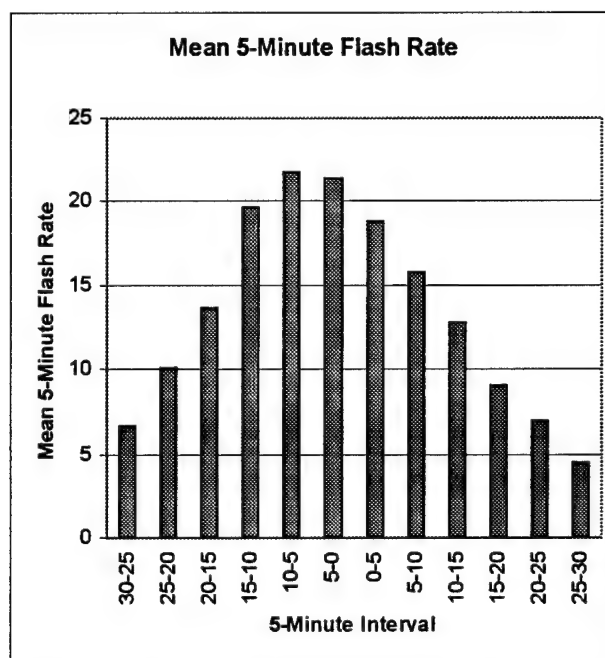
Fig. 22. Mean cloud-to-ground (CG) flash rate for each
5-minute interval 30 minutes before and after microbursts with
wind speeds greater than 34 knots using the 20x20 km grid box.
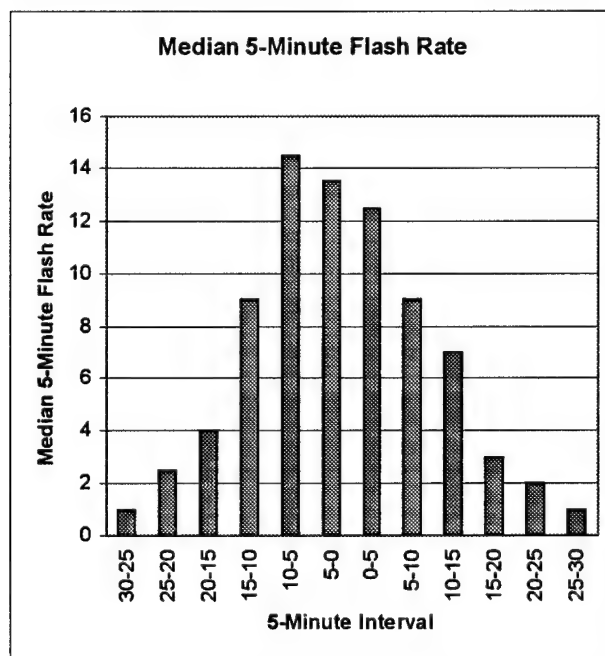
Fig. 23. Median cloud-to-ground (CG) flash rate for each
5-minute interval 30 minutes before and after microbursts with
wind speeds greater than 34 knots using the 20x20 km grid box.

microburst winds reached the wind tower. There were 41 cases of a distinct rise in the 5-minute flash rate 20-25 minutes before the microburst, 20 cases 15-20 minutes prior to the microburst, 16 cases 10-15 minutes before the microburst, and 9 cases 5-10 minutes before the microburst.

The total number of flashes recorded for each 5-minute interval before and after microbursts greater than 34 knots, using the area of study grid box, was plotted in Figure 24. The number of flashes increases sharply beginning 20-25 minutes before the microburst prior to reaching an apogee of 5238 flashes 10-15 minutes before the microburst. The number of flashes dips slightly to 5109 5-10 minutes prior to the microburst, but peaks again with a value of 5265 flashes 0-5 minutes before the microburst. After this, the number of flashes declines rapidly to a minimum 25-30 minutes after the microburst. This coincides well with the number of flashes plotted in Figure 21, with the exception of an earlier peak in the flash rate that occurs 10-15 minutes prior to the microburst. The mean and median 5-minute flash rate was shown in Figure 25 and Figure 26, respectively. Both of these figures reveal the same trend of increased flash rates before the microburst and decreased flash rates directly after the microburst that was indicative of the previous four figures.

Subsequently, the results for both the 20x20 km grid box and area of study grid box illuminate a signal of increased CG lightning flash rate before the microburst reaches the wind tower. Interestingly, the area of study grid box cases exhibited a stronger signal of the flash rate increase. This increased flash rate signal tends to begin most frequently 20-25 minutes before the microburst for the area of study grid box cases. This increase continues to a peak flash rate 10-15 minutes before the microburst. The majority of individual cases followed this pattern; however, some cases had quite erratic patterns or very few flashes. Similar results were found when all 213 microbursts were examined together using the 20x20 km grid box and area of study grid box (Appendix G). As a result, the Air Force forecasters at the 45th Weather Squadron may be able to use the CG lighting flash rate to alert KSC personnel of impending damaging microburst winds with a lead time up to 25 minutes.
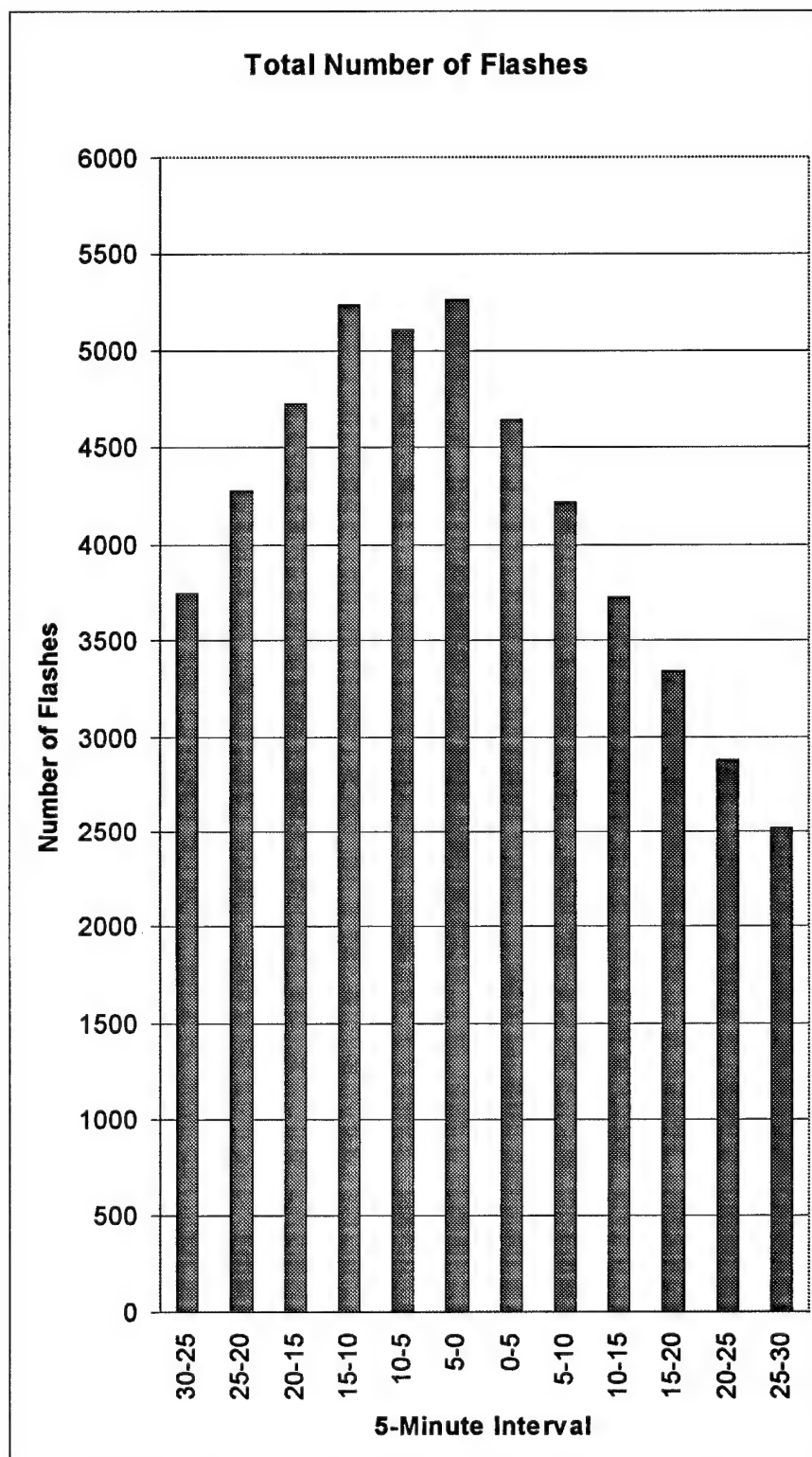
Fig. 24. Total number of cloud-to-ground (CG) flashes for each 5-minute interval 30 minutes before and after microbursts with wind speeds greater than 34 knots using the area of study grid box.

Mean 5-Minute Flash Rate

Fig. 25. Mean cloud-to-ground (CG) flash rate for each
5-minute interval 30 minutes before and after microbursts with
wind speeds greater than 34 knots using the area of study grid box.
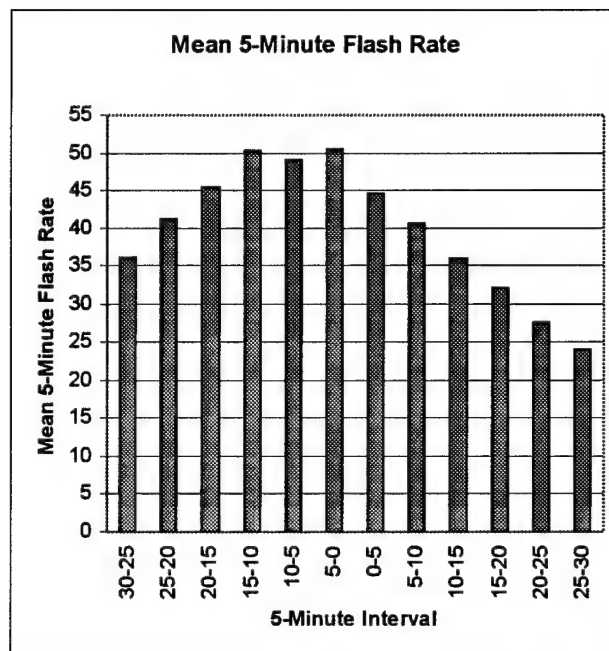
Median 5-Minute Flash Rate
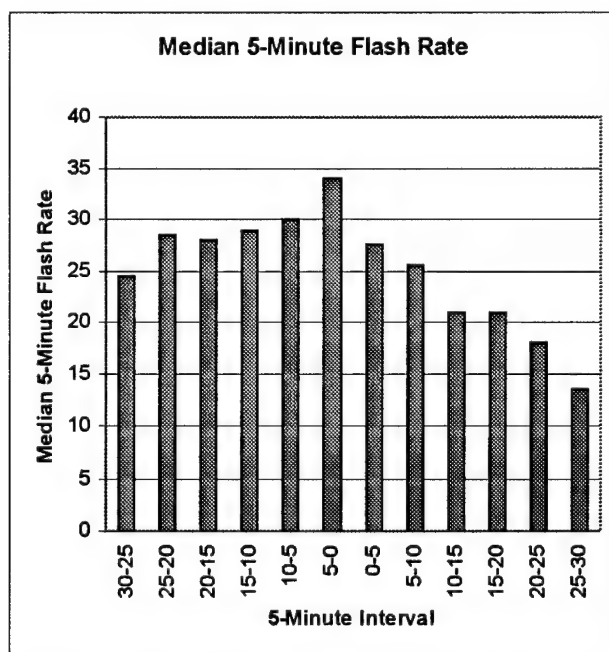
Fig. 26. Median cloud-to-ground (CG) flash rate for each
5-minute interval 30 minutes before and after microbursts with
wind speeds greater than 34 knots using the area of study grid box.

CHAPTER V
CONCLUSIONS

The first summertime microburst climatology in the United States was developed for the NASA Kennedy Space Center, Florida from 1995 through 1998 using wind data from the state of the art mesonet surrounding the Kennedy Space Center. This study of microbursts is an immense improvement on the three previous microburst projects. As a result, this climatology will provide Air Force forecasters with an important key to unlocking the secrets of microburst forecasting; however, this climatology only covers four years. Consequently, this data set must continue to increase in order to develop a ground-truth picture of microbursts at the Kennedy Space Center. Thus, this short-term climatology will serve as the foundation for a long-term climatology of 20 to 30 years for the Kennedy Space Center.

A total of 282 microbursts were observed during this 4-year period. The four-year average number of microbursts per year was 70.5. An evident decline in the number of microbursts was discovered in 1998. This precipitous drop in microbursts was only seen in May and June. It is hypothesized that this decrease may have been attributed to the strong El-Niño of 1997-1998.

There were 69 cases of microbursts that occurred without lightning. Some of these microbursts were quite strong . Consequently, more research into non-lightning microbursts is necessary.

There were a total of 114 microburst days recorded during the time of this study. The maximum number of microburst days was 31 in both 1995 and 1997. The minimum number of microburst days was 25 in 1998. This minimum corresponds well with the diminished number of microbursts observed in 1998.

Out of the 114 microburst days, 59 days had multiple microbursts. The four-year average number of multiple microburst days was 14.75. There was a maximum of 18 multiple microburst days found in 1996 and a minimum of 11 observed in 1998. The mean number of microbursts per microburst day is 2.17.

The most prominent months of microbursts are June, July, and August with July being the most dominant. In contrast, May and September contained a relatively small amount of the total microbursts. The monthly breakdown of microbursts was 36 in May, 53 in June, 86 in July, 64 in August, and 43 in September. The number of microburst days makes a rapid ascent from a minimum of 10 in May to peak of 31 in July; however, the number of microburst days only declined slightly to 29 in August and then to 21 in September.

Several important characteristics of wind speed and direction were found. The median microburst wind speed was 34 knots. The highest median microburst wind speed was 36 knots occurred in 1998. It is interesting that the peak median microburst wind speed occurred during the year with the least number of microbursts. The speed frequency distribution revealed that the most common wind speed for microbursts fell within the range of 25 and 44 knots, with two distinct peaks at 29 and 36 knots. The highest wind speed recorded, which occurred on two occasions, was 90 knots. As the wind speed increases above 43 knots, the frequency decreases exponentially, reaching virtually zero at 65 knots. These results coincide well with the NIMROD and JAWS studies; however, the exponential decay begins precipitously after the first peak. These different results may be due to the fact that this study consisted of a much larger and consistent data set of wet microbursts. Further research should attempt to unearth an average decay speed of microbursts. This will require using wind data that has a peak wind speed recorded each minute.

The winds associated with a microburst can come from any direction; however, it is less probable to experience microburst winds from 80° to 100° (east). The predominant wind direction of microbursts is from the southeast through the west-northwest with a maximum from the southwest. There were only a small number of microbursts with wind directions from northerly or easterly directions. These results fit well with the NIMROD and JAWS studies; however, the maximum wind direction frequency was from the west-northwest. It is hypothesized that the majority of microburst wind directions are from the southwest due to the fact that the most unstable and favorable regime for strong

convection, and hence, microbursts, is the southwest flow regime. The spatial variation of the microbursts revealed an striking pattern. The median frequency of microbursts for a given tower is 6; however, several towers received few, if any, microbursts during the four-year period, while others received a substantial amount. For instance, tower 61 received a maximum of 18 microbursts. It is hypothesized that this disparity in microburst frequency is a result of some towers residing in a favorable area of convergence near the intersection of river and sea breezes. Further research should examine the effects of the irregular coastline and inland waterways on the sea breeze in order to develop a model, such as MM5, that will be better able to predict convective development in the KSC area.

The diurnal variation of the microbursts also showed a revealing pattern. The most conducive time for microbursts is between 1600 UTC (12 P.M. EDT) and 2200 UTC (6 P.M. EDT) with the apex occurring between 2000 UTC (4 P.M. EDT) and 2200 UTC (6 P.M. EDT). A total of 99 microbursts were found within this two-hour period. After this peak, the number of microbursts for the next two-hour period is a meager 17. These diurnal variations of microbursts are in excellent agreement with the diurnal cycle of cloud-to-ground (CG) lightning and the previous microburst studies.

The temporal relationship between microbursts and cloud-to-ground (CG) lightning exhibits a strong correlation. In most cases, there is a vivid signal of increased flash rate preceding the microburst event with a fairly rapid decrease 0-5 minutes afterwards. Subsequently, it was found that Air Force forecasters at the 45th Weather Squadron could utilize this increased CG lightning flash rate signal to alert KSC personnel of impending damaging microburst winds with a lead-time of up to 25 minutes. However, more work on the relationship between microbursts and CG lightning flash rate needs to be accomplished before this indicator can be used as a reliable tool to forecast microbursts.

Several previous studies have focused on the microburst and total lightning (in-cloud and cloud-to-ground) peak flash rate temporal relationship. Unfortunately, since the total lightning peak flash rate usually occurs less than 10 minutes before a microburst, it can not be used to provide an adequate lead-time for safety of personnel and equipment at the

KSC. Also, the peak flash rate is not known until after the microburst has occurred. Moreover, the 45th Weather Squadron forecasters use NLDN lightning data, which only measures CG lightning activity.

The CG peak lightning flash rate performed better as a predictor of microbursts than in previous studies, where IC lightning was found to be the superior precursor to microbursts. These previous studies of lightning were for a fairly small sample size and took place nearly ten years ago. As a result, further studies need to examine both IC and CG lightning activity before microburst events for a larger sample size. Moreover, the focus should not be on the peak flash rate, but rather, on the signal of increased CG lightning flash rate preceding microbursts. One such study could utilize this microburst data set to compare the IC flash rate and CG flash rate 60 minutes before a microburst. It is hypothesized that IC lightning may be a better predictor than previously thought and could provide a lead-time on the order of 30-45 minutes. If this is the case, the KSC must be able to gain access to both IC and CG lightning data, otherwise, a valuable forecast tool that could save lives and money will be wasted.

REFERENCES

Abbs, D.J., 1983: Sea-breeze interactions along a concave coastline in southern Australia: Observations and numerical modeling study. *J. Atmos. Sci.,* **40,** 1999-2009.

Arritt, R.W., 1989: Numerical modeling of the offshore extent of sea breezes. *Quart. J. Roy. Meteor. Soc.,* **115,** 547-570.

Atchison, M.K., and G.E. Taylor, 1992: Analyzing and forecasting sea breeze conditions at the Kennedy Space Center. Preprints, *Symp. on Weather Forecasting,* Atlanta, GA, Amer. Meteor. Soc., 132-138.

Atkins, N.T., and R.M. Wakimoto, 1991: Wet microburst activity over the southeastern United States: implications for forecasting. *Wea. Forecasting.,* **6,** 470-482.

Bauman, W.H., III, and S. Businger, 1996: Nowcasting for Space Shuttle landings at Kennedy Space Center, Florida. *Bull. Amer. Meteor. Soc.,* **61,** 980-986.

Biedinger, R.E., and A.D. Stern, 1989: Introduction to WSFO Miami's lightning project through the examination of a severe weather event. Tech Attachment SR/SSD 89-14, NWS Southern Region Administrative Notes, 4 April 1989. [Available from National Weather Service Southern Headquarters, Fort Worth, TX.]

Boyd, B., J.T. Madura, and M.E. Adams: Meteorological support to the United States Air Force and NASA at the Eastern Range and Kennedy Space Center. *31st Aerospace Sciences Meeting and Exhibit,* Reno, NV, Amer. Inst. Aeronautics Astronautics, 1-10.

Buechler, D.E., S.J. Goodman and M.E. Weber, 1988: Cloud-to-ground lightning activity in microburst producing storms. Preprints: *Fifteenth Conference on Severe Local Storms,* Baltimore, Amer. Meteor. Soc., 496-500.

Byers, H.R., and H.R. Rodebush, 1948: Causes of thunderstorms of the Florida peninsula. *J. Meteor.,* **5,** 275-280.

Cautenet, S., and R. Rosset, 1989: Numerical simulation of sea breezes with vertical wind shear during dry season at Cape of Three Points, West Africa. *Mon. Wea. Rev.,* **117,** 329-339.

Cummins, K.L., E.A. Bardo, W.L. Hiscox, R.B. Pyle, and A.E. Pifer, 1995: NLDN '95: A combined TOA/MDF technology upgrade of the U.S. National Lightning Detection Network. *Int. Aerospace and Ground Conference on Lightning and Static Electricity,* Williamsburg, VA, 26-28 Sept. 95.

___, M.J. Murphy, E.A. Bardo, W.L. Hiscox, R.B. Pyle, and A.E. Pifer, 1998: A combined TOA/MDF technology upgrade of the U.S. National Lightning Detection Network. *J. Geophys. Res.,* **103,** 9035-9044.

Dodge, J., J. Arnold, G. Wilson, J. Evans. and T.T. Fujita, 1986: The Cooperative Huntsville Meteorological Experiment (COHMEX). *Bull. Amer. Meteor. Soc.,* **67,** 417-419.

Dye, J.E., J.J. Jones, W.P.Winn, T.A. Cerni, B. Gardiner, D.Lamb, R.L. Pitter, J. Hallett, and C.P.R. Saunders, 1986: Early electrification and precipitation development in a small isolated Montana cumulonimbus, *J. Geophys. Res.*, **91**, 1231-1247.

Frank, N.L., P.L. Moore, and G.E. Fisher, 1967: Summer shower distribution over the Florida peninsula as deduced from digitized radar data. *J. Appl. Meteor.*, **6**, 309-316.

Fujita, T.T., 1985: *The downburst.* SMRP Research Paper No. 210, The University of Chicago, 122 pp.

Gentry, R.C., and P.L. Moore, 1954: Relation of local and general wind interaction near the sea coast to time and location of air mass showers. *J. Meteor.*, **11**, 507-511.

Goodman, S.J., D.E. Buechler and P.J. Meyer, 1988a: Convective tendency images derived from a combination of lightning and satellite data. *Wea. Forecasting*, **3**, 173-188.

___, P.D. Wright and W.D. Rust, 1988b: Lightning and precipitation history of a microburst-producing storm. *Geophys. Res. Lett.*, **15**, 1185-1188.

Harms, D.E., A.A. Guiffrida, B.F. Boyd, L.H. Gross, G.D. Strohm, J.W. Weems, E.D. Priselac, K. Lammers, H.C. Herring, and F.J. Merceret, 1999: The many lives of a meteorologist in support a space launch. Submitted to the *8th Conference on Aviation, Range, and Aerospace Meteorology*, Dallas, TX.

Hinson, M.S., 1997: A study of the characteristics of thunderstorm cessation at the NASA Kennedy Space Center. Master's thesis, Dept. of Meteorology, Texas A&M University, 91 pp. [Available from Texas A&M University, Dept. of Meteorology, College Station, TX.]

Idone, V.P., D.A. Davis, P.K. Moore, Y. Wang, R.W. Henderson, M. Ries, and P.F. Jamason, 1998: Performance evaluation of the U.S. National Lightning Detection Network in eastern New York, 2, Location accuracy. *J. Geophys. Res.*, **103**, 9038-9041.

Jayaratne, E.R., C.P.R. Saunders, and J. Hallet, 1983: Laboratory studies of the charging of soft hail during ice crystal interactions, *Q.J. Roy. Meteor. Soc.*, **106**, 609-630

Kane, R.J., 1991: Correlating lightning to severe local storms in the northeastern United States. *Wea. Forecasting.*, **6**, 3-12.

Kelly, D.L., J.T. Schaefer, and C.A. Doswell III, 1985: Climatology of nontornadic severe thunderstorm events in the United States. *Mon. Wea. Rev.*, **123**, 2913-2933.

Khrebiel, P.R., 1981: An analysis of the electric field change produced by lightning. PhD. thesis, Univ. of Manchester, England.

Laird, N.F., D.A.R. Kristovich, R.M. Rauber, H.T. Ochs III, and L.J. Miller, 1995. The Cape Canaveral sea and river breezes: kinematic structure and convective initiation. *Mon. Wea. Rev.*, **123**, 2942-2956.

Lhermitte, R.M., and P.R. Krehbiel, 1979: Doppler radar and radio observations of thunderstorms. *IEEE Trans.Geosci. Electron.*, **GE-17**, 162-171.

___, and E.R. Williams, 1985: Thunderstorm electrification: A case study. *J. Geophys. Res.,* **90,** 6071-6078.

Lyons, W.A., R.L. Walko, M.E. Nicholls, R.A. Pielke, W.R. Cotton, and C.S. Keen, 1992: Observational and numerical modeling investigations of Florida thunderstorms generated by multi-scale surface thermal forcing. Preprints, *Fifth Conf. on Mesoscale Processes,* Atlanta, GA, Amer. Meteor. Soc., 85-90.

McPherson, R.D., 1970: A numerical study of the effect of a coastal irregularity on the sea breeze. *J. Appl. Meteor.,* **9,** 767-777.

Maier, M.W., and E.P. Krider, 1982: A comparative study of cloud-to-ground lightning characteristics in Florida and Oklahoma thunderstorms. Preprints: *Twelfth Conference on Severe Local Storms,* San Antonio, Amer. Meteor. Soc., 334-337.

Maier, L.M., E.P. Krider, and M.W. Maier, 1984: Average diurnal variation of summer lightning over the Florida peninsula. *Mon. Wea. Rev.,* **112,** 1134-1140.

Neumann, C.J., 1968: Frequency and duration of thunderstorms at Cape Kennedy, Part 1. ESSA Tech Memo. WBTM SOS-2, 34 pp. [U.S. Department of Commerce, Springfield].

___, 1971: The thunderstorm forecasting system at the Kennedy Space Center. *J. Appl. Meteor.,* **10,** 921-936.

Nicholls, M.E., R.A. Pielke, and W.R. Cotton, 1991: A two-dimensional numerical investigation of the interaction between sea-breezes and deep convection over the Florida peninsula. *Mon. Wea. Rev.,* **119,** 298-323.

Orville, R.E., 1991: Lightning ground flash density in the contiguous United States: 1989. *Mon. Wea. Rev.,* **119,** 573-577.

___, 1994: Cloud-to-ground lightning flash characteristics in the contiguous United States: 1989-1991. *J. Geophys. Res.,* **99,** 10833-10841.

Pielke, R.A., 1974: A three-dimensional numerical model of the sea breezes over south Florida. *Mon. Wea. Rev.,* **102,** 115-139.

Simpson, G.C., and F.J. Scrase, 1937: The distribution of electricity in thunderclouds. *Proc. R. Soc. London, Ser. A,* **161,** 309-352.

Srivastava, R.C., 1985: A simple model of evaporatively driven downdraft: Application to microburst downdraft. *J. Atmos. Sci.* **42,** 1004-1023.

___, 1987: A model of intense downdrafts driven by melting and evaporation of precipitation. *J. Atmos. Sci.,* **44,** 1752-1773.

Taylor, W., 1983: Lightning location and progression using VHF space-time mapping technique. *Proceedings in Atmospheric Electricity,* Hampton, VA, 381-384.

Watson, A.L., R.E. Lopez, R.L. Holle, and J.R. Daugherty, 1987: The relationship of lightning to surface convergence at Kennedy Space Center: A preliminary study. *Wea. Forecasting,* **2,** 140-157.

Wheeler, M., 1997: 1997 MDPI Results. *AMU Memorandum,* 10 Nov 97, 4 pp. [Available from 45th Weather Squadron, Kennedy Space Center, FL]

Williams, E.R., M.E. Weber, and R.E. Orville, 1989: Relationship between lightning type and convective state of thunderclouds. *J. Geophys. Res.,* **94,** 13213-13220.

Wilson, C.T.R., 1916: On some determinations of the sign and magnitude of electric discharges in lightning flashes. *Proc. R. Soc. London Ser.* A, **92,** 555-574.

Workman, E.J., and S.E. Reynolds, 1949: Electrical activity as related to thunderstorm cell growth. *Bull. Amer. Meteor. Soc,* **30,** 142

Zhong, S., J.M. Leone Jr., and E.S. Takle, 1991: Interaction of the sea breeze with a river breeze in an area of complex coastal heating. *Bound.-Layer Meteor.,* **56,** 101-139.

___, and E.S. Takle, 1993: The effects of large-scale winds on the sea-land breeze circulations in an area of complex coastal heating. *J. Appl. Meteor.,* **32,** 1181-1195.

APPENDIX A

MICROBURSTS ASSOCIATED WITH HURRICANE ERIN

Table A1. List of microbursts that were associated with Hurricane Erin.

Number	Date	Time	Tower	Height	Direction	Speed	Gust
1	2 Aug 95	0025	509	54	50	22	36
2	2 Aug 95	0035	803	12	37	8	25
3	2 Aug 95	0150	1101	162	61	34	50
4	2 Aug 95	0205	513	30	46	19	43
5	2 Aug 95	0225	412	54	43	25	39
6	2 Aug 95	0225	513	30	45	20	46
7	2 Aug 95	0240	1007	54	37	35	48
8	2 Aug 95	0350	3131	54	49	22	41
9	2 Aug 95	0500	1101	162	60	36	54
10	2 Aug 95	0505	311	54	45	26	46
11	2 Aug 95	0525	805	12	49	11	36
12	2 Aug 95	0540	415	54	47	22	41
13	2 Aug 95	0910	9001	54	101	23	54
14	2 Aug 95	1120	9001	54	121	19	39
15	2 Aug 95	1825	9001	54	95	16	40
16	2 Aug 95	2235	1000	54	140	19	36

APPENDIX B

KENNEDY SPACE CENTER MICROBURST PLOT
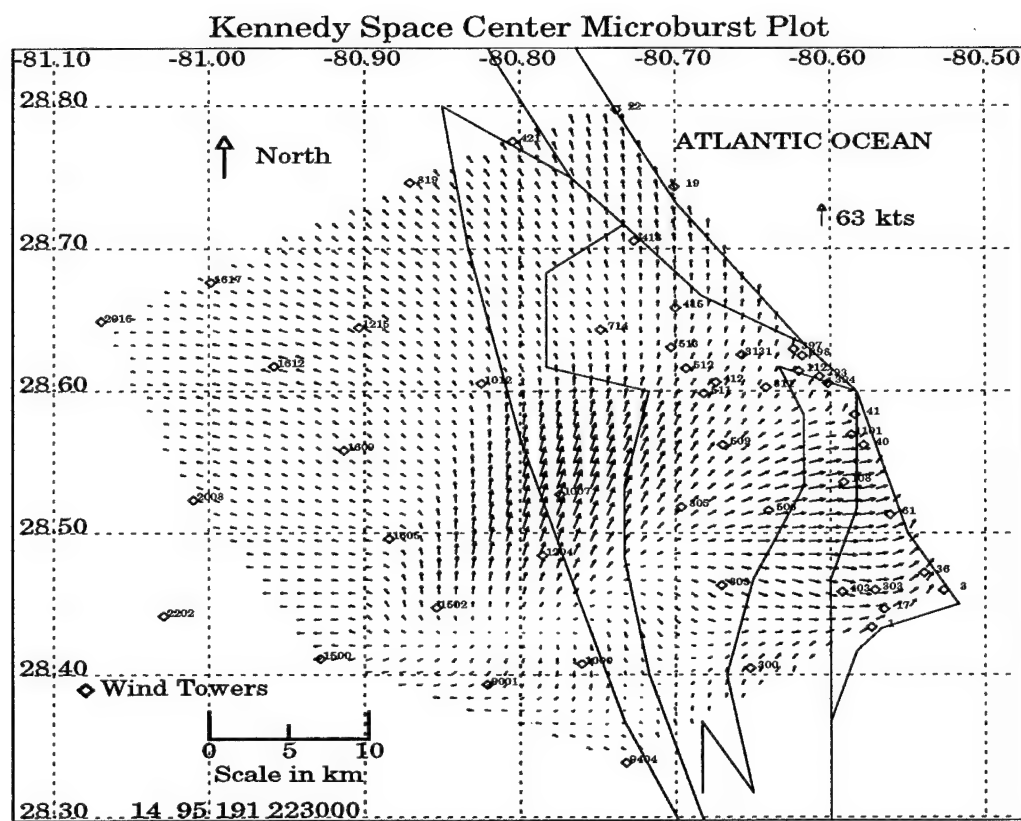
Fig. B1. Wind vector plot of all towers for the microburst event that occurred on 10 July 1995 at 2230 UTC (630 P.M. EDT). The microburst of 63 knots was observed at tower 1007.

APPENDIX C

LIST OF MICROBURSTS

TABLE C1. List of all microbursts according to number, year, day, time, tower, height, wind direction, wind speed, and peak wind gust.

Number	Year	Day	Time	Tower	Height	Direction	Speed	Gust
1	1995	11-May	2045	819	54	300	15	36
2	1995	11-May	2120	415	54	303	13	29
3	1995	11-May	2130	3131	162	344	28	40
4	1995	11-May	2215	300	54	325	21	41
5	1995	20-May	0500	9001	54	284	14	30
6	1995	20-May	0950	513	30	273	15	27
7	1995	20-May	0955	1007	54	278	18	29
8	1995	20-May	1000	394	60	262	21	36
9	1995	23-May	2020	2008	54	79	16	32
10	1995	5-Jun	1700	300	54	240	22	41
11	1995	10-Jun	2005	2202	54	326	25	44
12	1995	12-Jun	1645	1	54	261	21	39
13	1995	12-Jun	1700	393	60	257	16	30
14	1995	12-Jun	1700	398	60	257	16	35
15	1995	12-Jun	1850	2016	54	295	13	23
16	1995	12-Jun	1920	421	54	272	39	50
17	1995	12-Jun	2010	509	12	263	8	22
18	1995	12-Jun	2340	303	54	252	11	20
19	1995	12-Jun	2345	36	90	249	15	32
20	1995	18-Jun	1825	1000	54	39	13	26
21	1995	25-Jun	1950	511	30	196	15	41
22	1995	25-Jun	2005	412	54	172	11	21
23	1995	25-Jun	2015	1000	54	230	19	32
24	1995	26-Jun	2025	819	54	290	15	32
25	1995	26-Jun	2040	9001	54	259	14	34
26	1995	26-Jun	2050	403	54	262	12	37
27	1995	10-Jul	1840	412	54	299	13	27
28	1995	10-Jul	1850	394	60	318	19	36
29	1995	10-Jul	1850	398	60	303	25	46
30	1995	10-Jul	1925	506	54	171	14	36
31	1995	10-Jul	1930	1	54	231	13	30
32	1995	10-Jul	1935	3	54	256	15	30
33	1995	10-Jul	1935	61	162	319	13	28
34	1995	10-Jul	1935	108	12	147	2	21
35	1995	10-Jul	2125	2008	54	234	7	25
36	1995	10-Jul	2140	3131	54	302	13	27
37	1995	10-Jul	2210	509	12	328	15	34
38	1995	10-Jul	2230	1007	54	199	39	63

TABLE C1. Cont.

Number	Year	Day	Time	Tower	Height	Direction	Speed	Gust
39	1995	13-Jul	1745	1612	54	250	15	28
40	1995	17-Jul	1750	398	60	239	3	21
41	1995	20-Jul	1820	805	54	105	15	32
42	1995	20-Jul	1855	3	54	263	19	32
43	1995	21-Jul	2000	1007	54	274	15	27
44	1995	21-Jul	2035	1	54	295	14	36
45	1995	21-Jul	2100	1101	162	206	21	39
46	1995	24-Jul	2035	513	30	234	13	27
47	1995	27-Jul	1555	403	12	168	12	23
48	1995	28-Jul	2145	397	60	109	16	37
49	1995	28-Jul	2145	398	60	109	18	40
50	1995	29-Jul	0930	311	54	162	15	29
51	1995	29-Jul	0935	412	54	134	13	29
52	1995	30-Jul	2050	397	60	66	18	29
53	1995	1-Aug	1520	819	54	72	9	25
54	1995	23-Aug	1615	61	54	101	16	30
55	1995	23-Aug	2235	61	54	109	22	39
56	1995	24-Aug	0600	1101	54	145	23	43
57	1995	24-Aug	0735	803	54	129	15	37
58	1995	24-Aug	0750	506	54	149	22	40
59	1995	24-Aug	0755	3131	54	150	23	49
60	1995	24-Aug	0830	108	12	162	7	27
61	1995	24-Aug	0840	511	30	140	18	36
62	1995	24-Aug	1100	1101	162	149	34	50
63	1995	24-Aug	1420	19	54	146	36	55
64	1995	24-Aug	1450	412	54	145	20	39
65	1995	26-Aug	2145	108	54	231	16	26
66	1995	27-Aug	1840	303	54	257	8	22
67	1995	27-Aug	2030	397	60	250	20	34
68	1995	31-Aug	0755	513	30	111	11	23
69	1995	12-Sep	1540	393	60	194	6	22
70	1995	13-Sep	1425	511	30	126	12	26
71	1995	25-Sep	0305	403	12	222	9	30
72	1995	26-Sep	0435	3131	162	182	13	32
73	1995	28-Sep	0025	513	30	169	16	34
74	1995	28-Sep	0200	1	54	60	25	42
75	1996	28-May	1950	40	54	153	4	43
76	1996	28-May	1950	61	204	289	13	37
77	1996	28-May	1950	311	54	15	16	39
78	1996	28-May	1950	3131	12	341	12	27
79	1996	28-May	1955	394	60	19	15	32
80	1996	28-May	2010	108	12	1	8	27
81	1996	31-May	0130	1	54	220	18	42
82	1996	31-May	0130	61	204	246	34	53
83	1996	31-May	0135	3	54	233	34	48
84	1996	9-Jun	1925	714	54	216	11	25

TABLE C1. Cont.

Number	Year	Day	Time	Tower	Height	Direction	Speed	Gust
85	1996	9-Jun	2230	509	54	212	20	37
86	1996	19-Jun	2115	36	90	291	20	41
87	1996	20-Jun	1905	512	30	202	15	26
88	1996	20-Jun	1910	509	54	261	22	48
89	1996	26-Jun	1910	513	30	206	14	48
90	1996	27-Jun	2235	393	60	349	9	29
91	1996	4-Jul	1825	415	54	238	15	36
92	1996	4-Jul	1830	61	12	235	11	29
93	1996	4-Jul	1830	112	54	248	25	40
94	1996	4-Jul	1830	397	60	234	26	44
95	1996	5-Jul	2025	1101	162	156	14	25
96	1996	5-Jul	2035	311	54	161	8	20
97	1996	5-Jul	2115	1101	204	139	20	36
98	1996	5-Jul	2135	803	54	172	21	40
99	1996	6-Jul	1940	803	12	223	6	20
100	1996	6-Jul	1945	506	54	206	14	30
101	1996	6-Jul	2140	512	30	200	15	26
102	1996	6-Jul	2145	394	60	258	16	33
103	1996	6-Jul	2145	397	60	209	16	32
104	1996	6-Jul	2200	512	30	329	12	32
105	1996	11-Jul	2000	805	54	325	15	27
106	1996	11-Jul	2115	61	204	315	15	27
107	1996	23-Jul	2135	9001	54	269	9	29
108	1996	24-Jul	1930	393	60	265	20	44
109	1996	24-Jul	2055	1	54	258	13	30
110	1996	24-Jul	2055	403	54	253	13	23
111	1996	24-Jul	2100	805	54	194	11	32
112	1996	1-Aug	1745	1612	54	174	13	22
113	1996	1-Aug	1825	311	54	264	19	34
114	1996	1-Aug	1825	412	12	175	12	29
115	1996	3-Aug	1935	3131	204	248	16	33
116	1996	11-Aug	1730	512	30	224	16	90
117	1996	11-Aug	1735	3131	12	259	9	23
118	1996	13-Aug	1830	513	30	357	13	27
119	1996	15-Aug	2015	714	54	250	15	43
120	1996	15-Aug	2015	1204	54	323	15	39
121	1996	15-Aug	2025	61	204	295	22	34
122	1996	15-Aug	2025	1204	54	69	14	36
123	1996	15-Aug	2030	513	30	164	12	90
124	1996	15-Aug	2035	61	162	265	22	43
125	1996	19-Aug	2250	311	54	106	15	27
126	1996	19-Aug	2300	394	60	66	21	29
127	1996	20-Aug	0915	61	54	85	13	25
128	1996	20-Aug	1630	1605	54	84	15	35
129	1996	20-Aug	2100	421	54	68	15	29
130	1996	2-Sep	1715	1204	54	260	9	22

TABLE C1. Cont.

Number	Year	Day	Time	Tower	Height	Direction	Speed	Gust
131	1996	2-Sep	1745	311	54	197	11	25
132	1996	2-Sep	1750	418	54	118	12	25
133	1996	2-Sep	1755	397	60	182	16	48
134	1996	2-Sep	1755	398	60	211	18	49
135	1996	6-Sep	0025	394	60	181	20	30
136	1996	7-Sep	0020	3131	54	263	8	29
137	1996	10-Sep	0710	41	54	321	3	20
138	1996	10-Sep	1245	1204	54	102	13	43
139	1996	10-Sep	1325	1204	54	92	11	39
140	1996	11-Sep	1635	394	60	276	14	29
141	1996	11-Sep	2005	1204	54	236	8	35
142	1996	17-Sep	1725	506	54	248	13	29
143	1996	17-Sep	1840	394	60	221	13	23
144	1996	17-Sep	2340	511	30	279	18	35
145	1996	18-Sep	2050	300	54	310	15	29
146	1997	3-May	1815	805	54	201	9	26
147	1997	3-May	1955	61	204	196	21	40
148	1997	3-May	2010	61	204	200	15	35
149	1997	3-May	2015	397	60	198	19	36
150	1997	3-May	2015	3131	295	194	27	37
151	1997	3-May	2020	41	54	206	14	35
152	1997	3-May	2020	1101	162	230	18	36
153	1997	3-May	2025	421	54	225	39	64
154	1997	3-May	2030	22	54	219	25	42
155	1997	28-May	0105	803	54	19	8	36
156	1997	28-May	0115	803	54	20	3	30
157	1997	28-May	1525	3	54	56	22	36
158	1997	31-May	1900	1012	54	182	8	25
159	1997	31-May	2205	3	12	259	11	22
160	1997	31-May	2205	112	54	223	18	39
161	1997	1-Jun	1750	509	54	215	22	55
162	1997	1-Jun	1755	415	54	268	12	25
163	1997	1-Jun	1805	512	30	233	19	41
164	1997	1-Jun	1825	403	54	264	28	42
165	1997	2-Jun	1520	3131	12	293	7	20
166	1997	2-Jun	2115	36	90	298	15	29
167	1997	12-Jun	1910	511	30	109	15	29
168	1997	12-Jun	2020	403	12	156	11	22
169	1997	12-Jun	2025	1	54	141	18	34
170	1997	12-Jun	2105	805	54	339	9	27
171	1997	14-Jun	1710	61	54	201	15	36
172	1997	14-Jun	1710	108	12	199	6	25
173	1997	14-Jun	1730	61	204	230	21	39
174	1997	14-Jun	1745	513	30	221	20	42
175	1997	17-Jun	1745	61	162	294	28	48
176	1997	19-Jun	2015	512	30	34	15	27

TABLE C1. Cont.

Number	Year	Day	Time	Tower	Height	Direction	Speed	Gust
177	1997	19-Jun	2025	394	60	7	21	43
178	1997	19-Jun	2045	412	54	130	15	39
179	1997	19-Jun	2100	1000	54	33	18	28
180	1997	19-Jun	2110	3	54	332	22	48
181	1997	24-Jun	1730	2016	54	43	11	22
182	1997	27-Jun	1715	393	60	258	11	23
183	1997	29-Jun	2030	421	54	227	14	27
184	1997	1-Jul	0035	108	54	268	12	36
185	1997	1-Jul	2130	412	54	213	11	33
186	1997	1-Jul	2130	511	30	110	11	32
187	1997	5-Jul	1925	714	54	135	15	28
188	1997	5-Jul	1935	1012	54	195	12	30
189	1997	9-Jul	2110	805	54	328	15	39
190	1997	19-Jul	2045	300	54	288	20	36
191	1997	26-Jul	1835	1612	54	283	9	34
192	1997	26-Jul	1900	1012	54	274	16	49
193	1997	26-Jul	1925	714	54	322	11	46
194	1997	27-Jul	2020	393	60	317	23	37
195	1997	29-Jul	2130	421	54	154	22	43
196	1997	3-Aug	2105	41	54	239	19	36
197	1997	4-Aug	1905	393	60	281	22	48
198	1997	6-Aug	2225	819	54	309	8	20
199	1997	10-Aug	2005	19	54	298	34	50
200	1997	10-Aug	2005	805	12	315	5	28
201	1997	10-Aug	2025	509	54	188	18	33
202	1997	10-Aug	2125	61	162	273	15	34
203	1997	19-Aug	1805	1101	162	115	22	43
204	1997	19-Aug	1810	112	12	53	4	20
205	1997	19-Aug	1825	1500	54	247	8	25
206	1997	19-Aug	1835	311	12	209	7	20
207	1997	20-Aug	2150	513	30	326	23	43
208	1997	20-Aug	2155	3131	295	299	23	42
209	1997	23-Aug	2040	803	54	45	6	29
210	1997	1-Sep	1040	3	54	68	18	28
211	1997	1-Sep	1105	393	60	121	22	34
212	1997	1-Sep	1320	3	54	75	23	32
213	1997	1-Sep	1530	803	54	71	6	26
214	1997	3-Sep	2005	3131	162	289	13	29
215	1997	23-Sep	0750	506	54	212	15	36
216	1997	25-Sep	2025	1000	54	244	16	34
217	1997	26-Sep	1755	1612	54	205	12	27
218	1997	26-Sep	1820	803	54	220	16	29
219	1997	26-Sep	1835	61	204	194	18	36
220	1997	26-Sep	1840	3131	12	173	9	28
221	1997	26-Sep	1845	397	60	215	18	34
222	1998	4-May	1900	112	54	293	14	32

TABLE C1. Cont.

Number	Year	Day	Time	Tower	Height	Direction	Speed	Gust
223	1998	4-May	1950	1000	54	283	19	41
224	1998	5-May	1745	1007	54	213	16	53
225	1998	7-Jun	1925	9001	54	336	18	47
226	1998	21-Jun	0105	418	54	227	22	43
227	1998	21-Jun	2130	300	54	309	19	35
228	1998	21-Jun	2140	300	54	337	11	39
229	1998	26-Jun	1830	1101	54	238	22	39
230	1998	26-Jun	1845	41	54	201	13	34
231	1998	6-Jul	1925	1612	54	75	32	55
232	1998	6-Jul	2005	1612	54	248	11	30
233	1998	7-Jul	1640	1007	54	231	16	29
234	1998	11-Jul	1825	300	54	292	14	26
235	1998	18-Jul	2215	511	30	248	18	33
236	1998	18-Jul	2215	512	30	224	28	44
237	1998	18-Jul	2215	513	30	192	25	43
238	1998	18-Jul	2250	819	54	225	13	36
239	1998	26-Jul	1930	819	54	221	12	29
240	1998	28-Jul	0220	1000	54	203	3	26
241	1998	28-Jul	0230	303	54	208	13	35
242	1998	28-Jul	0300	108	54	311	18	43
243	1998	28-Jul	0300	112	12	177	13	27
244	1998	28-Jul	0300	1101	162	188	36	57
245	1998	28-Jul	2105	421	54	8	16	29
246	1998	28-Jul	2120	421	54	340	18	34
247	1998	28-Jul	2135	418	54	308	18	39
248	1998	28-Jul	2145	714	12	21	11	32
249	1998	28-Jul	2150	112	54	353	11	33
250	1998	28-Jul	2150	398	60	336	20	35
251	1998	28-Jul	2150	1101	204	14	16	36
252	1998	28-Jul	2200	397	60	316	26	51
253	1998	28-Jul	2200	398	60	307	15	41
254	1998	28-Jul	2200	513	30	189	5	36
255	1998	28-Jul	2200	3131	295	354	29	44
256	1998	28-Jul	2225	1007	54	274	13	47
257	1998	29-Jul	1745	311	54	32	9	26
258	1998	5-Aug	1855	1000	54	7	21	42
259	1998	6-Aug	1750	805	54	135	15	32
260	1998	10-Aug	1935	714	54	259	8	28
261	1998	13-Aug	1955	421	54	7	22	41
262	1998	13-Aug	2015	714	54	13	21	40
263	1998	13-Aug	2045	3131	204	351	30	43
264	1998	14-Aug	1900	819	54	137	18	43
265	1998	14-Aug	1955	61	204	288	25	36
266	1998	14-Aug	2020	1000	54	73	16	32
267	1998	17-Aug	1645	311	54	114	12	26
268	1998	21-Aug	0615	3131	204	129	22	36

TABLE C1. Cont.

Number	Year	Day	Time	Tower	Height	Direction	Speed	Gust
269	1998	22-Aug	0220	311	54	137	14	34
270	1998	22-Aug	0220	397	60	144	22	37
271	1998	22-Aug	0220	398	60	139	26	40
272	1998	31-Aug	1805	1007	54	13	21	39
273	1998	31-Aug	1815	714	54	251	18	35
274	1998	3-Sep	0030	300	54	135	15	30
275	1998	3-Sep	1815	9001	54	238	14	39
276	1998	3-Sep	1825	803	12	234	9	28
277	1998	3-Sep	1830	403	54	244	18	40
278	1998	3-Sep	1835	108	54	245	27	43
279	1998	3-Sep	1900	421	54	214	27	46
280	1998	7-Sep	2145	513	30	169	19	33
281	1998	24-Sep	1230	311	54	67	18	29
282	1998	25-Sep	2055	3	54	162	25	34

APPENDIX D

NUMBER OF MICROBURSTS RECORDED AT EACH TOWER

TABLE D1. Number of microbursts recorded for each wind tower.

Tower	Number	Tower	Number
1	7	509	6
2	0	511	7
3	9	512	7
17	0	513	12
19	2	714	8
22	1	803	9
36	3	805	8
40	1	819	7
41	4	1000	8
61	18	1007	7
108	8	1012	3
112	6	1101	10
300	8	1204	6
303	3	1215	0
311	11	1500	1
393	8	1502	0
394	9	1605	1
397	10	1609	0
398	8	1612	6
403	7	1617	0
412	7	2008	2
415	3	2016	2
418	3	3131	17
421	9	9001	5
506	5	9404	0

APPENDIX E

MICROBURST AND FLASH RATE TEMPORAL RELATIONSHIP FOR ALL MICROBURSTS GREATER THAN 34 KNOTS USING 10X10 KM GRID BOX
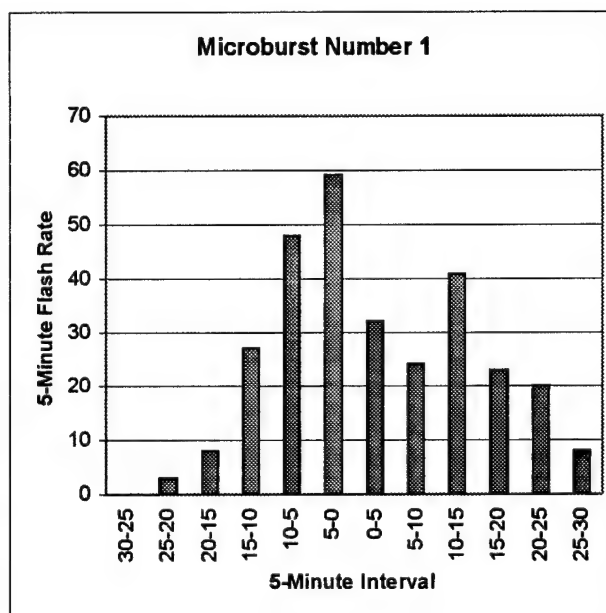
Fig. E1. Microburst and cloud-to-ground (CG) flash rate temporal relationship starting 30 minutes before the and ending 30 minutes after microbursts greater than 34 knots using the 20x20 km grid box. The CG flash rate is divided into i5-minute intervals. The microburst number corresponds to Table C1 in Appendix C.
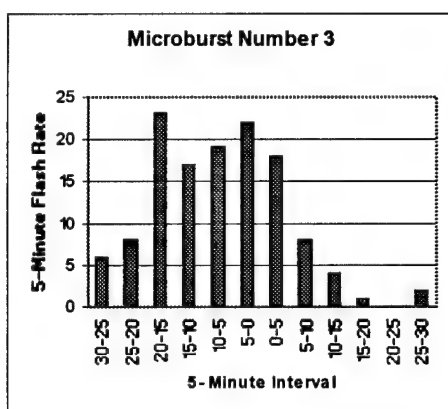
Fig. E2. As in Fig. E1 except for microburst number 3.
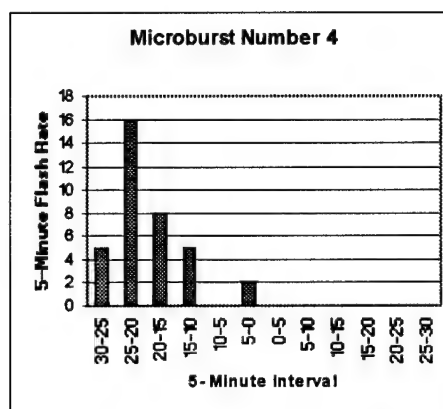
Fig. E3. As in Fig. E1 except for microburst number 4.
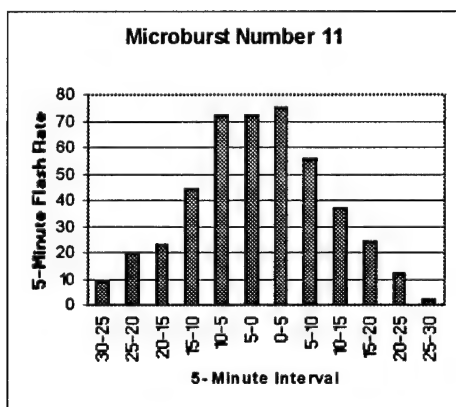
Fig. E4. As in Fig. E1 except for microburst number 11.
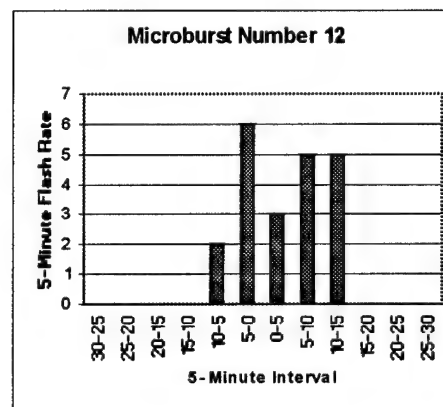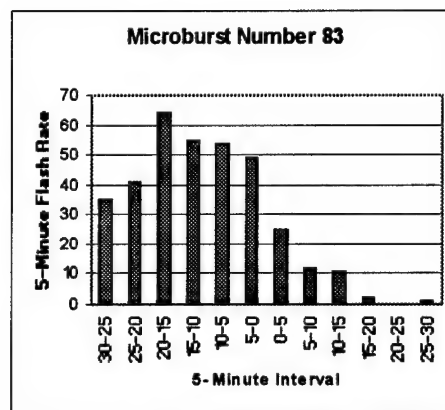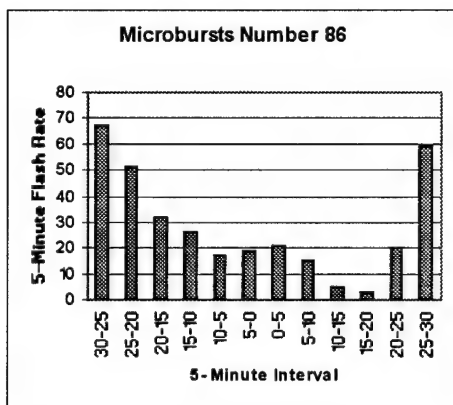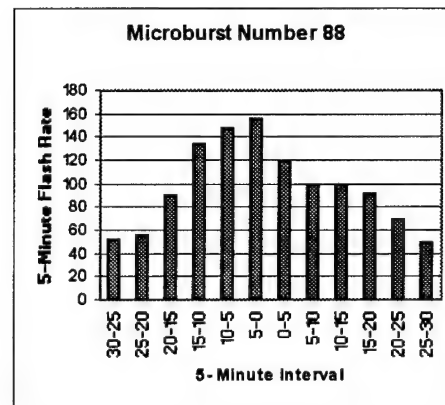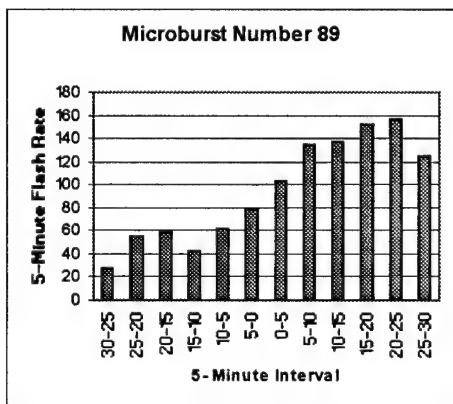

Fig. E5. As in Fig. E1 except for microburst number 12.
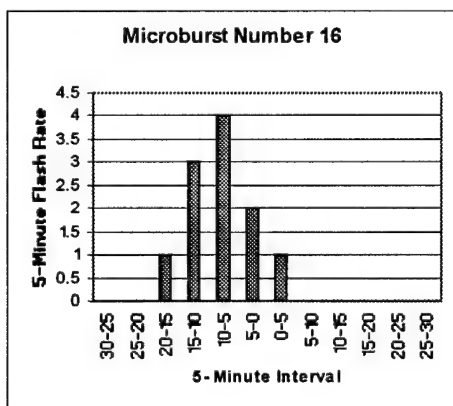
Fig. E6. As in Fig. E1 except for microburst number 16.
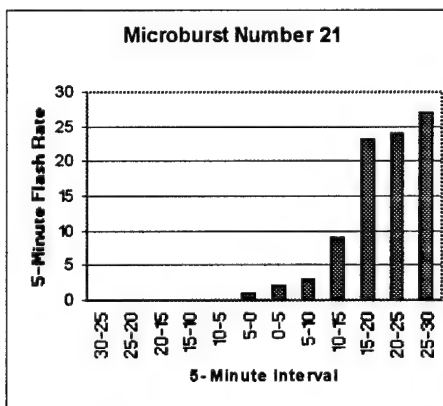
Fig. E7. As in Fig. E1 except for microburst number 21.

77
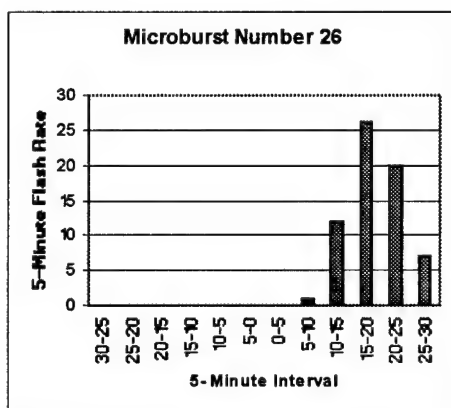
Fig. E8. As in Fig. E1 except for microburst number 26.
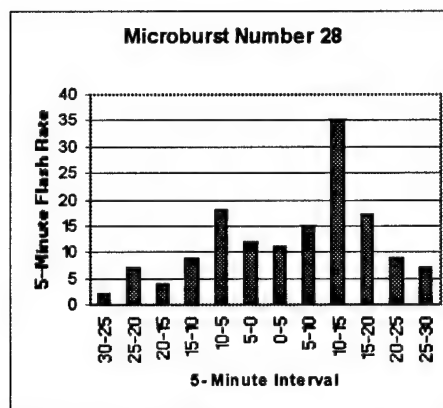
Fig. E9. As in Fig. E1 except for microburst number 28.
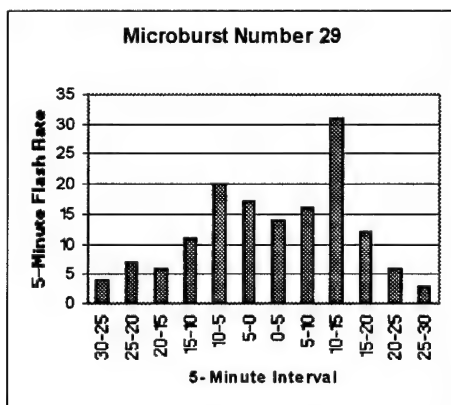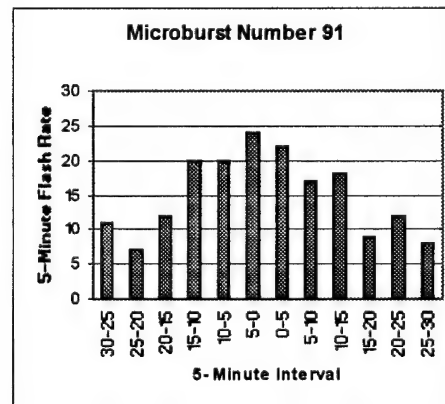

Fig. E10. As in Fig. E1 except for microburst number 29.
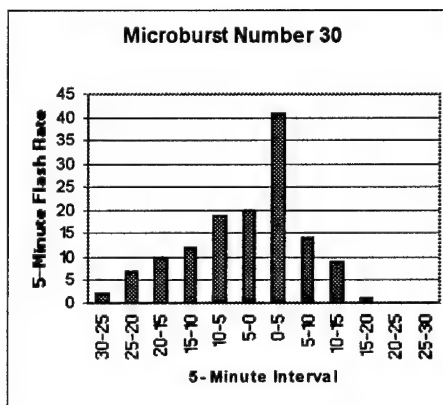
Fig. E11. As in Fig E1 except for microburst number 30.
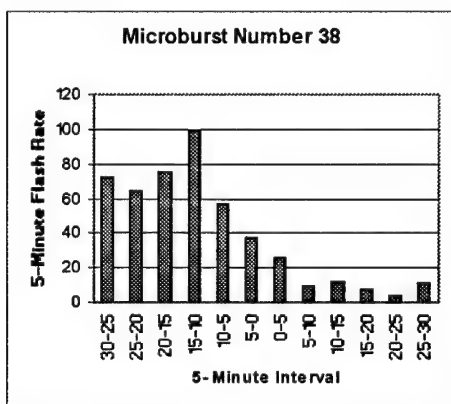
Fig. E12. As in Fig. E1 except for microburst number 38
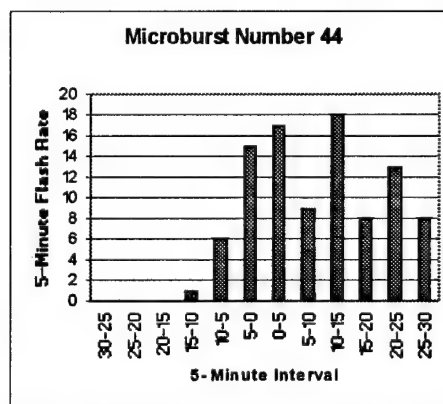
Fig. E13. As in Fig. E1 except for microburst number 44.
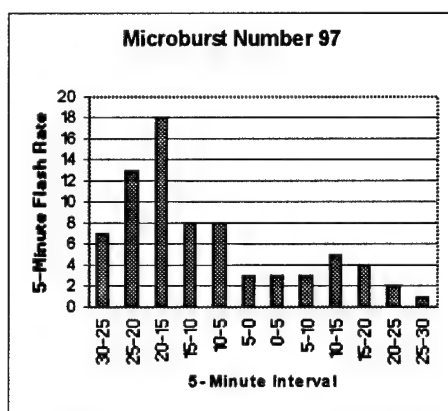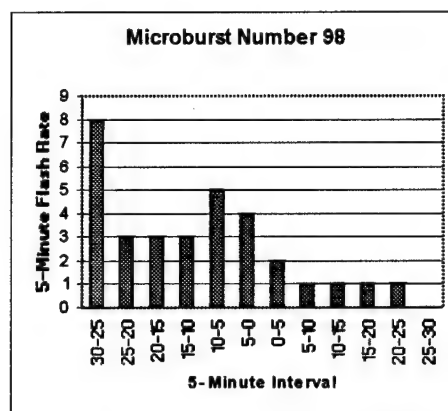
Microburst Number 45
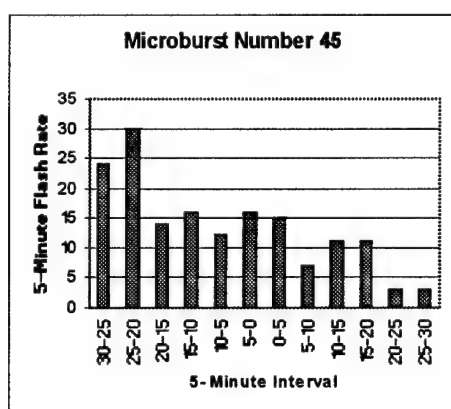
Fig. E14. As in Fig. E1 except for microburst number 45.

Microburst Number 74
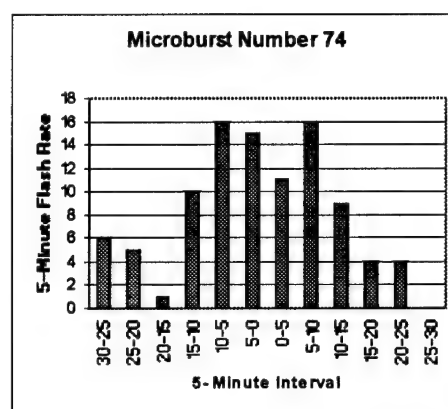
Fig. E15. As in Fig. E1 except for microburst number 74.

Microburst Number 75
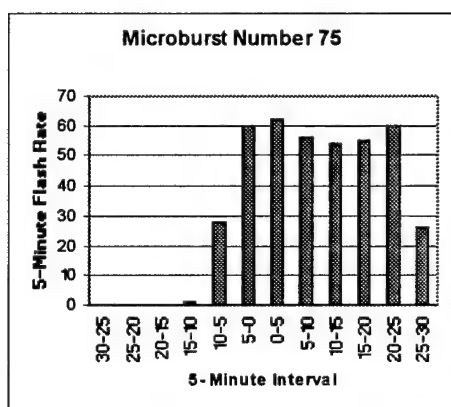
Fig. E16. As in Fig. E1 except for microburst number 75.

Microburst Number 76
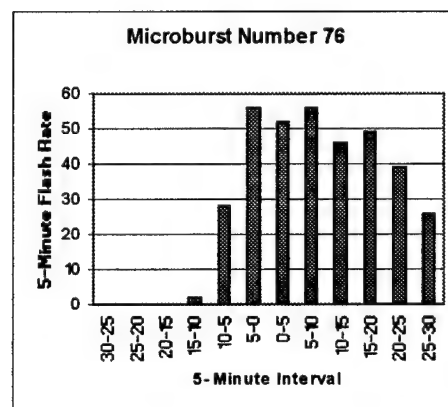
Fig. E17. As in Fig. E1 except for microburst number 76.

Microburst Number 77
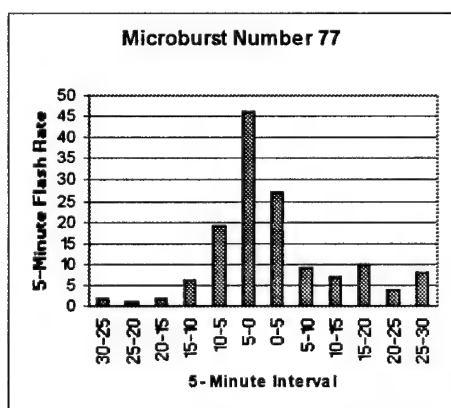
Fig. E18. As in Fig. E1 except for microburst number 77.

Microburst Number 81
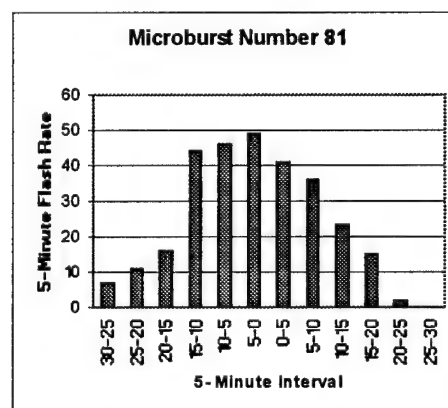
Fig. E19. As in Fig. E1 except for microburst number 81.
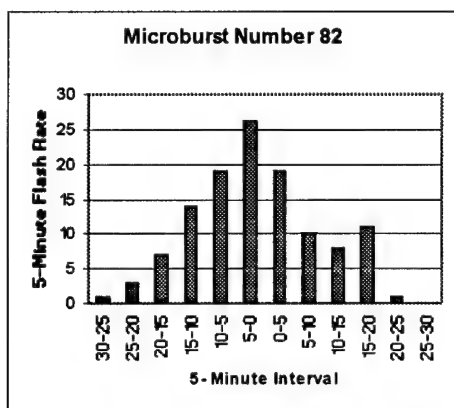
Fig. E20. As in Fig. E1 except for microburst number 82.
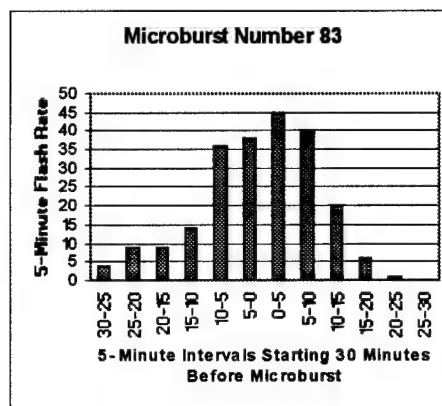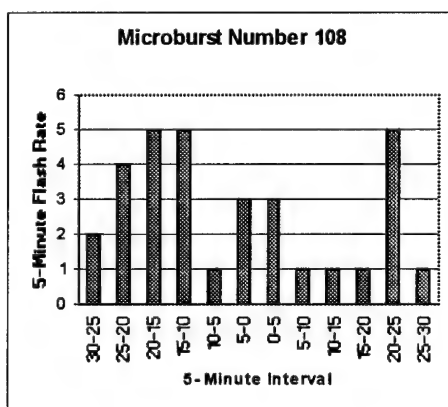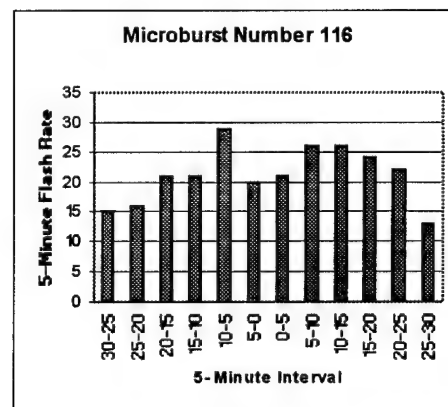

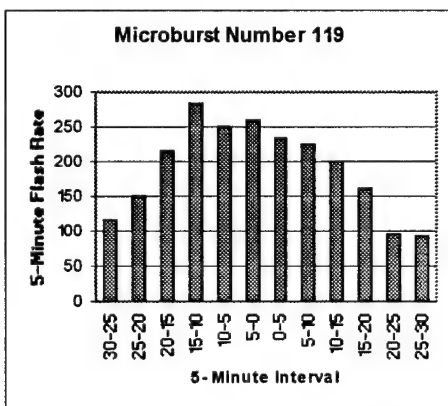Fig. E21. As in Fig. E1 except for microburst number 83.
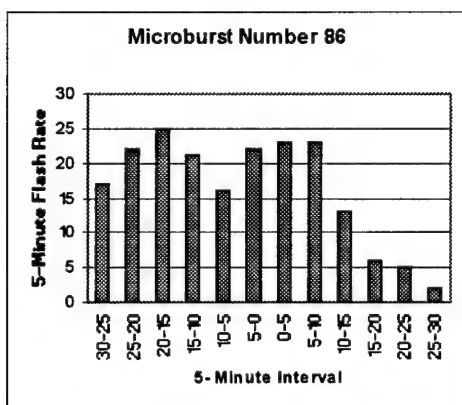
Fig. E22. As in Fig. E1 except for microburst number 86.
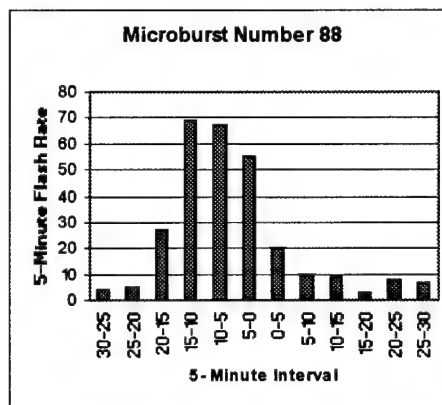
Fig. E23. As in Fig. E1 except for microburst number 88.
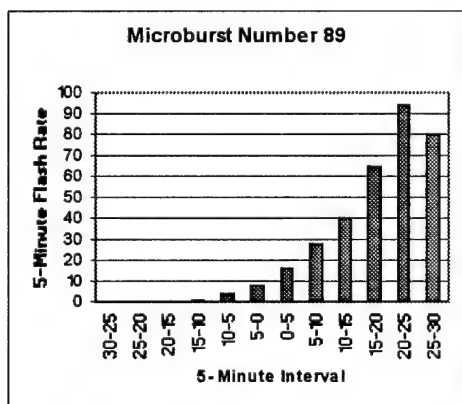
Fig. E24. As in Fig. E1 except for microburst number 89.
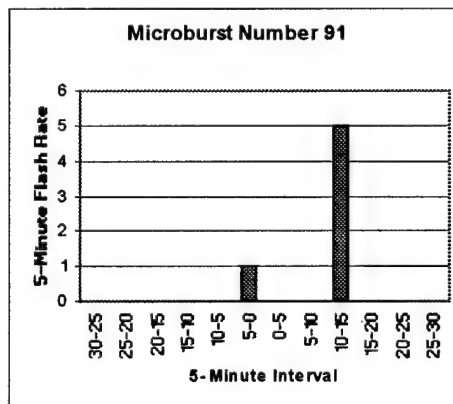
Fig. E25. As in Fig. E1 except for microburst number 91.
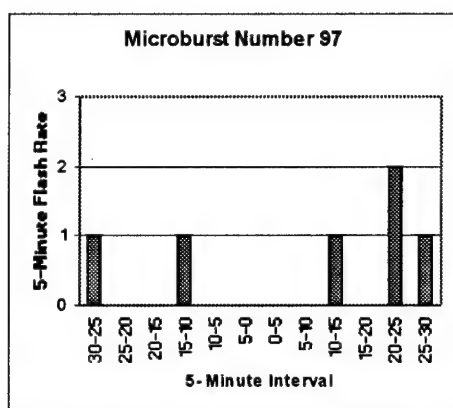
Fig. E26. As in Fig. E1 except
for microburst number 97.
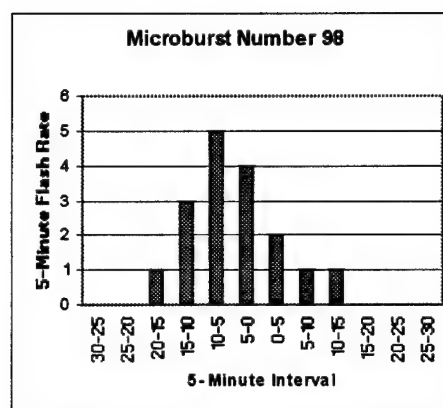
Fig. E27. As in Fig. E1 except
for microburst number 98.
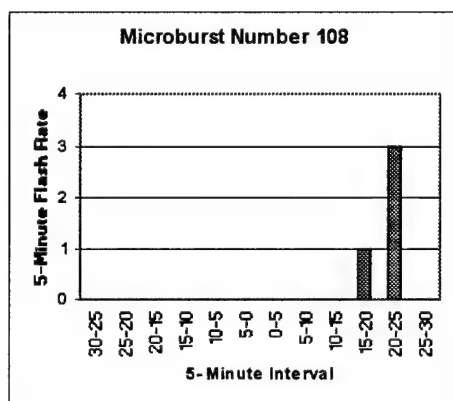
Fig. E28. As in Fig. E1 except
for microburst number 108.
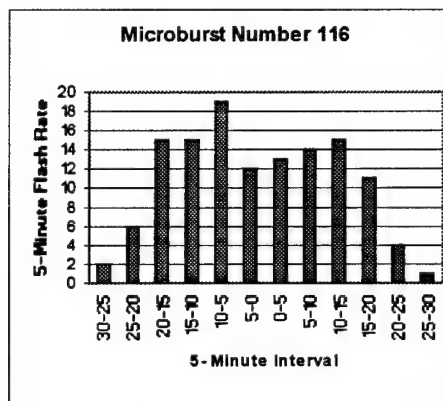
Fig. E29. As in Fig. E1 except
for microburst number 116.
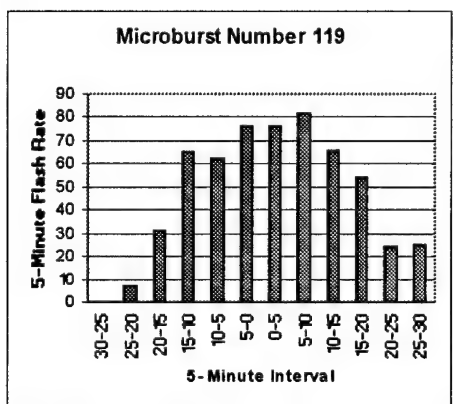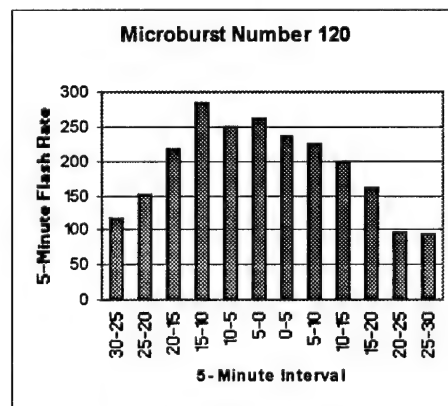
Fig. E30. As in Fig. E1 except
for microburst number 119.
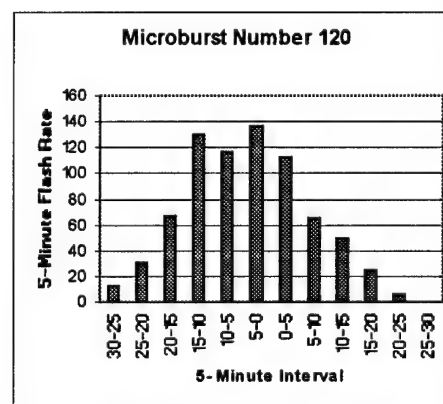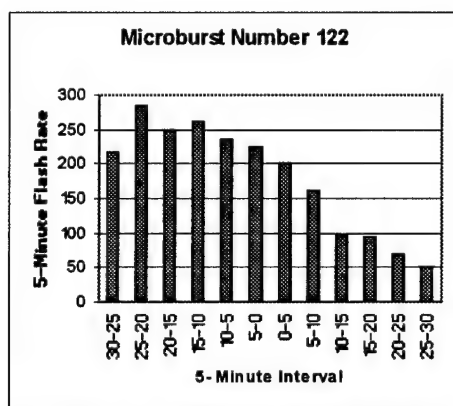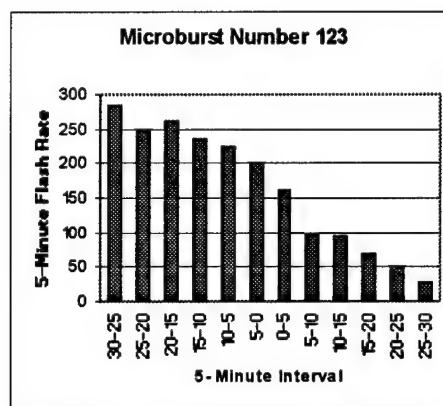
Fig. E31. As in Fig. E1 except
for microburst number 120.

Microburst Number 122
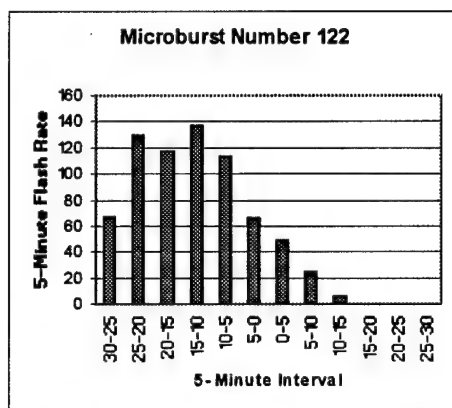
Fig. E32. As in Fig. E1 except
for microburst number 122.

Microburst Number 123
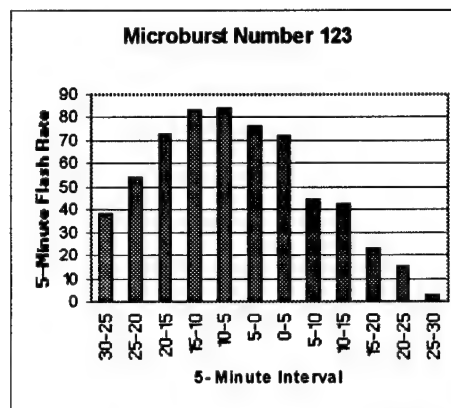
Fig. E33. As in Fig. E1 except
for microburst number 123.

Microburst Number 124
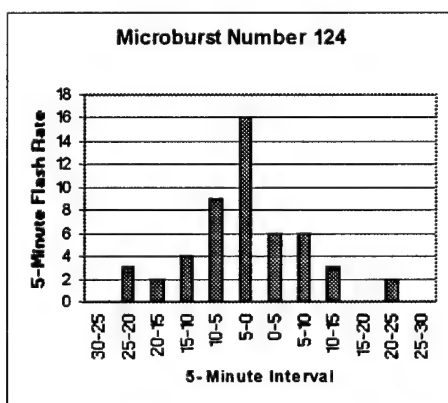
Fig. E34. As in Fig. E1 except
for microburst number 124.

Microburst Number 133
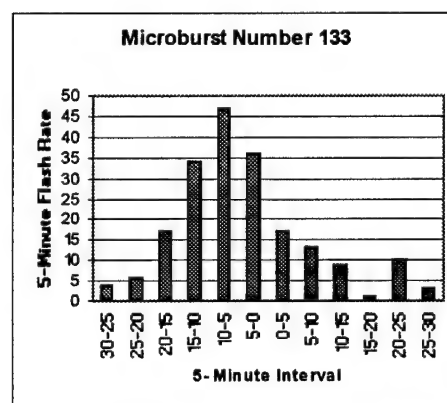
Fig. E35. As in Fig. E1 except
for microburst number 133.

Microburst Number 134
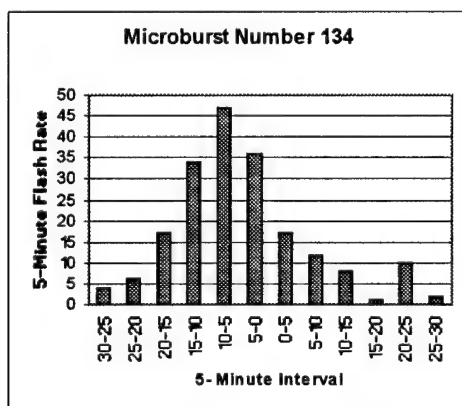
Fig. E36. As in Fig. E1 except
for microburst number 134.

Microburst Number 141
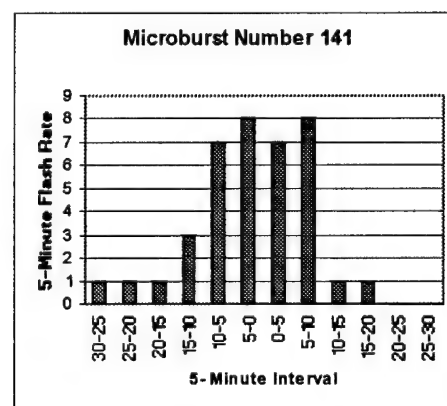
Fig. E37. As in Fig. E1 except
for microburst number 141.
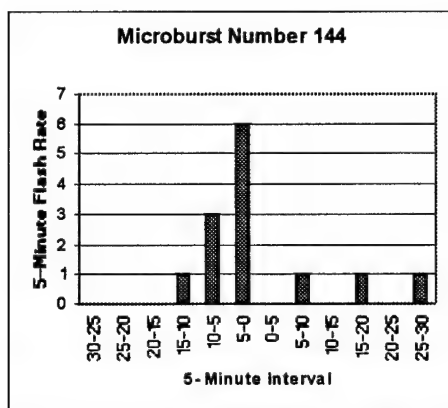
Fig.E38. As in Fig. E1 except for microburst number 144.
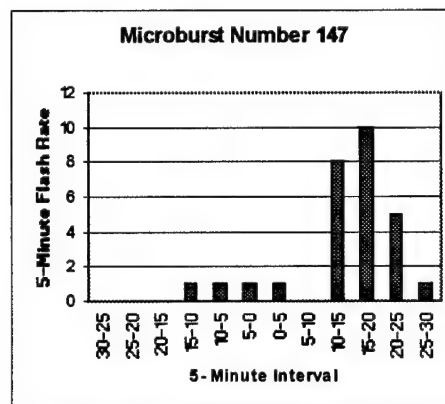
Fig. E39. As in Fig. E1 except for microburst number 147.
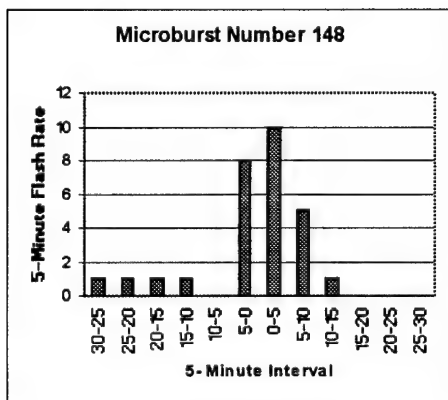
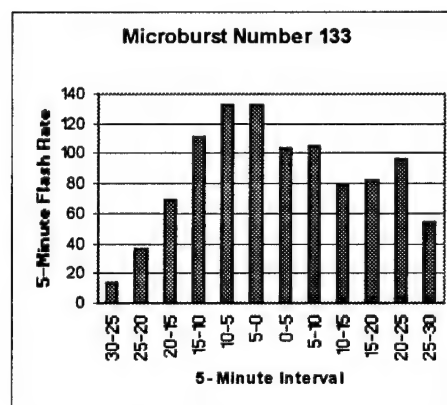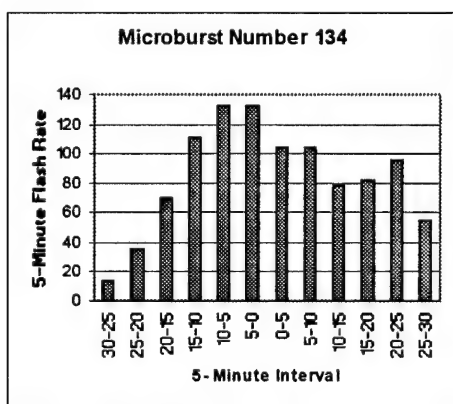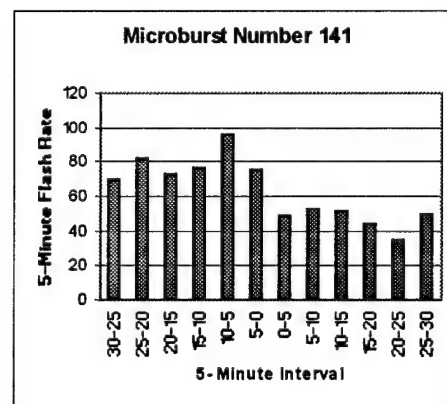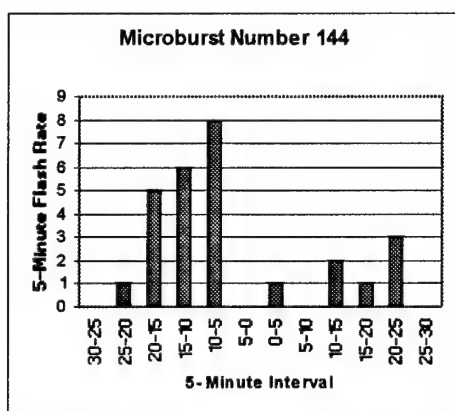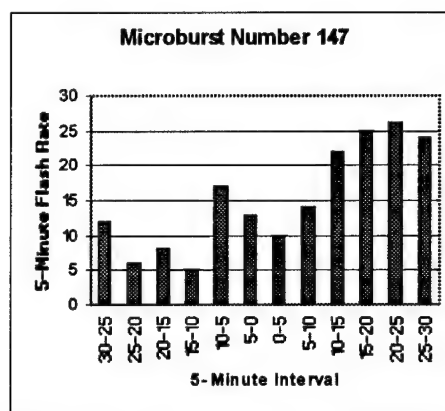Fig. E40. As in Fig. E1 except for microburst number 148.
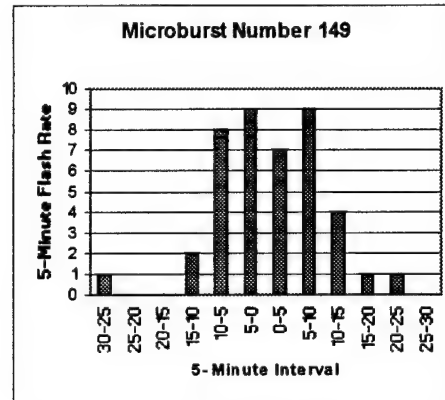
Fig. E41. As in Fig. E1 except for microburst number 149.
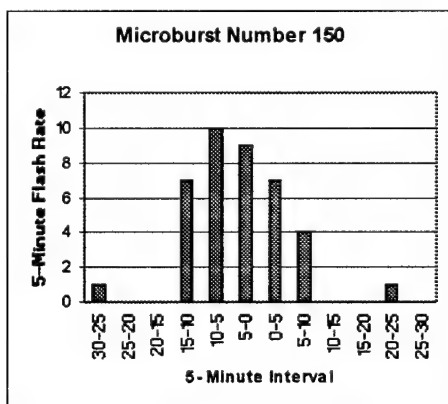
Fig. E42. As in Fig. E1 except for microburst number 150.
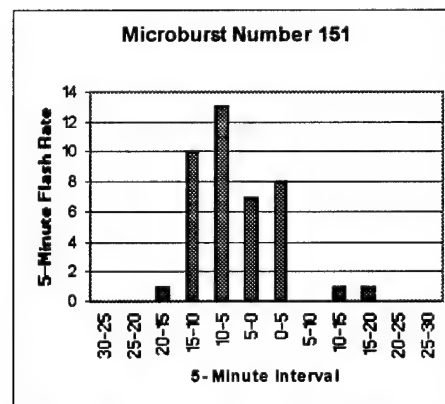
Fig. E43. As in Fig. E1 except for microburst number 151.

Microburst Number 152
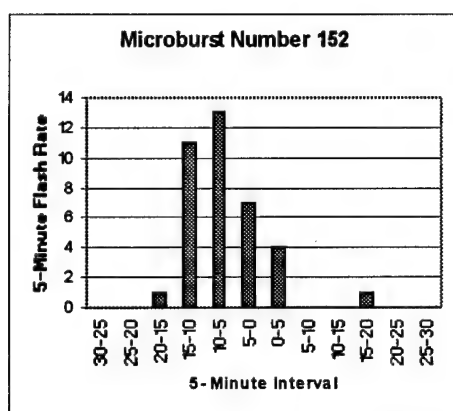
Fig. E44. As in Fig. E1 except for microburst number 152.

Microburst Number 153
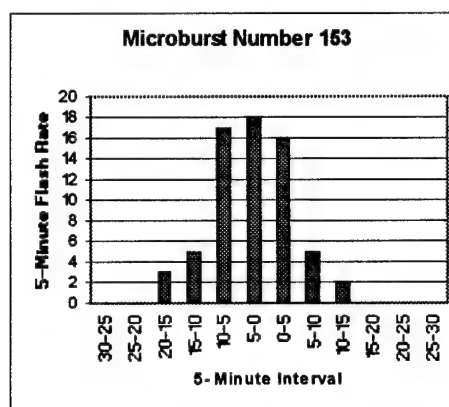
Fig. E45. As in Fig. E1 except for microburst number 153.

Microburst Number 154
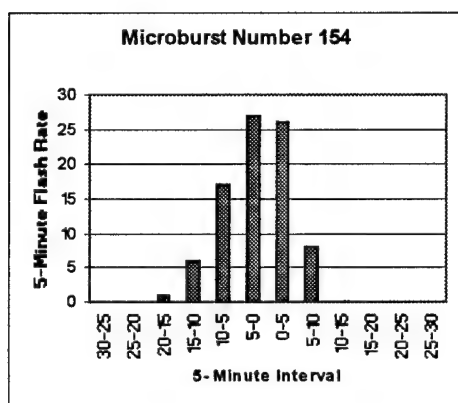
Fig. E46. As in Fig. E1 except for microburst number 154.

Microburst Number 155
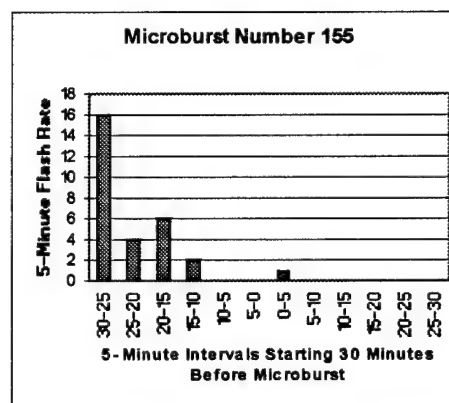
Fig. E47. As in Fig. E1 except for microburst number 155.

Microburst Number 160
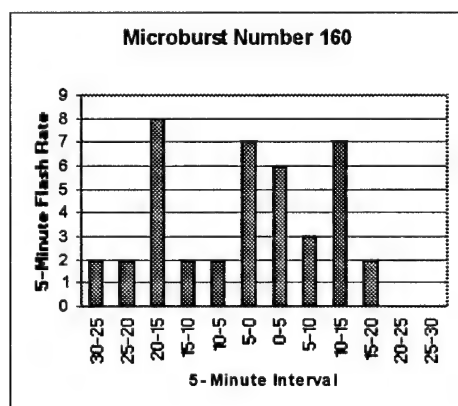
Fig. E48. As in Fig. E1 except for microburst number 160.

Microburst Number 161
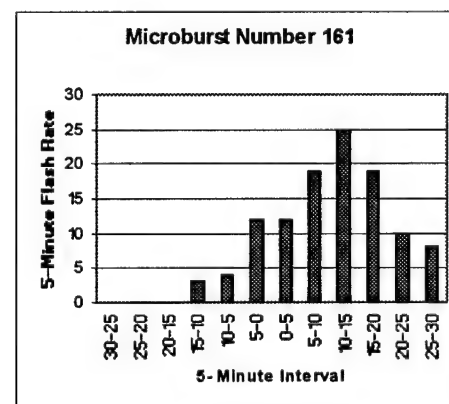
Fig. E49. As in Fi. E1 except for microburst number 161.
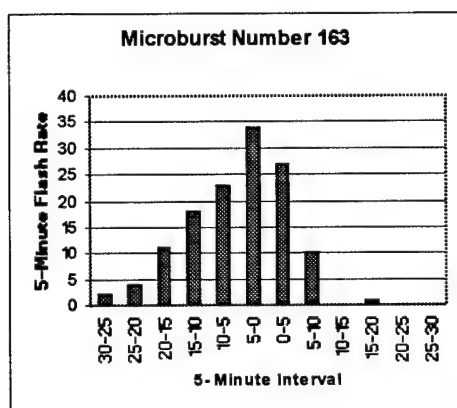
Fig. E50. As in Fig. E1 except for microburst number 163.
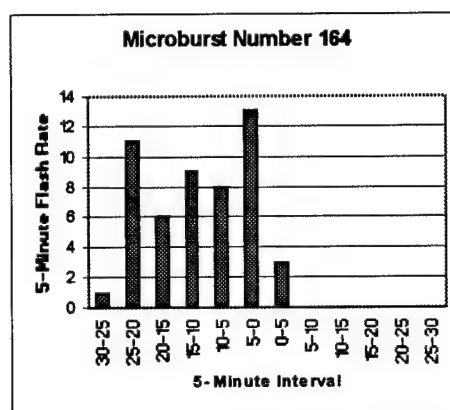
Fig. E51. As in Fig. E1 except for microburst number 164.
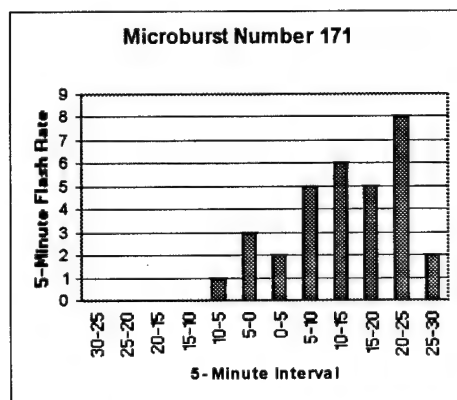
Fig. E52. As in Fig. E1 except for microburst number 171.
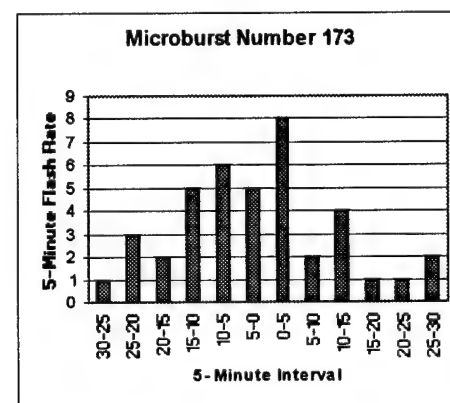
Fig. E53. As in Fig. E1 except for microburst number 173.
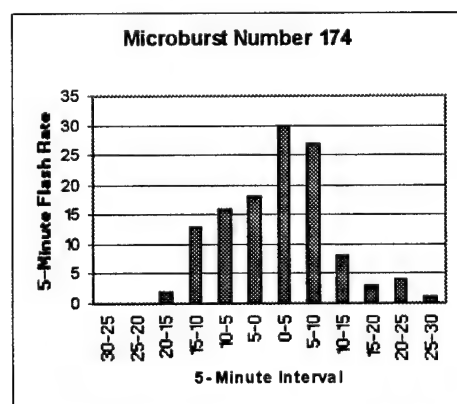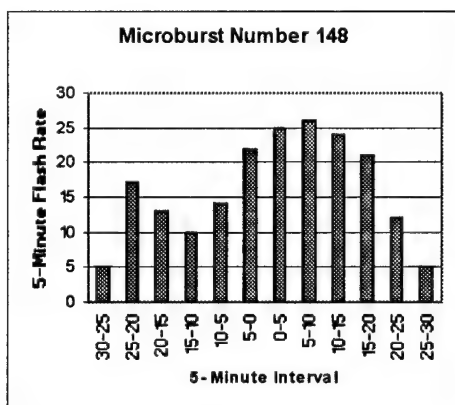

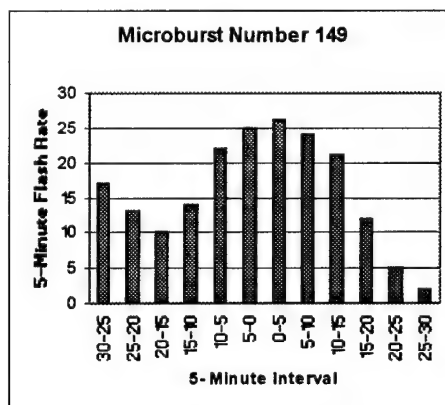Fig. E54. As in Fig. E1 except for microburst number 174.
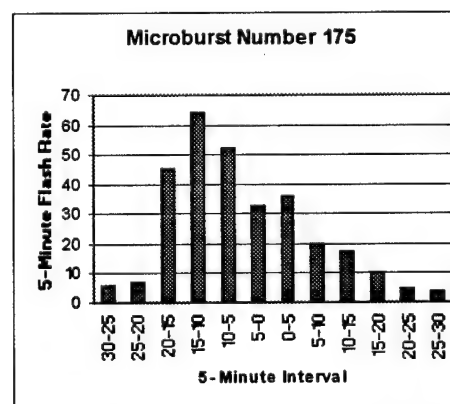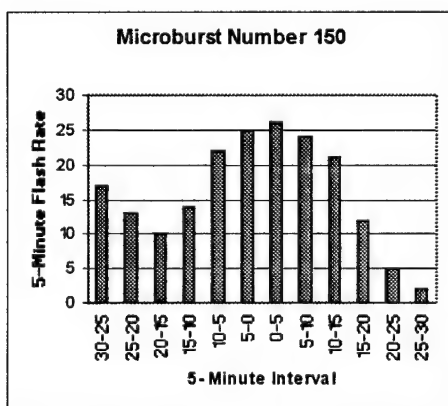

Fig. E55. As in Fig. E1 except for microburst number 175.
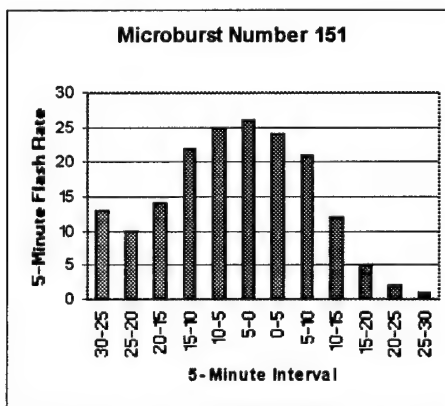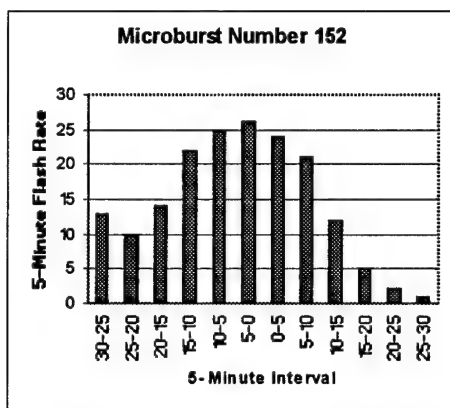
Microburst Number 177
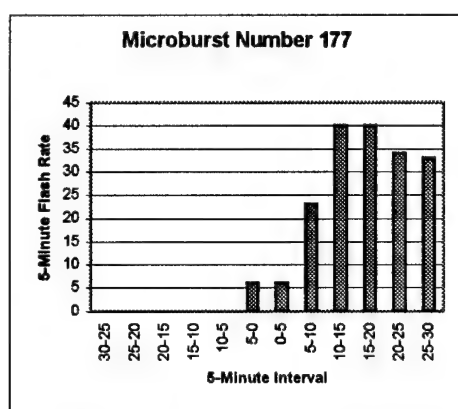
Fig. E56. As in Fig. E1 except for microburst number 176.

Microburst Number 178
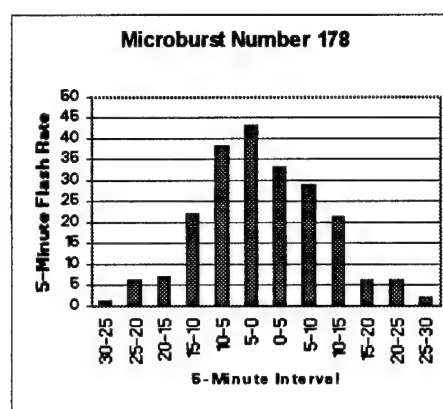
Fig. E57. As in Fig. E1 except for microburst number 178.

Microburst Number 180
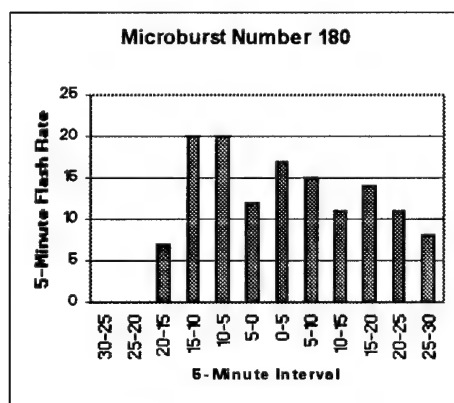
Fig. E58. As in Fig. E1 except for microburst number 180.

Microburst Number 184
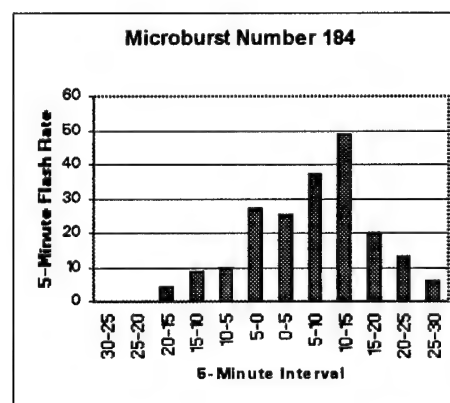
Fig. E59. As in Fig E1 except for microburst number 184.

Microburst Number 189
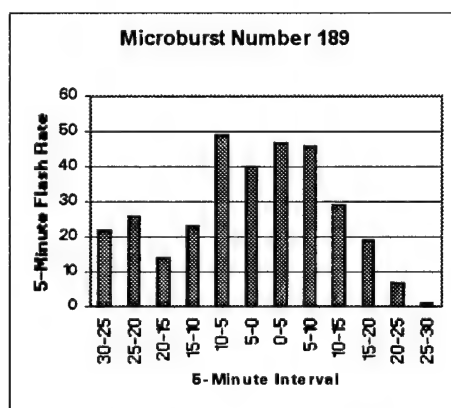
Fig. E60. As in Fig. E1 except for microburst number 189.

Microburst Number 190
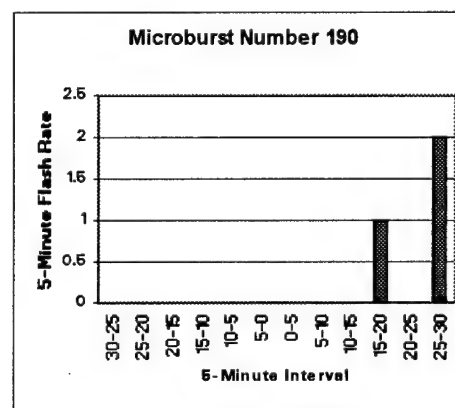
Fig. E61. As in Fig. E1 except for microburst number 190.
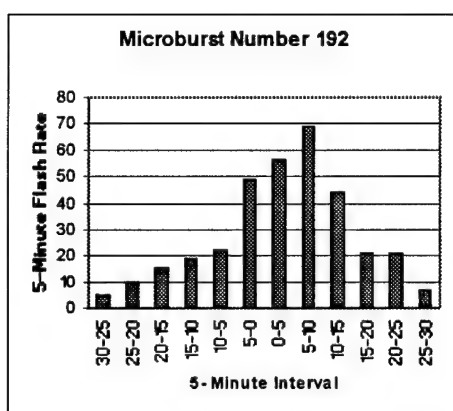
Fig. E62. As in Fig. E1 except for microburst number 192.
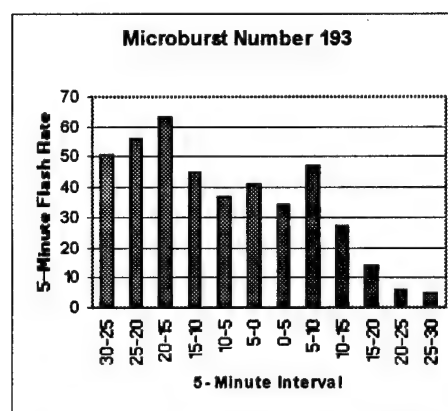
Fig. E63. As in Fig. E1 except for microburst number 193.
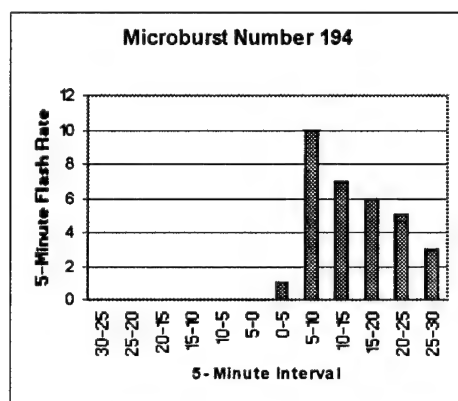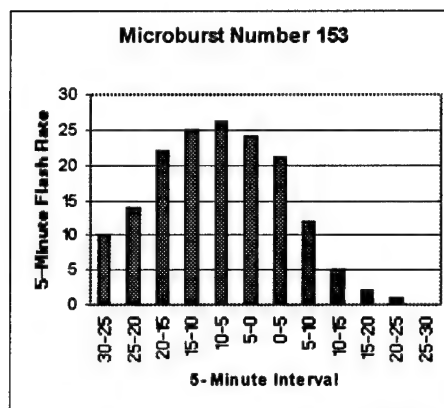

Fig. E64. As in Fig. E1 except for microburst number 194.
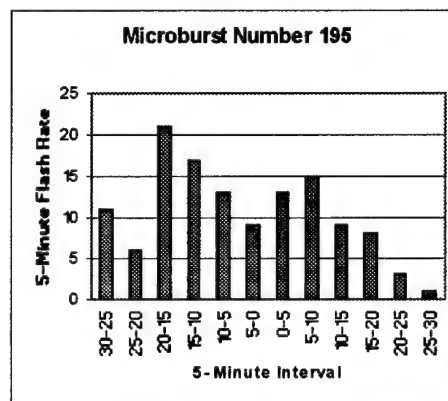
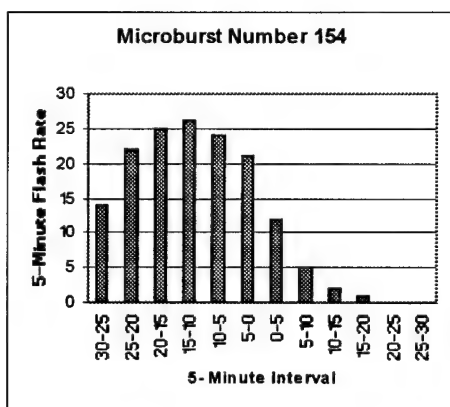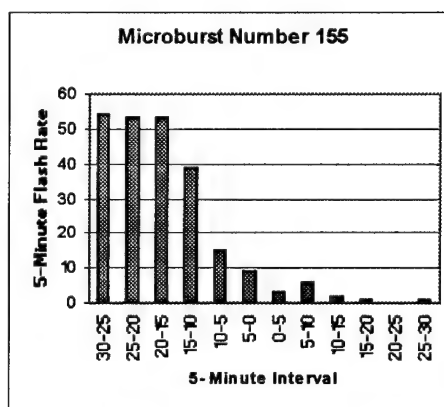Fig. E65. As in Fig. E1 except for microburst number 195.
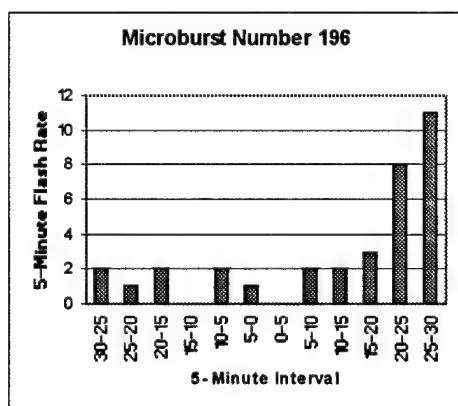
Fig. E66. As in Fig. E1 except for microburst number 196.
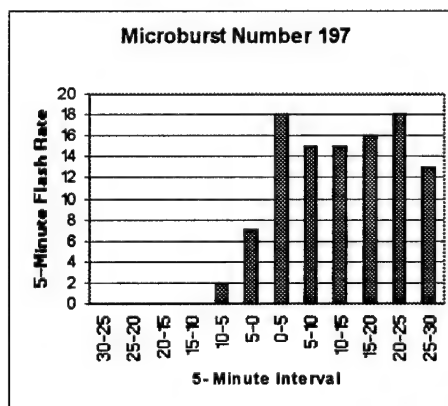
Fig. E67. As in Fig. E1 except for microburst number 197.
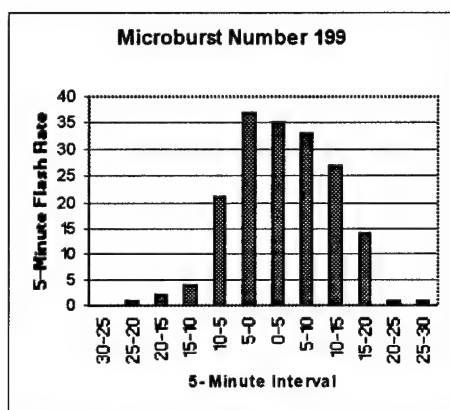
Fig. E68. As in Fig. E1 except for microburst number 199.
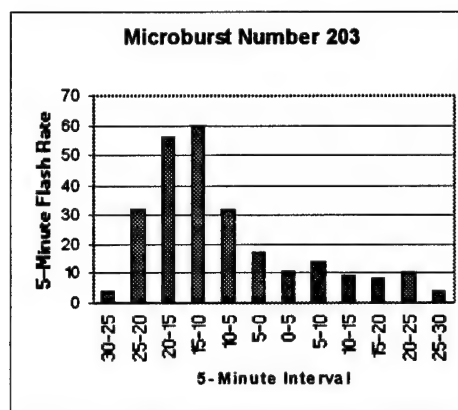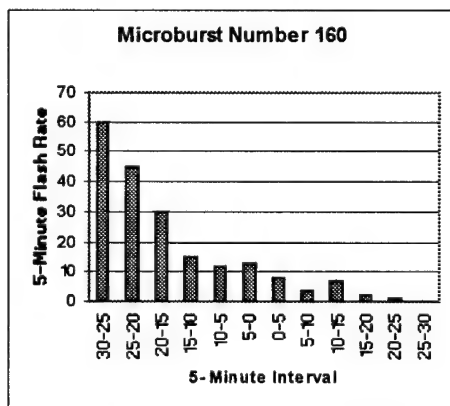

Fig. E69. As in Fig. E1 except for microburst number 203.
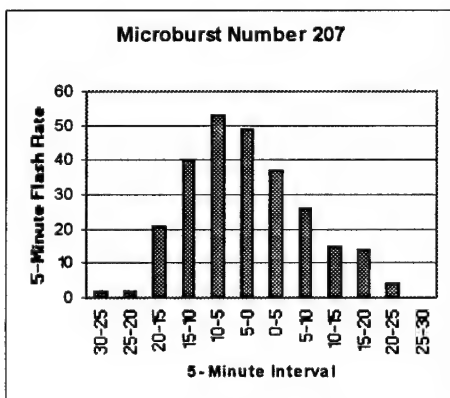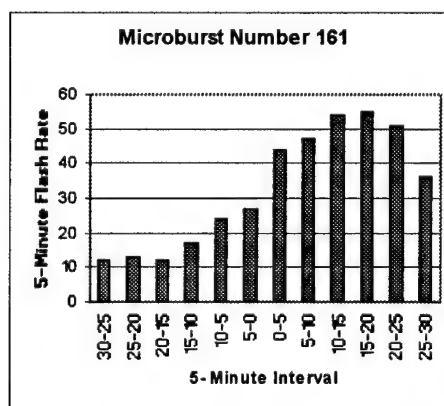

Fig. E70. As in Fig. E1 except for microburst number 207.
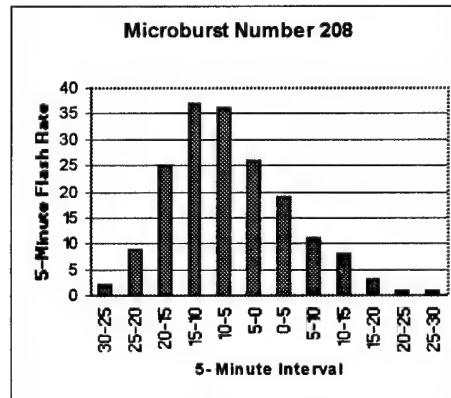
Fig. E71. As in Fig. E1 except for microburst number 208.
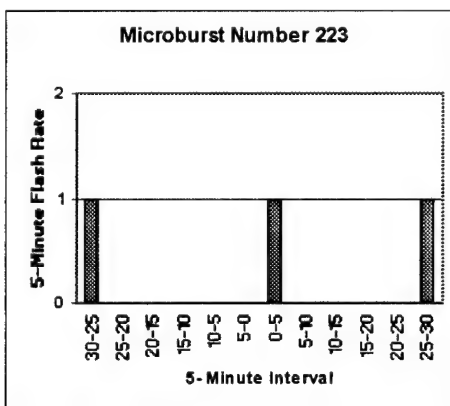
Fig. E72. As in Fig. E1 except for microburst number 223.
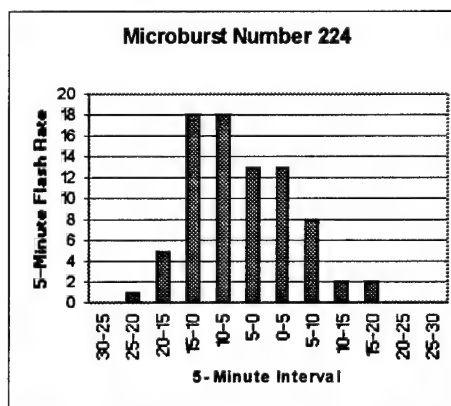
Fig. E73. As in Fig. E1 except for microburst number 224.
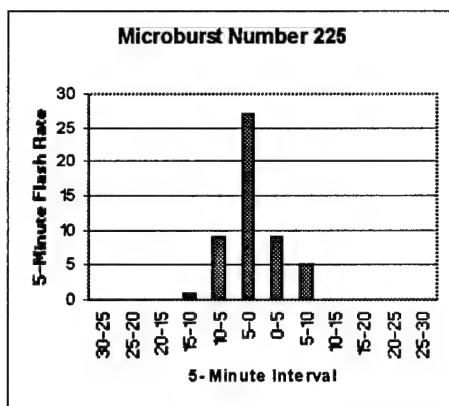
Fig. E74. As in Fig. E1 except for microburst number 225.
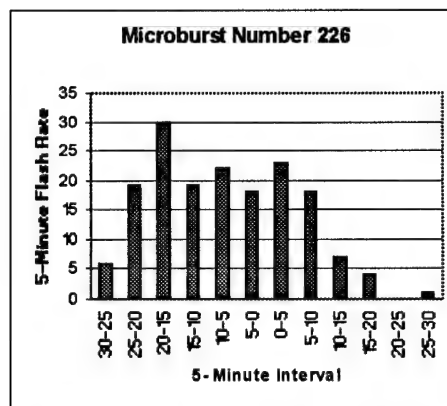
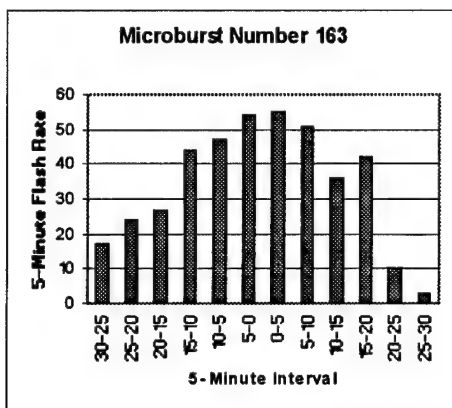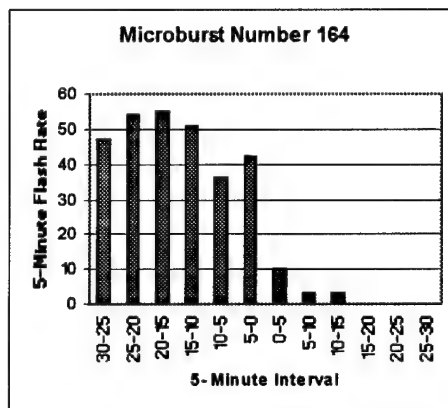Fig. E75. As in Fig. E1 except for microburst number 226.
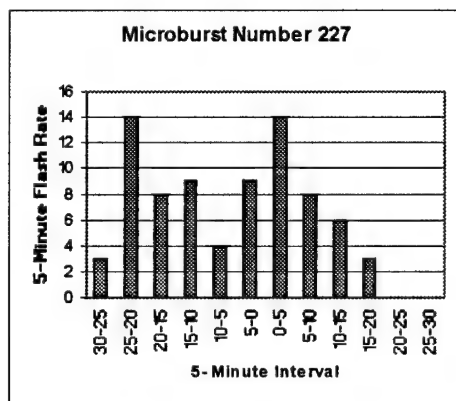
Fig. E76. As in Fig. E1 except for microburst number 227.
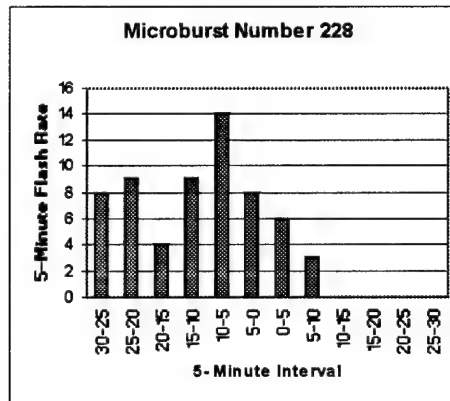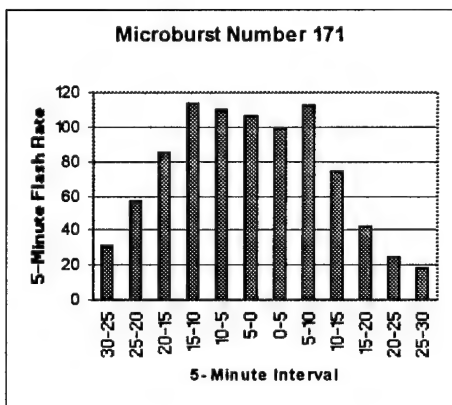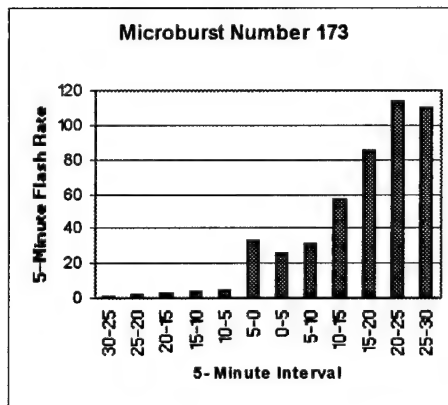

Fig. E77. As in Fig. E1 except for microburst number 228.
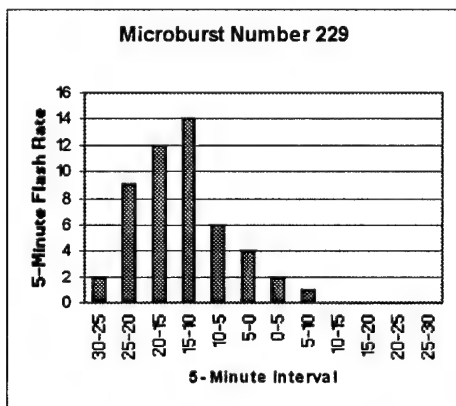
Fig. E78. As in Fig. E1 except for microburst number 229.
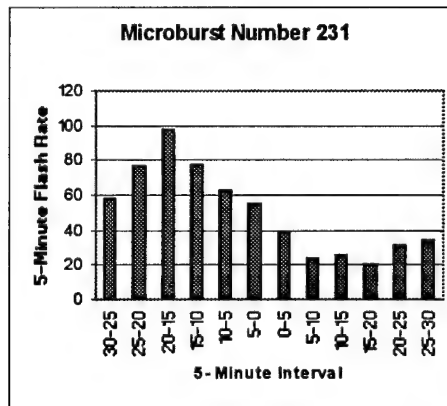
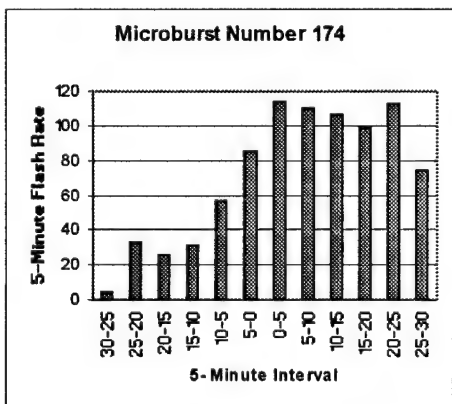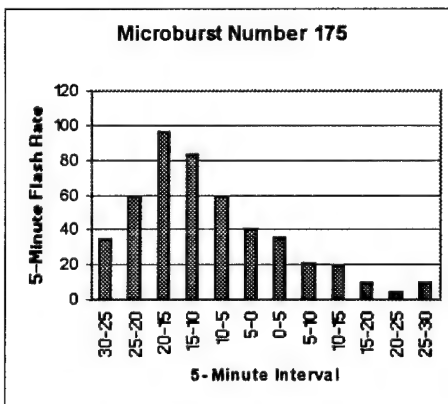Fig. E79. As in Fig. E1 except for microburst number 231.

Microburst Number 236
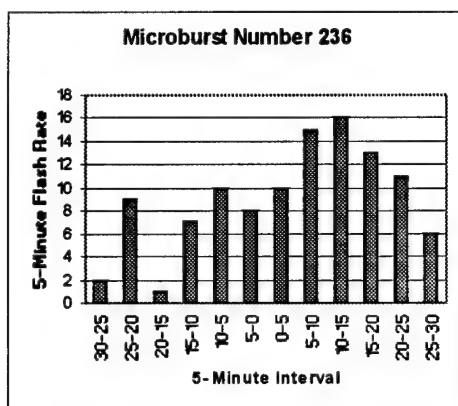
Fig. E80. As in Fig. E1 except for microburst number 236.

Microburst Number 237
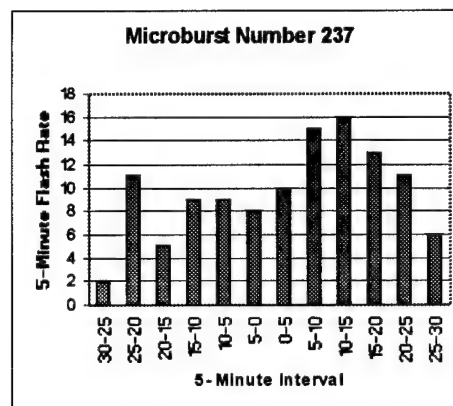
Fig. E81. As in Fig. E1 except for microburst number 237.

Microburst Number 238
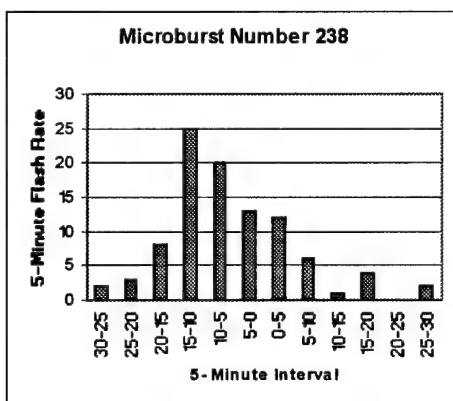
Fig. E82. As in Fig. E1 except for microburst number 238.

Microburst Number 241
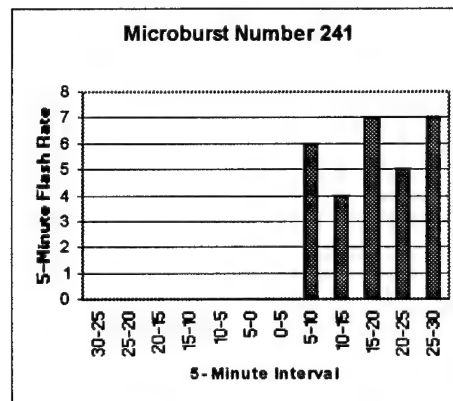
Fig. E83. As in Fig. E1 except for microburst number 241.

Microburst Number 242
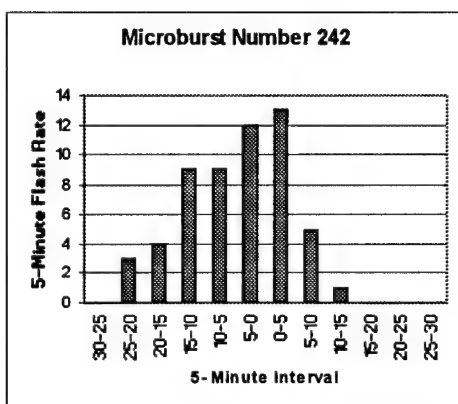
Fig. E84. As in Fig. E1 except for microburst number 242.

Microburst Number 244
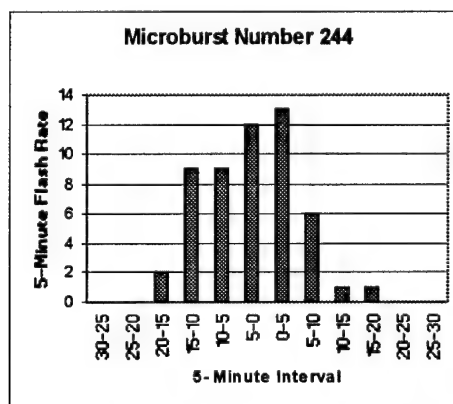
Fig. E85. As in Fig. E1 except for microburst number 244.

Microburst Number 247
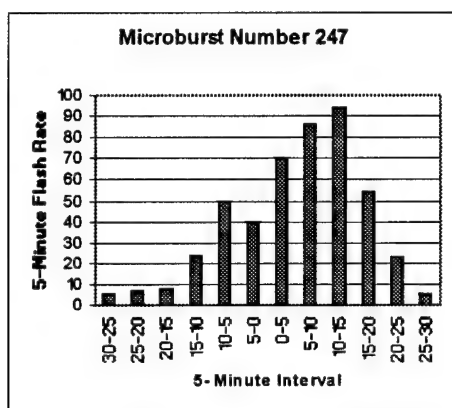
Fig. E86. As in Fig. E1 except for microburst number 246.

Microburst Number 250
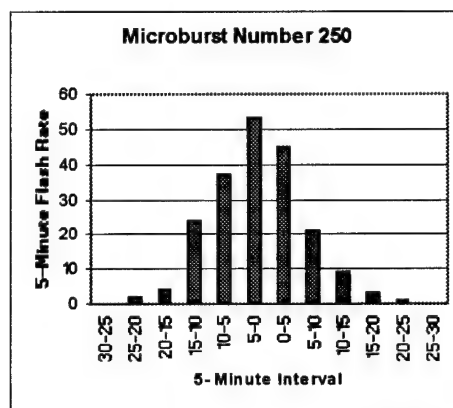
Fig. E87. As in Fig. E1 except for microburst number 250.

Microburst Number 251
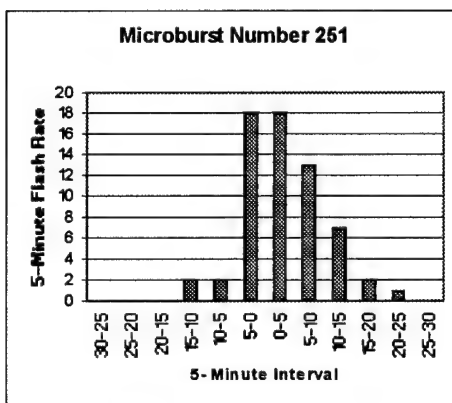
Fig. E88. As in Fig. E1 except for microburst number 251.

Microburst Number 252
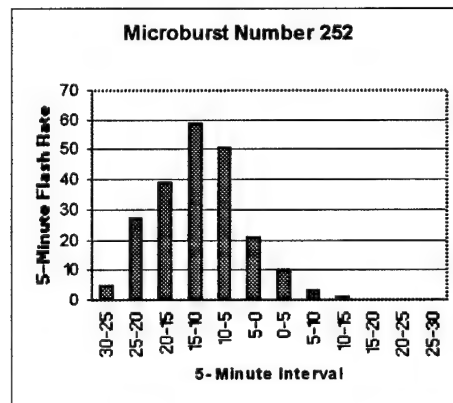
Fig. E89. As in Fig. E1 except for microburst number 252.

Microburst Number 253
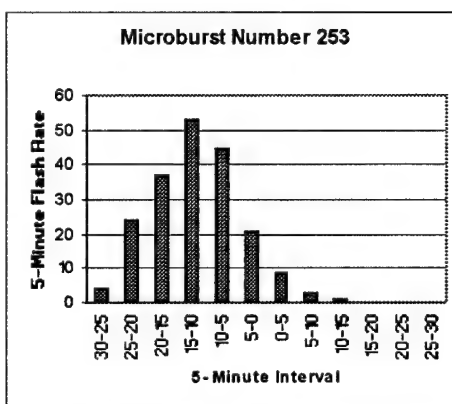
Fig. E90. As in Fig. E1 except for microburst number 253.

Microburst Number 254
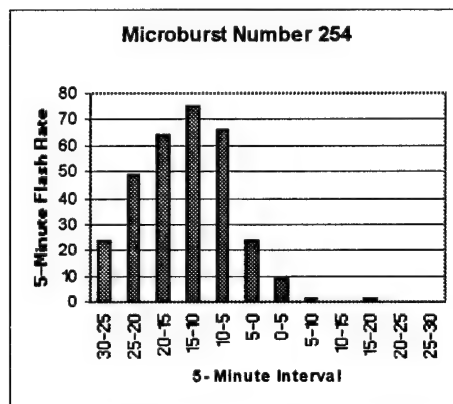
Fig. E91. As in Fig. E1 except for microburst number 254.
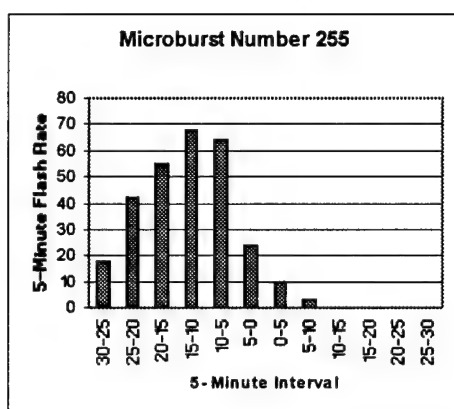
Fig. E92. As in Fig. E1 except for microburst number 255.
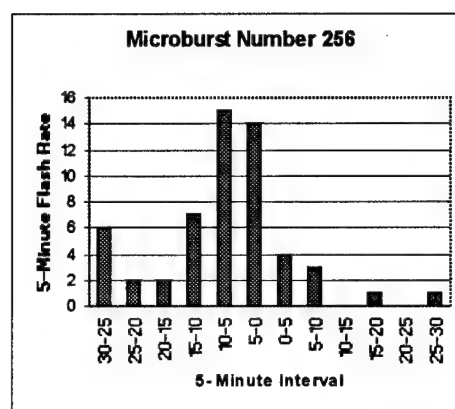
Fig. E93. As in Fig. E1 except for microburst number 256.
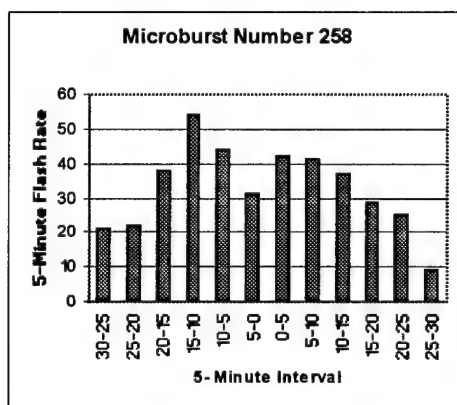
Fig. E94. As in Fig. E1 except for microburst number 258.
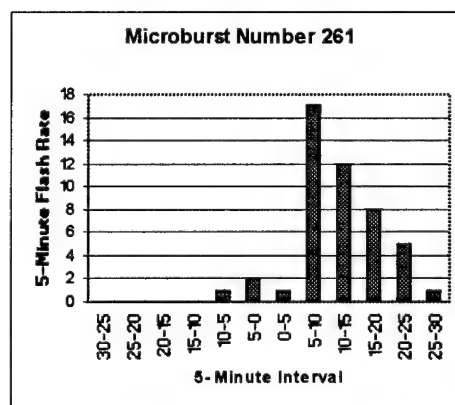
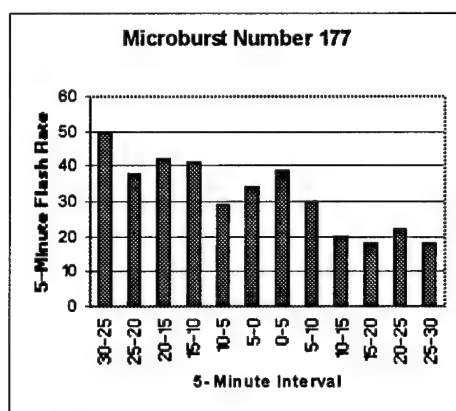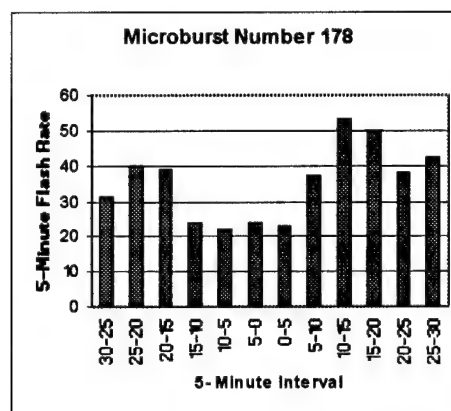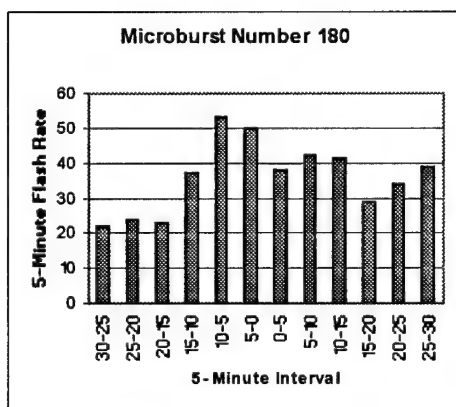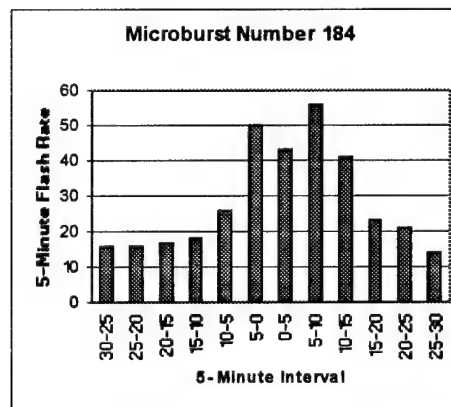Fig. E95. As in Fig. E1 except for microburst number 261.
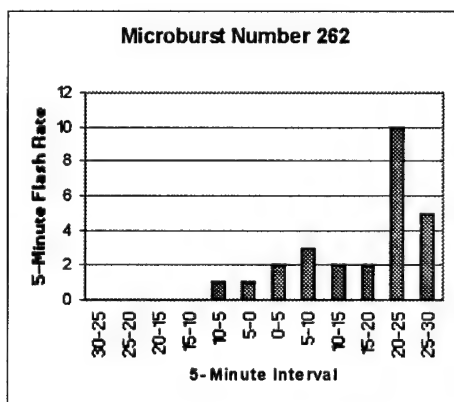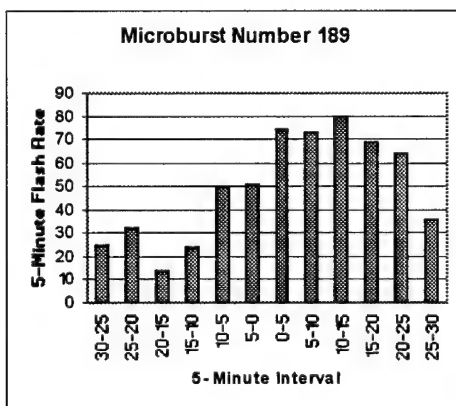

Fig. E96. As in Fig. E1 except for microburst number 262.
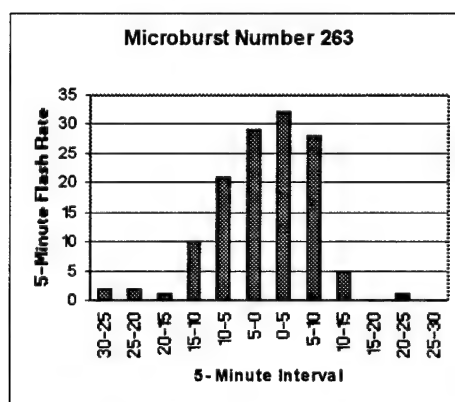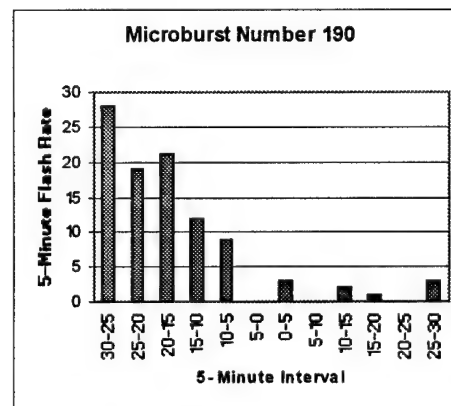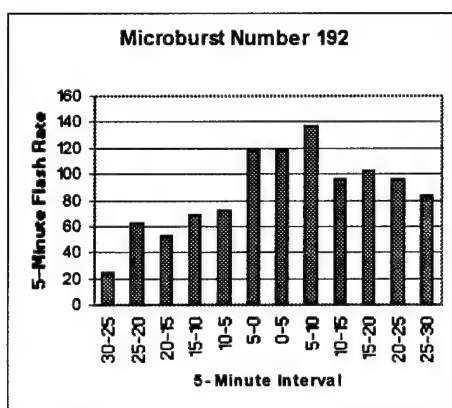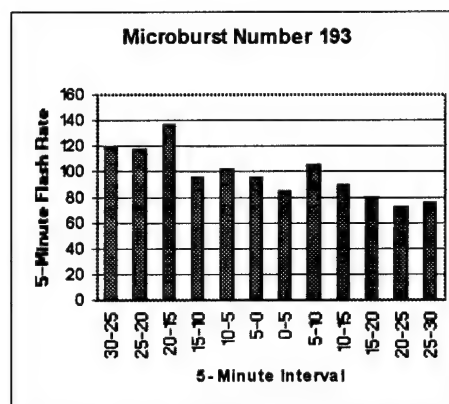

Fig. E97. As in Fig. E1 except for microburst number 263.

Microburst Number 264
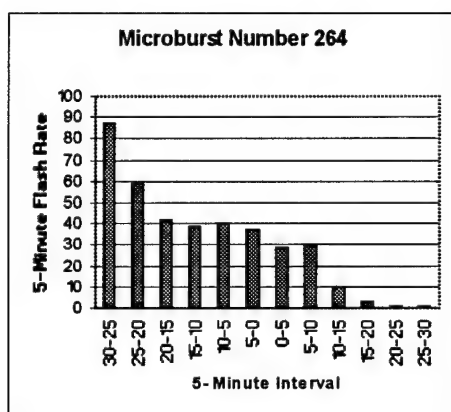
Fig. E98. As in Fig E1 except for microburst number 264.

Microburst Number 265
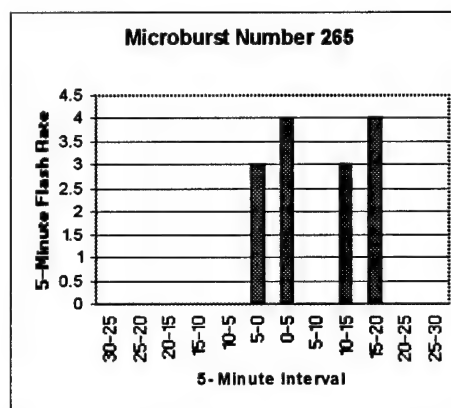
Fig. E99. As in Fig. E1 except for microburst number 265.

Microburst Number 272
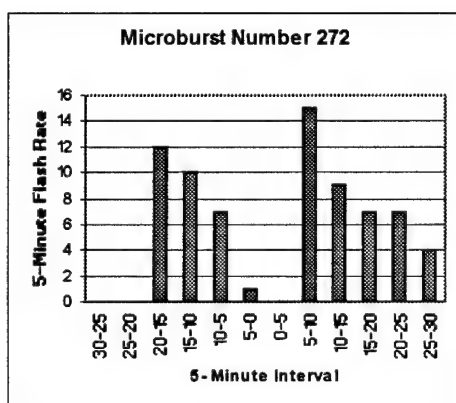
Fig. E100. As in Fig. E1 except for microburst number 272.

Microburst Number 273
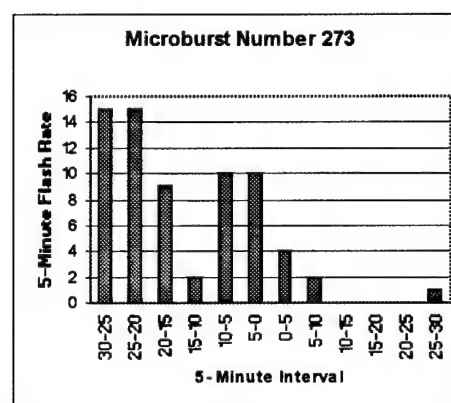
Fig. E101. As in Fig. E1 except for microburst number 273.

Microburst Number 275
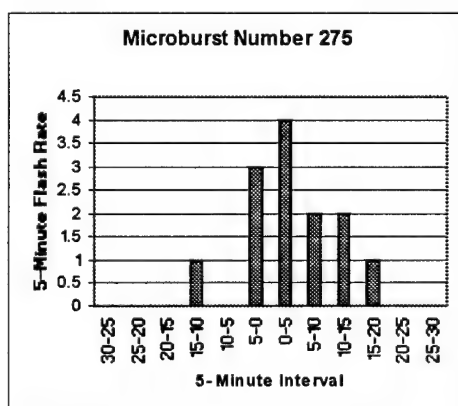
Fig. E102. As in Fig. E1 except for microburst number 275.

Microburst Number 277
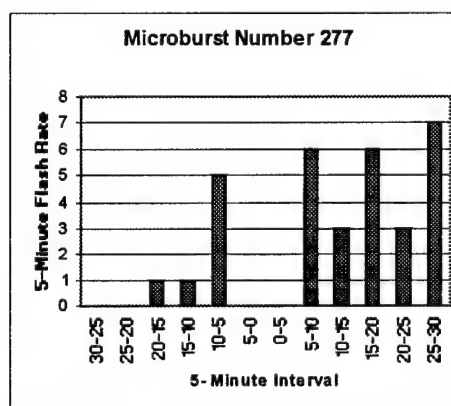
Fig. E103. As in Fig. E1 except for microburst number 277.
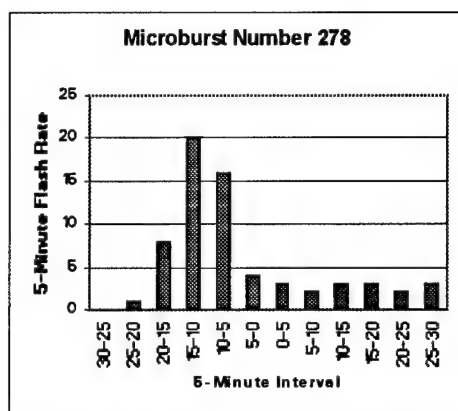
Fig. E104. As in Fig.E1 except
for microburst number 278.

APPENDIX F

MICROBURST AND FLASH RATE TEMPORAL RELATIONSHIP FOR ALL

MICROBURSTS GREATER THAN 34 KNOTS USING AREA OF STUDY GRID

BOX
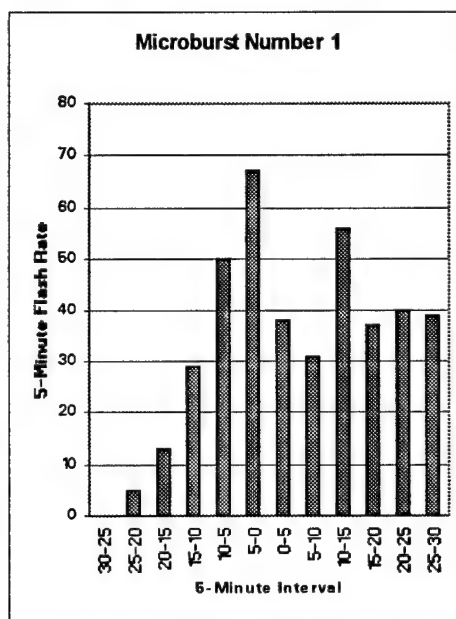
Fig. F1. Microburst and cloud-to-ground (CG) flash rate temporal relationship starting 30 minutes before and ending 30 minutes after microbursts greater than 34 knots using the area of study grid box The CG flash rate is divided into 5-minute intervals. The microburst number corresponds to Table C1 in Appendix C.
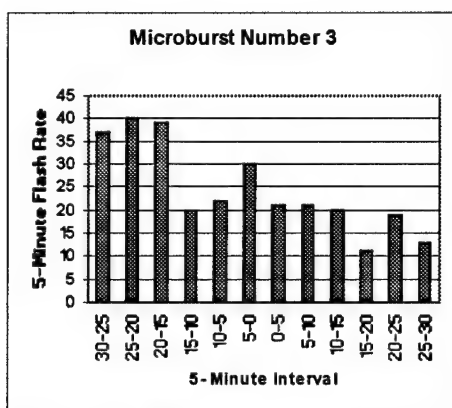
Fig. F2. As in Fig. F1 except for microburst number 3.
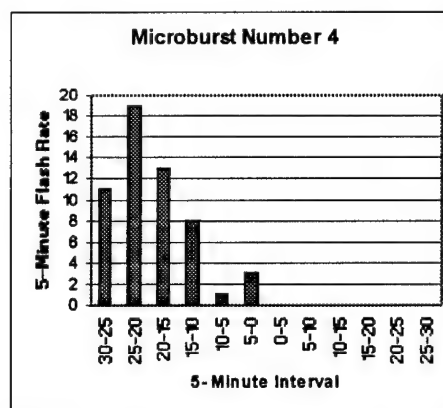
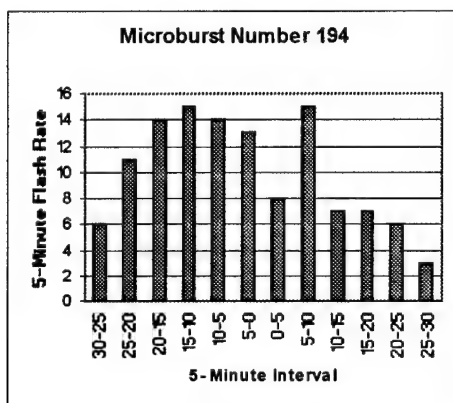Fig. F3. As in Fig. F1 except for microburst number 4.
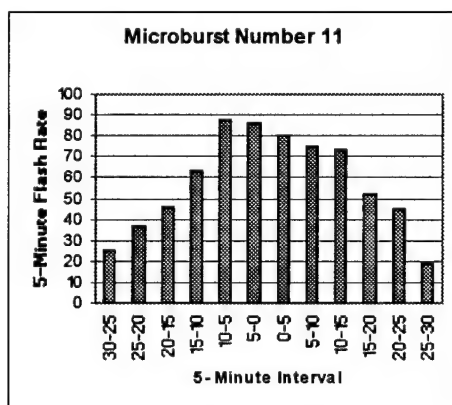
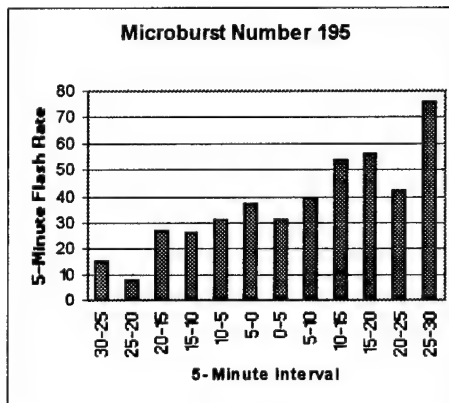Fig. F4. As in Fig. F1 except for microburst number 11.
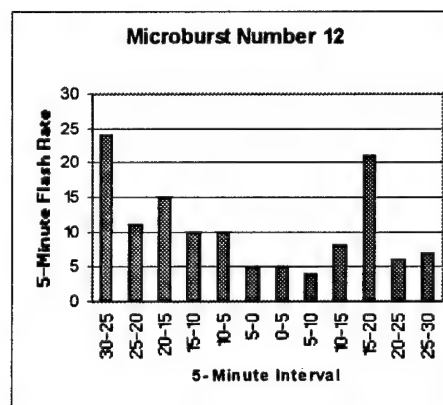
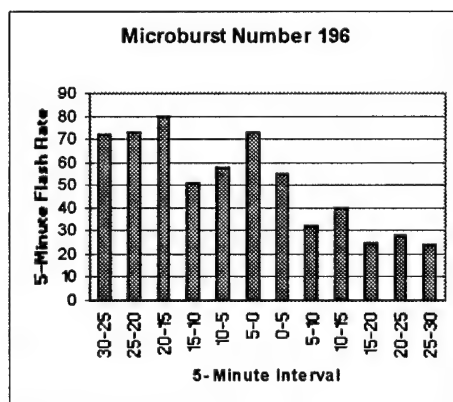
Fig. F5. As in Fig. F1 except for microburst number 12.
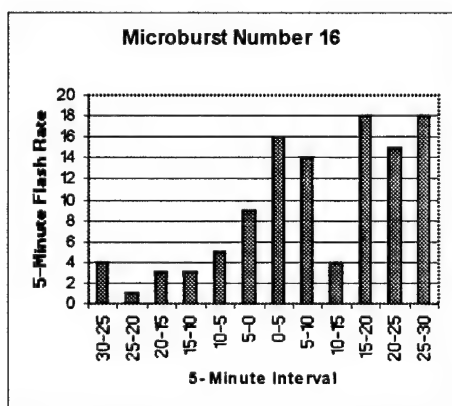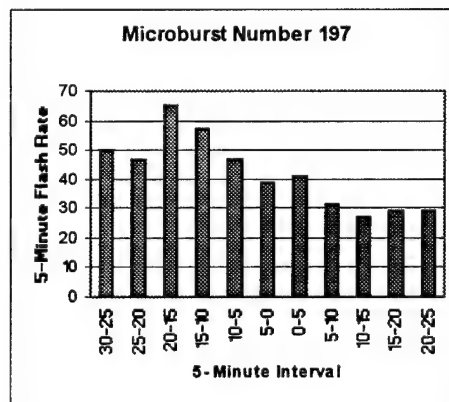

Fig. F6. As in Fig. F1 except for microburst number 16.
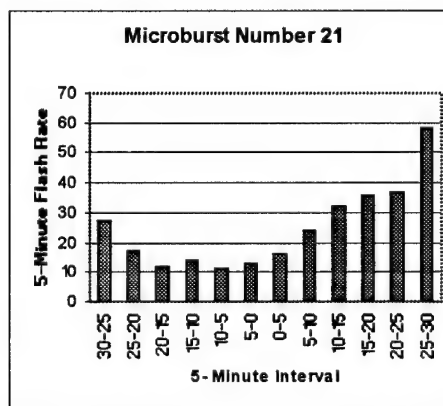
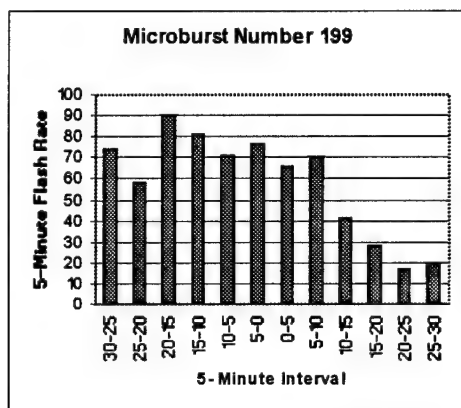

Fig. F7. As in Fig. F1 except for microburst number 21.
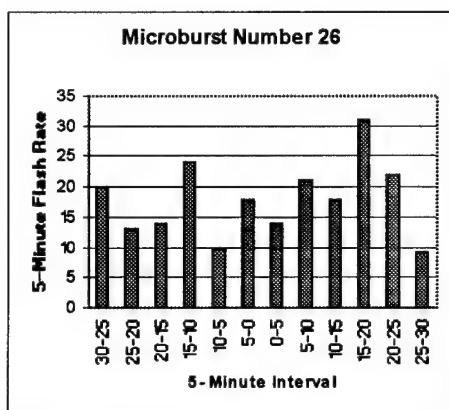
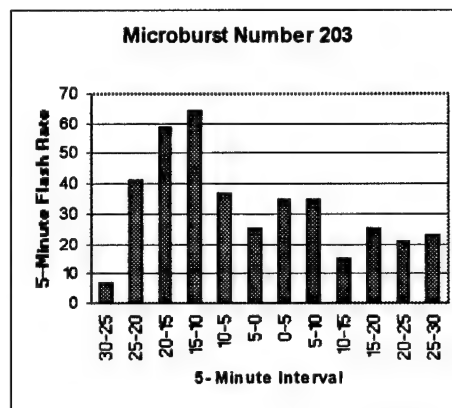Fig. F8. As in Fig. F1 except for microburst number 26.
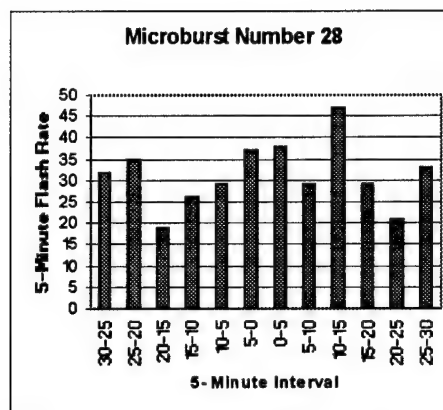
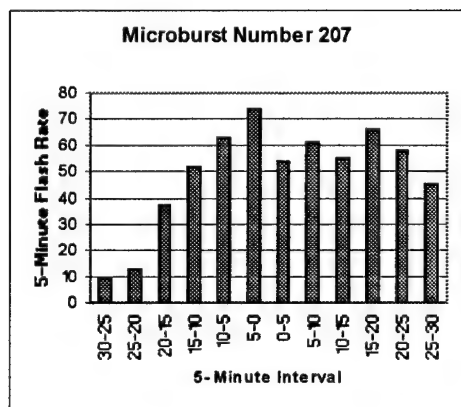Fig. F9. As in Fig. F1 except for microburst number 28.
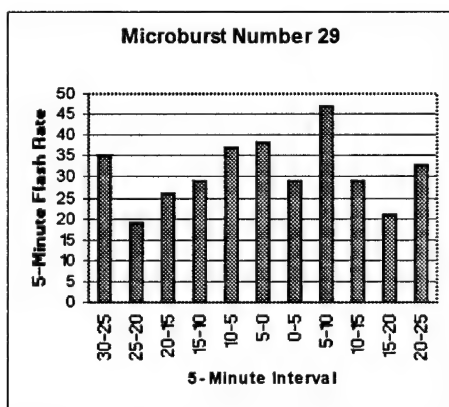
Fig. F10. As in Fig. F1 except for microburst number 29.
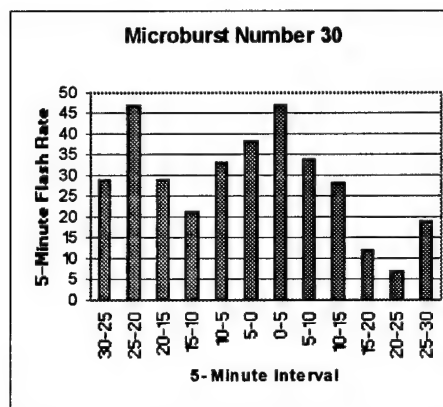
Fig. F11. As in Fig. F1 except for microburst number 30.
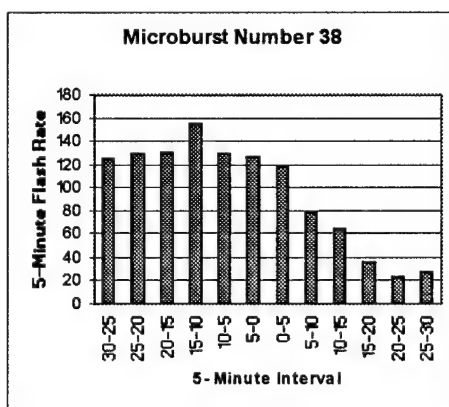
Fig. F12. As in Fig. F1 except for microburst number 38.
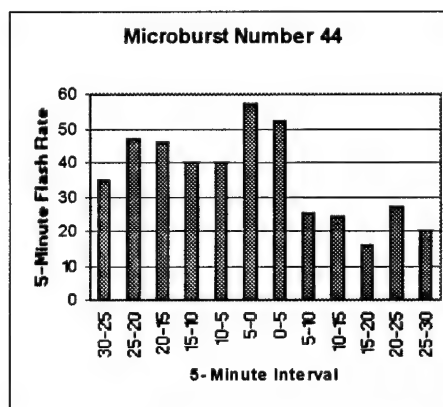
Fig. F13. As in Fig. F1 except for microburst number 44.
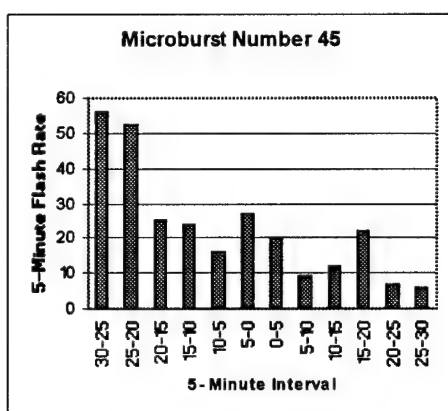
Fig. F14. As in Fig. F1 except for microburst number 45.
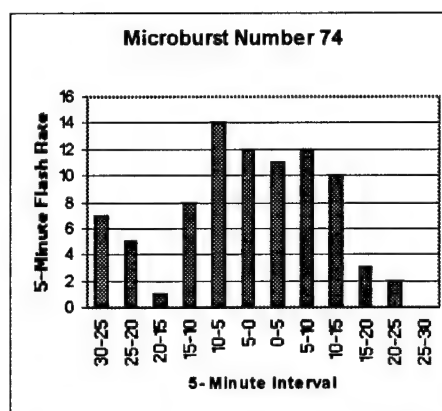
Fig. F15. As in Fig. F1 except for microburst number 74.
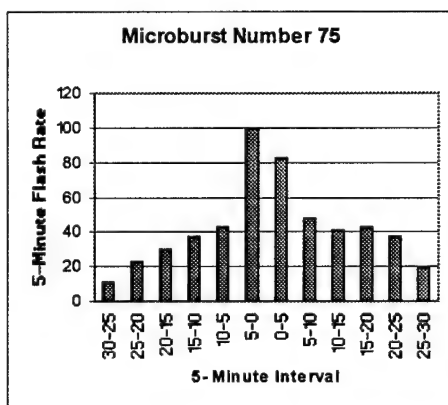
Fig. F16. As in Fig. F1 except for microburst number 75.
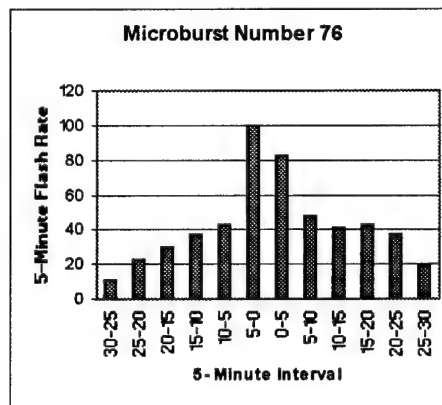
Fig. F17. As in Fig. F1 except for microburst number 76.
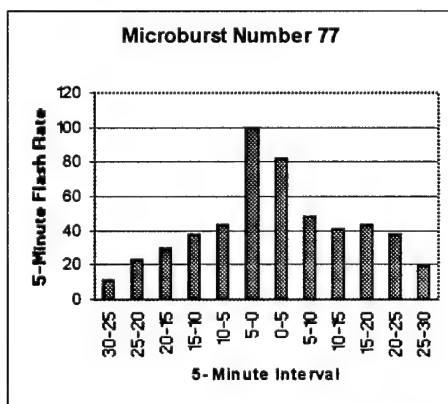
Fig. F18. As in Fig. F1 except for microburst number 77.
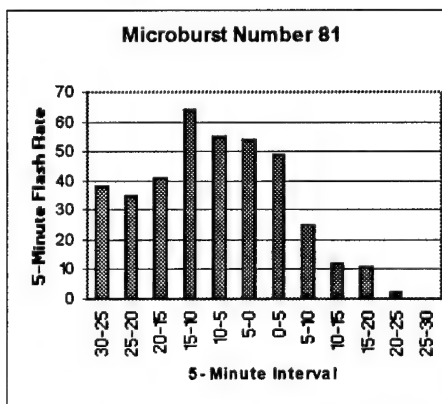
Fig. F19. As in Fig. F1 except for microburst number 81.
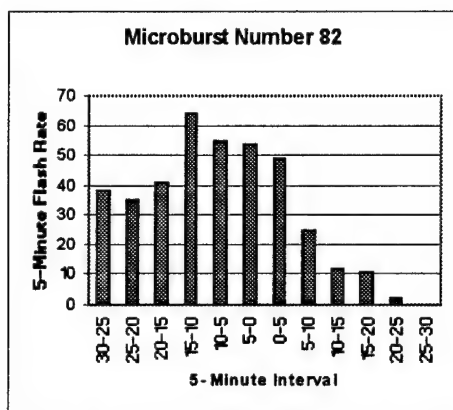
Fig. F20. As in Fig. F1 except for microburst number 82.
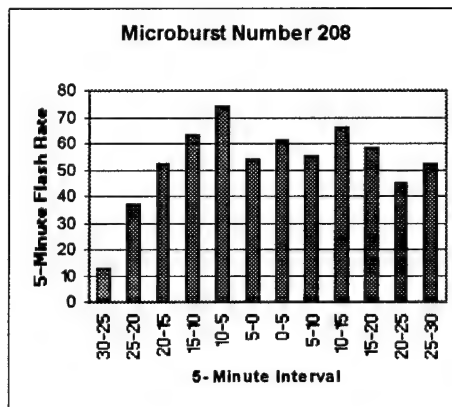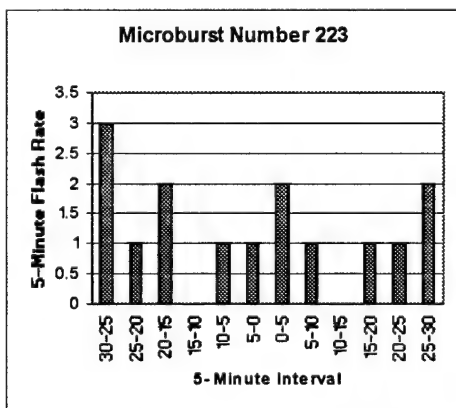
Fig. F21. As in Fig. F1 except for microburst number 83.
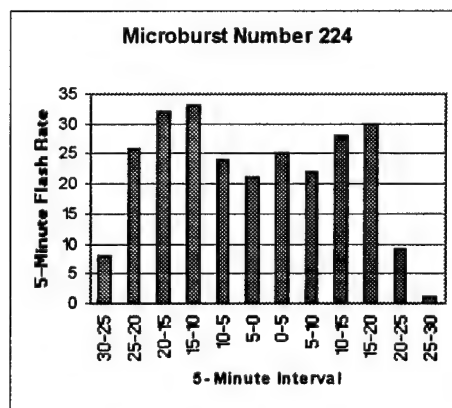
Fig. F22. As in Fig. F1 except for microburst number 86.

Fig. F23. As in Fig. F1 except for microburst number 88.
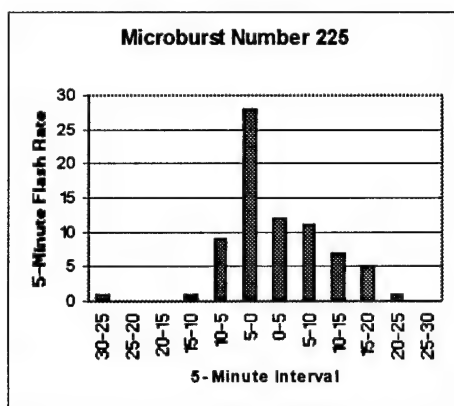
Fig. F24. As in Fig. F1 except for microburst number 89.

Fig. F25. As in Fig. F1 except for microburst number 91.

Fig. F26. As in Fig. F1 except for microburst number 97.

Fig. F27. As in Fig. F1 except for microburst number 98.

Fig. F28. As in F1 except for microburst number 108.

Fig. F29. As in Fig. F1 except for microburst number 116.

Fig. F30. As in Fig. F1 except for microburst number 119.

Fig. F31. As in Fig. F1 except for microburst number 120.

Fig. F32. As in Fig. F1 except for microburst number 122.

Fig. F33. As in Fig. F1 except for microburst number 123.
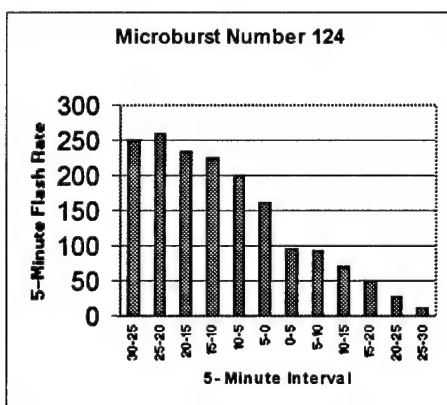
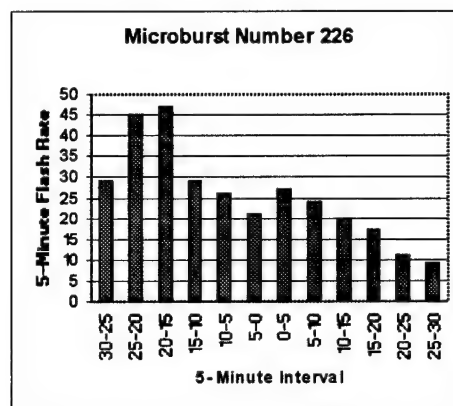Fig. F34. As in Fig. F1 except for microburst number 124.

Fig. F35. As in Fig. F1 except for microburst number 133.
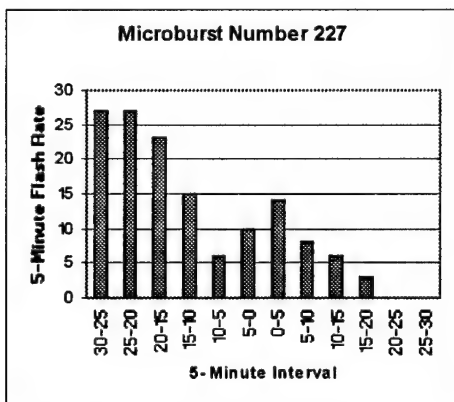
Fig. F36. As in Fig. F1 except for microburst number 134.
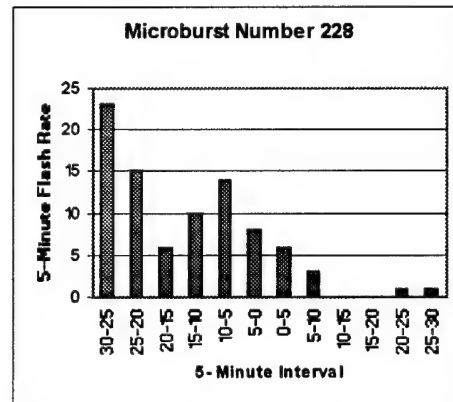
Fig. F37. As in Fig. F1 except for microburst number 141.
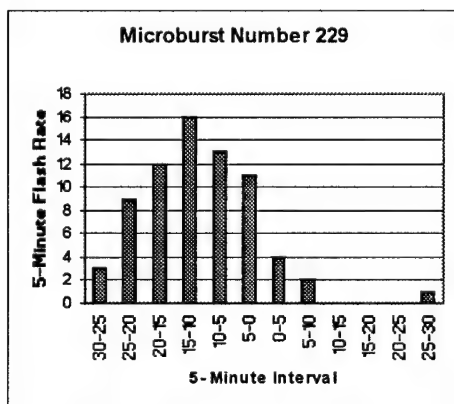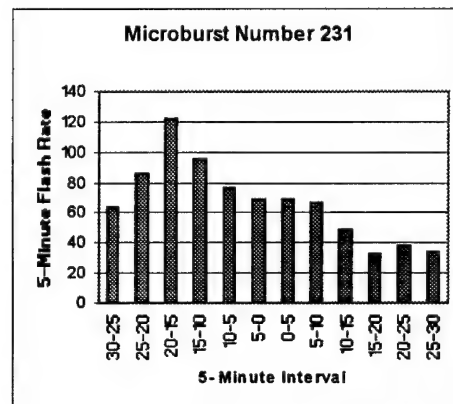
Microburst Number 144

Fig. F38. As in Fig. F1 except for microburst number 38.

Microburst Number 147

Fig. F39. As in Fig. F1 except for microburst number 147.

Microburst Number 148

Fig. F40. As in Fig. F1 except for microburst number 148.

Microburst Number 149

Fig. F41. As in Fig. F1 except for microburst number 149.

Microburst Number 150

Fig. F42. As in Fig. F1 except for microburst number 150.

Microburst Number 151

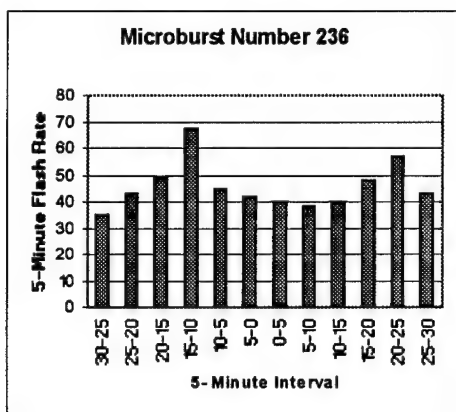Fig. F43. As in Fig. F1 except for microburst number 151.

Fig. F44. As in Fig. F1 except for microburst number 152.

Fig. F45. As in Fig. F1 except for microburst number 153.

Fig. F46. As in Fig. F1 except for microburst number 154.

Fig. F47. As in Fig. F1 except for microburst number 155.

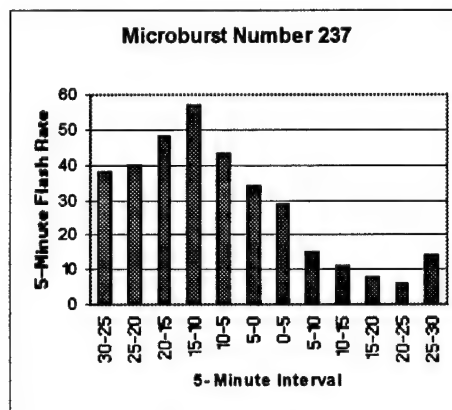Fig. F48. As in Fig. F1 except for microburst number 160.

Fig. F49. As in Fig. F1 except for microburst number 161.

Fig. F50. As in Fig. F1 except for microburst number 163.
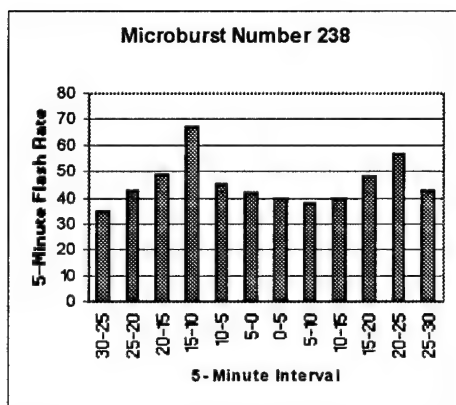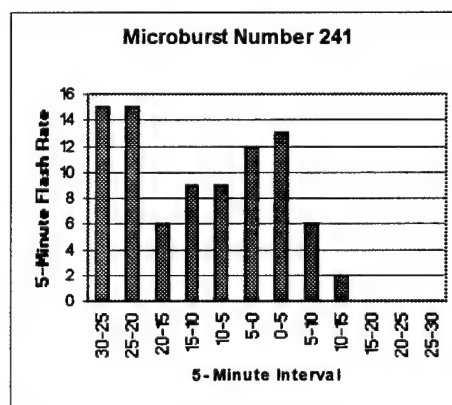

Fig. F51. As in Fig. F1 except for microburst number 164.

Fig. F52. As in Fig. F1 except for microburst number 171.
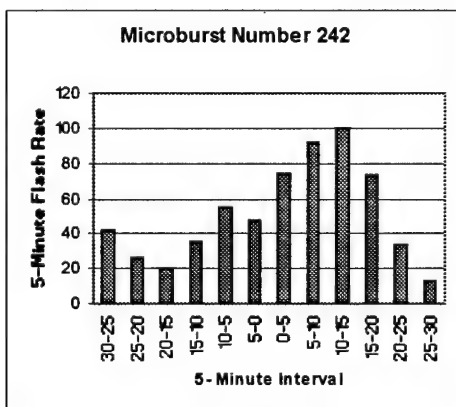

Fig. F53. As in Fig. F1 except for microburst number 173.

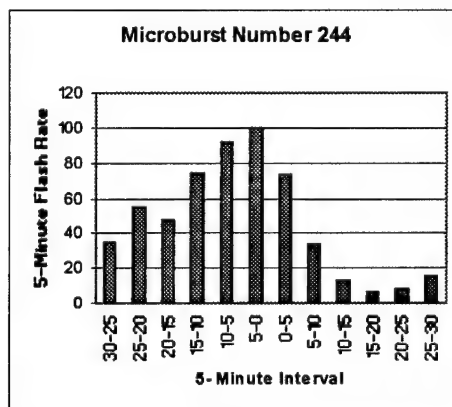Fig. F54. As in Fig. F1 except for microburst number 174.
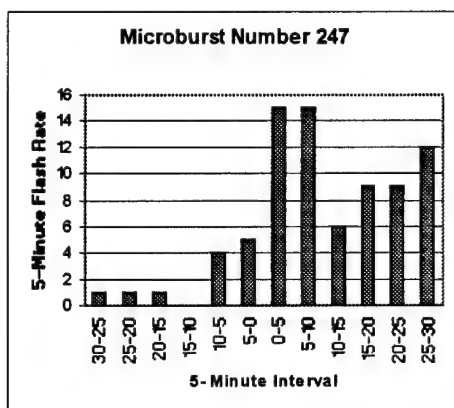

Fig. F55. As in Fig. F1 except for microburst number 175.

Microburst Number 177

Fig. F56. As in Fig. F1 except for microburst number 177.

Microburst Number 178

Fig. F57. As in Fig. F1 except for microburst number 178.

Microburst Number 180

Fig. F58. As in Fig. F1 except for microburst number 180.

Microburst Number 184

Fig. F59. As in Fig. F1 except for microburst number 184.

Microburst Number 189

Fig. F60. As in Fig.1 except for microburst number 189.

Microburst Number 190

Fig. F61. As in Fig. 1 except for microburst number 190.

Fig. F62. As in Fig. F1 except for microburst number 192.

Fig. F63. As in Fig. F1 except for microburst number 193.

Fig. F64. As in Fig. F1 except for microburst number 194.

Fig. F65. As in Fig. F1 except for microburst number 195.

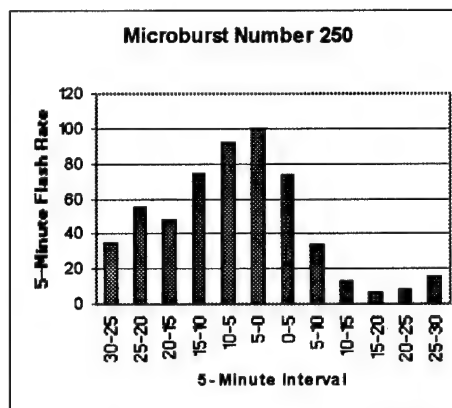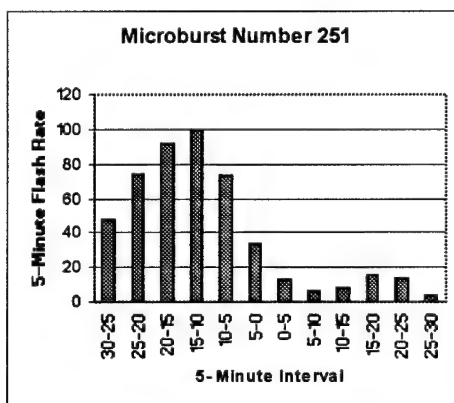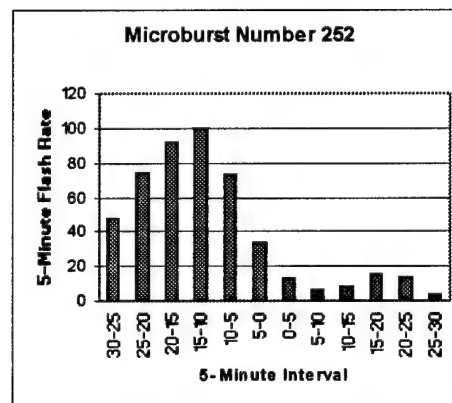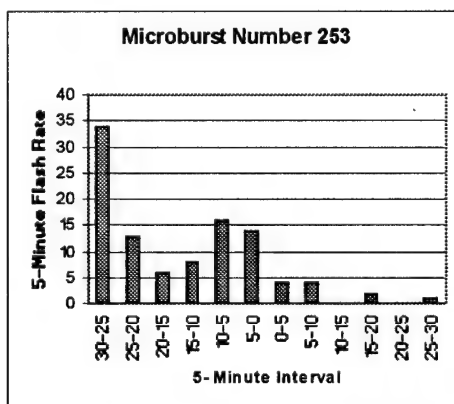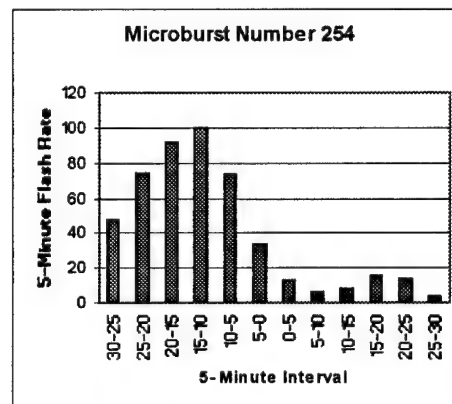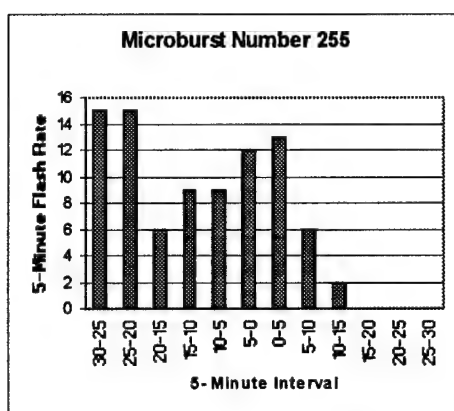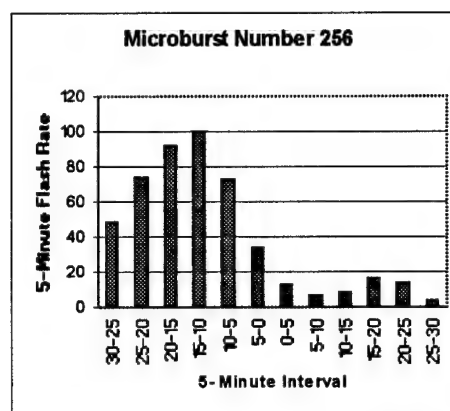Fig. F66. As in Fig. F1 except for microburst number 196.

Fig. F67. As in Fig. F1 except for microburst number 197.

Microburst Number 199

Fig. F68. As in Fig. F1 except for microburst number 199.

Microburst Number 203

Fig. F69. As in Fig. F1 except for microburst number 203.

Microburst Number 207

Fig. F70. As in Fig. F1 except for microburst number 207.

Microburst Number 208

Fig. F71. As in Fig. F1 except for microburst number 208.

Microburst Number 223

Fig. F72. As in Fig. F1 except for microburst number 223.

Microburst Number 224

Fig. F73. As in Fig. F1 except for microburst number 224.

Microburst Number 225

Fig. F74. As in Fig. F1 except for microburst number 225.

Microburst Number 226

Fig. F75. As in Fig. F1 except for microburst number 226.

Microburst Number 227

Fig. F76. As in Fig. F1 except for microburst number 227.

Microburst Number 228

Fig. F77. As in Fig. F1 except for microburst number 228.

Microburst Number 229

Fig. F78. As in Fig. F1 except for microburst number 229.

Microburst Number 231

Fig. F79. As in Fig. F1 except for microburst number 231.

Microburst Number 236

Fig. F80. As in Fig. F1 except for microburst number 236.

Microburst Number 237

Fig. F81. As in Fig. F1 except for microburst number 237.

Microburst Number 238

Fig. F82. As in Fig. F1 except for microburst number 238.

Microburst Number 241

Fig. F83. As in Fig. F1 except for microburst number 241.

Microburst Number 242

Fig. F84. As in Fig. F1 except for microburst number 242.

Microburst Number 244

Fig. F85. As in Fig. F1 except for microburst number 244.

Fig. F86. As in Fig. F1 except for microburst number 246.

Fig. F87. As in Fig. F1 except for microburst number 250.

Fig. F88. As in Fig. F1 except for microburst number 251.

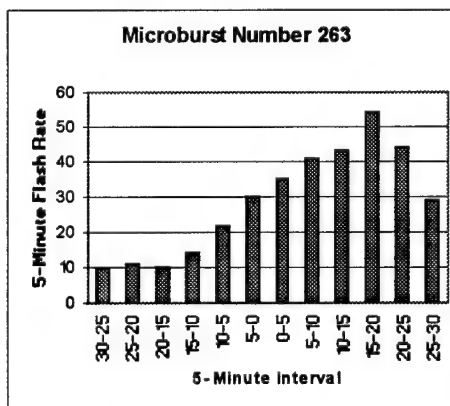Fig. F89. As in Fig. F1 except for microburst number 252.

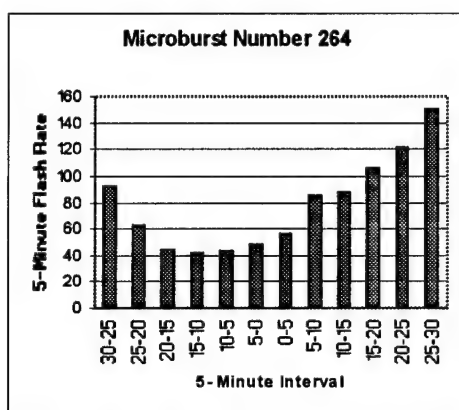Fig. F90. As in Fig. F1 except for microburst number 253.

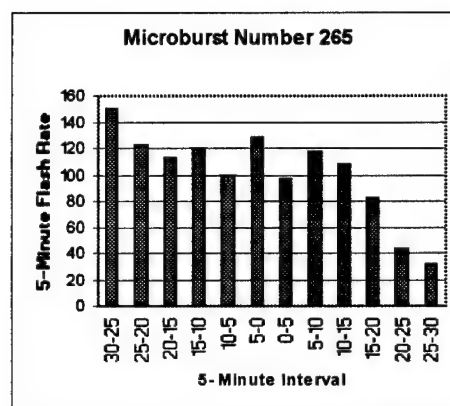Fig. F91. As in Fig. F1 except for microburst number 254.

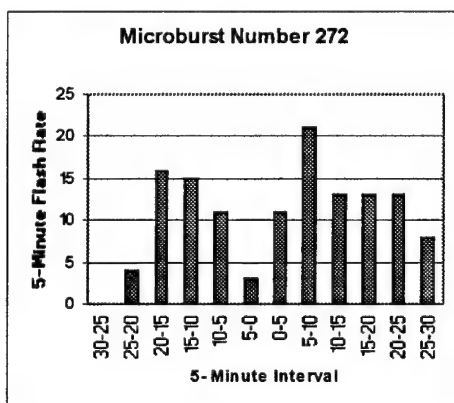Fig. F92. As in Fig. F1 except for microburst number 255.

Fig. F93. As in Fig. F1 except for microburst number 256.
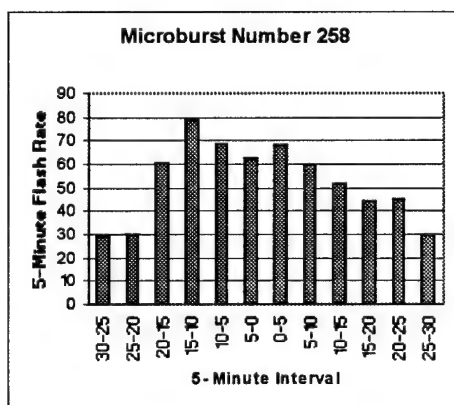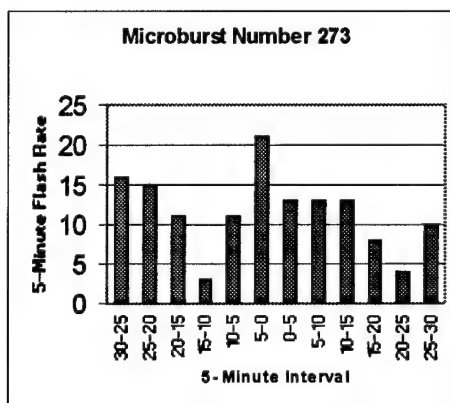
Fig. F94. As in Fig. F1 except for microburst number 258.
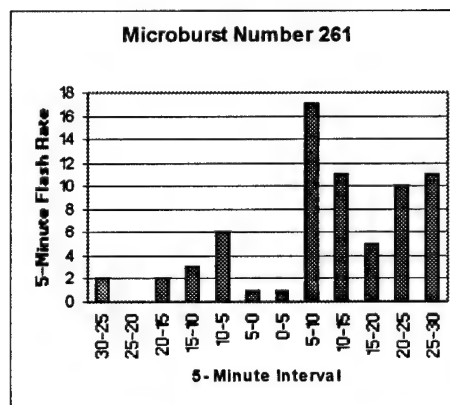
Fig. F95. As in Fig. F1 except for microburst number 261.
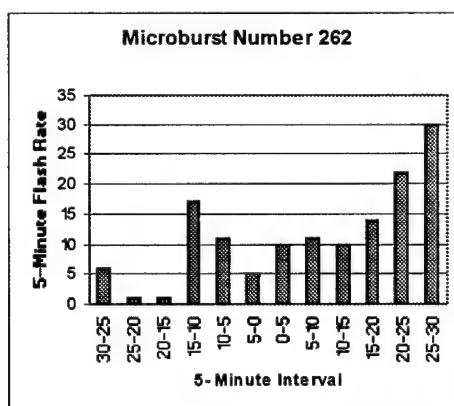
Fig. F96. As in Fig. F1 except for microburst number 262.

Fig. F97. As in Fig. F1 except for microburst number 263.

Fig. F98. As in Fig. F1 except
for microburst number 264.

Fig. F99. As in Fig. F1 except
for microburst number 265.

Fig. F100. As in F1 except
for microburst number 272.

Fig. F101. As in Fig. F1 except
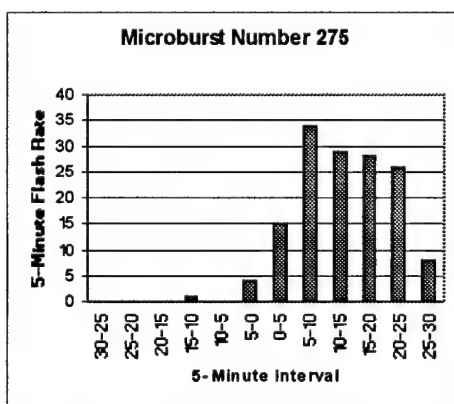for microburst number 273.

Fig. F102. As in Fig. F1 except
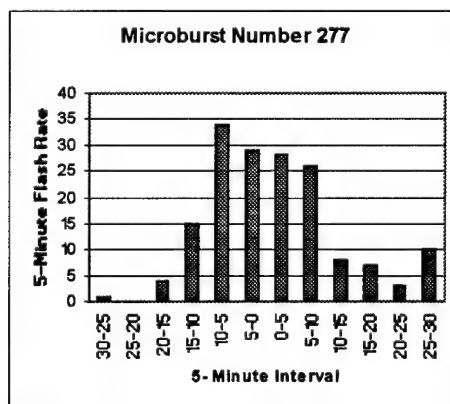for microburst number 275.

Fig. F103. As in Fig. F1 except
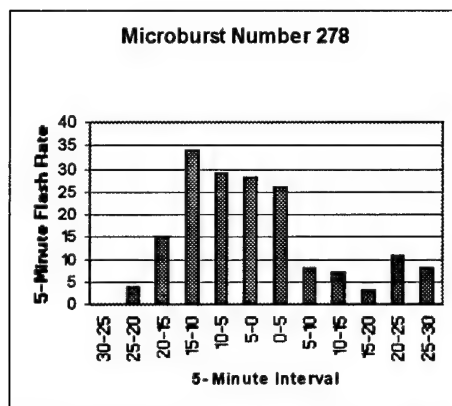for microburst number 277.

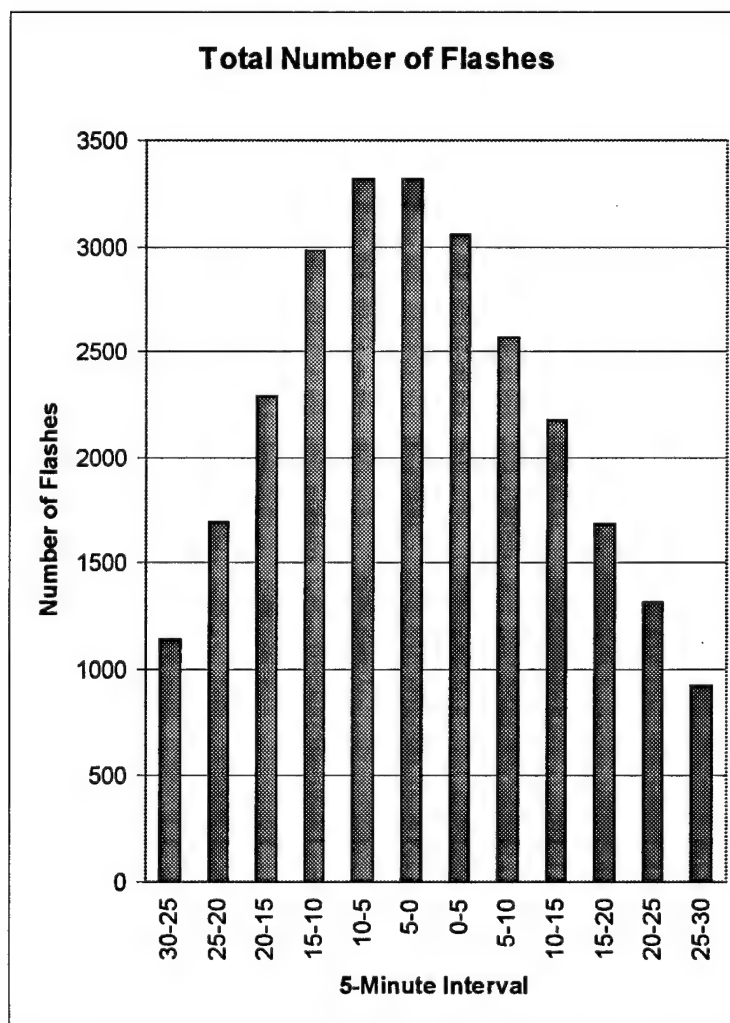Fig. F104. As in Fig F1 except for microburst number 278.

APPENDIX G

MICROBURST AND CLOUD-TO-GROUND LIGHTNING FLASH RATE
TEMPORAL RELATIONSHIP FOR ALL CASES OF MICROBURSTS

Total Number of Flashes

Fig. G1. Total number of cloud-to-ground (CG) flashes for each 5-minute interval 30 minutes before and and after all microburst cases using the 20x20 km grid box.
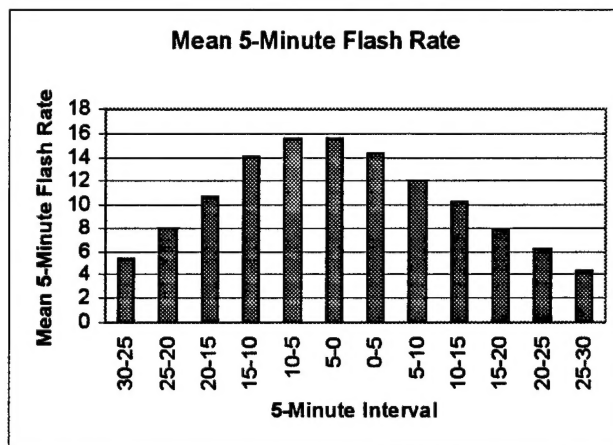
Fig. G2. Mean cloud-to-ground (CG) flash rate for each 5-minute interval 30 minutes before and after all cases of microbursts using the 20x20 km grid box.
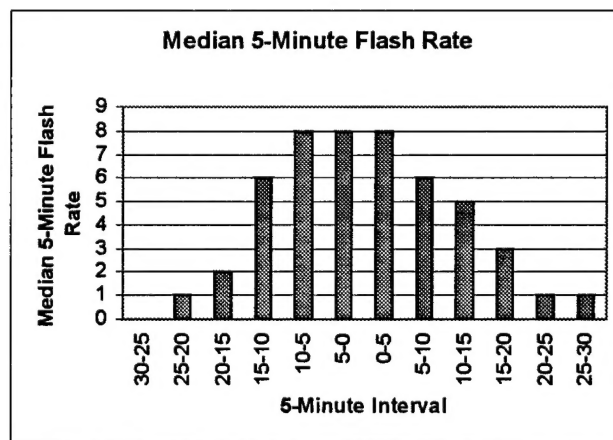

Fig. G3. Median cloud-to-ground (CG) flash rate for each 5-minute interval 30 minutes before and after all cases of microbursts using the 20x20 km grid box.
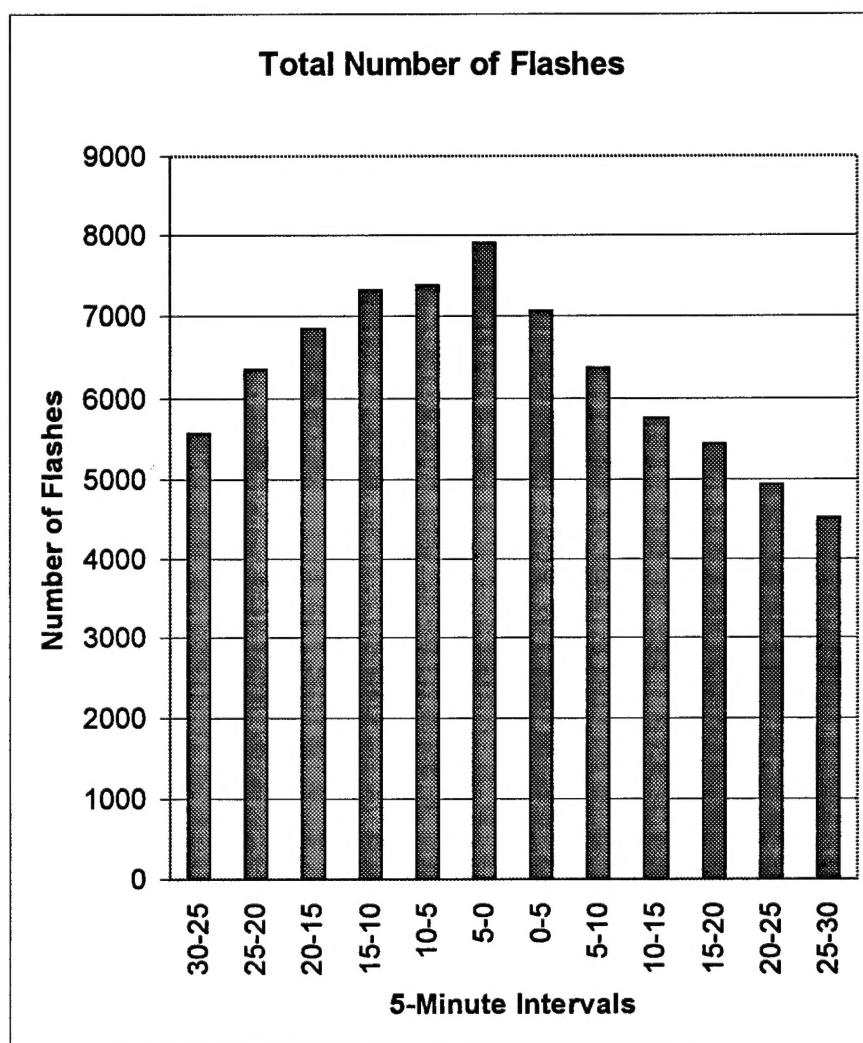
Total Number of Flashes

Fig. G4. Total number of cloud-to-ground (CG) flashes for each 5-minute interval 30 minutes before and after all cases of microbursts using the area of study grid box.

Mean Flash 5-Minute Flash Rate

Fig. G5. Mean cloud-to-ground (CG) flash rate for each 5-minute interval 30 minutes before and after all cases of microbursts using the area of study grid box.

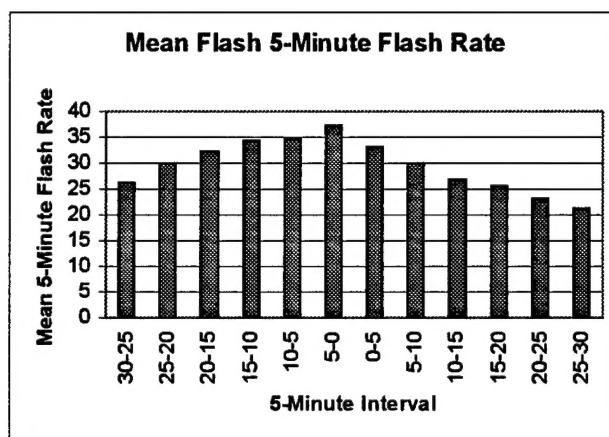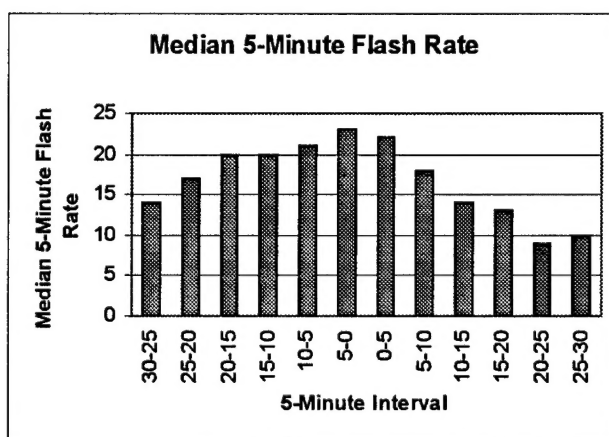**Median 5-Minute Flash Rate**

Fig. G6. Median cloud-to-ground (CG) flash rate for each 5-minute interval 30 minutes before and after all cases of microbursts using the area of study grid box.

VITA

Neil Thomas Sanger was born in Columbus, Ohio, on January 3, 1972 to Stephen and Jeannette Sanger. His father's duties as an Air Force officer took Neil, his brother, and sister all across the U.S., where they attended a number of parochial and public schools. Neil graduated from Niceville Senior High School, Niceville, Florida, in 1990. In April 1994, he earned a B.S. in Meteorology from Florida State University and his commission as a Second Lieutenant in the United States Air Force through the Air Force Reserve Officer Training Corps.

Lieutenant Sanger's first assignment, in June 1994, was to Fort Polk, Louisiana, in support of the Joint Readiness Training Center as the Staff Weather Officer. In July 1996, he was assigned to Osan Air Base, Republic of Korea, as the Instructor Meteorologist for the 51st Fighter Wing where he earned the Air Force Commendation Medal. While stationed at Osan Air Base, he earned a M.S. in Human Relations from the University of Oklahoma.

In April 1997, Lieutenant Sanger was accepted into the Air Force Institute of Technology (AFIT) Advanced Degree Program at Texas A&M University. He will receive his M.S. in Meteorology in August 1999.

While at Texas A&M University, Lieutenant Sanger was promoted to the rank of Captain. On July 12, 1998, Captain Sanger proposed to Miss Lily Landaverde. They will be married on June 17, 2000, in College Station, Texas.

Neil is stationed at the Air Force Combat Climatology Center (AFCCC) in Asheville, NC where he awaits Lily to join him. His permanent address is 1197 Irwin Court, Winter Springs, Florida, 32708.